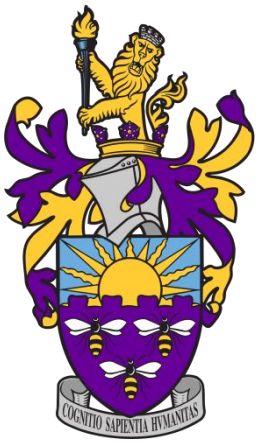

Cryo-EPR of light-driven NADPH:protochlorophyllide oxidoreductase

Guillem Brandariz de Pedro

A THESIS SUBMITTED TO THE UNIVERSITY OF MANCHESTER

FOR THE DEGREE OF

Doctor of Philosophy

IN THE FACULTY OF SCIENCE AND ENGINEERING

2018

School of Chemistry

The University of Manchester

For my parents

List of contents

Total word count: 37,797

List of figures

List of tables

Chapter 4. Excited-state studies on the triplet state of protochlorophyllide analogues at cryogenic temperatures

Abstract

Cryo-EPR of light-driven NADPH:protochlorophyllide oxidoreductase

A thesis submitted to The University of Manchester for the degree of Doctor of Philosophy (PhD) in the Faculty of Science and Engineering by Guillem Brandariz, 2018.

Protochlorophyllide (Pchlide) is the substrate of the light-driven reaction catalysed by the protochlorophyllide oxidoreductase (POR) enzyme. This reaction is a crucial step for chlorophyll biosynthesis in plants, it plays an important role in plant development and it has been suggested to also play a photoprotective role in plant cells.

The POR reaction is one of the very few enzymatic reactions activated by light. The fact that the reaction can be triggered with a single laser pulse makes it a unique model to study enzyme catalysis. A crystal structure of POR is to date unavailable and this lack has thwarted a full elucidation of the reaction mechanism as well as the determination of the protein ternary structure and the exact active state geometry. The substrate, Pchlide, has unique excited-state properties and the decay kinetics including what was presumed to be a long-lived triplet state.

We have used time-resolved absorption and electron paramagnetic resonance (EPR) spectroscopy at cryogenic temperatures to provide direct evidence of the triplet state of Pchlide and the characterisation of its EPR signature. We have found that the triplet state of Pchlide reacts with solvated oxygen, and that POR-binding reduces the triplet lifetime, supporting the theory of POR playing a photoprotective role. We were able to stabilise and characterise a highly transient reaction intermediate by means of cryo-trapping as well as identifying changes in its structure, a matter where there is currently no clear consensus. By studying substrate analogues we have been able to expand current knowledge on which and how different regions of Pchlide are important for the reaction photochemistry.

The work in this thesis opens up this crucial biological system to a whole new range of experimental techniques that can prove instrumental in elucidating the still unclear reaction mechanism of light-driven POR.

Declaration

No portion of the work referred to in the thesis has been submitted in support of an application for another degree or qualification of this or any other university or other institute of learning.

Copyright statement

Acknowledgements

This four-year long journey would not have been possible without the help and support from many. First of all I would like to thank Dearg and the UoM staff who were not involved with research but took care of us from day one. Thanks to the people in HR, career service, to those organising workshops and to the staff serving us lunch every day, but especially, I want to thank Terry for his caring and dedication towards the girls and I. Thanks for putting a smile on our faces every time you came to tidy up the office and for checking on us when times were tough. Get better soon, this one goes to you.

Any academic progress I've made in Manchester has been thanks to the constant and priceless support, guidance and help from my supervisors Alistair, Derren and Sam. There's no way I could have got this far without you. I'd like to extend my gratitude to David, Floriana, Nick, Michi and all the colleagues in MIB and PSI. I also want to thank the Weber group for hosting and taking care of me in Freiburg, especially Daniel.

I also am thankful to the UB GMMF and CH groups, especially to Arnald, Nuria and Guillem helping me prepare for this challenge. I could also not forget my dear friends from "cats", Lidi, amic guapo, Javi, Llucia, Helena, Retek and many more whom I've seldom seen but whose support I always felt. Thanks to my friends from the Netherlands. To Akis for his sense of humour, to George for loving me despite having the empathy skills of a chicken nugget, to Iris & fam for being the voice of reason, to Eli for being the most encouraging grumpy ex ever, to Miri for inspiration and, of course, thank you Remi for being the best accountabilibuddy I could have asked for. You truly did make a difference and I'm sure you will continue to.

Many thanks to my UK friends too for making this experience unforgettable. Thanks to the DLH crew, especially Hattie, Oli and Emma for looking after me and making me feel home in London. Thanks to Paul and Stephen (and the Serbians!) for the most ridiculously fun weekends. I'm also truly thankful to Alina 🐻, Ana, Alex, Toby (+football team) and to my fabulous ex-flatmates for all the memories and support.

If there's one treasure I'm getting from the PhD that has to be meeting *the gurlz*. What an incredible set of office, PhD, conference, travel and life partners I've met.

Much love to the Psyders, Joan&Marius, Maricas and Oops families who changed my life in Spain. A little extra love for Lina, Mario, Erika, Angel, Roly, our german superstars, Gisela (+our lovely group) and Eze/Jowy. An enormous hug goes to Maria, Du, Daria, Alli, Andrea and Vico for being the most adorable, inspiring and supporting bebs. You mean a lot to me.

Hug, Jane and tetis: you are the pillars of my life and a constant source of inspiration.

Finally, my deepest and most sincere gratefulness is for my parents and my family for making sure over the last years that I had nothing to worry about but getting the most out of this experience. I did.

1 Introduction

1.1 Outline

The work carried out during this Ph.D. project followed a natural progression of research objectives. The outcomes of this research are presented as an alternative format thesis consisting of three manuscripts.

Considering the broad range of topics involved in this project, an introduction to photochemistry, light-activated catalysis, the protochlorophyllide oxidoreductase (POR) enzyme system and the main techniques used is presented prior to the aforementioned manuscripts.

The studies carried out during this Ph.D. involved extensive work and training at the EPSRC national service for electron paramagnetic resonance (EPR) spectroscopy. All work involving cell culture, protein purification and time-resolved absorption spectroscopy was carried out at the Biophysics facility of the Manchester Institute of Biotechnology. Most of the pulsed EPR work in this thesis was carried out at the EPR facility of the Manchester Institute of Biotechnology.

This project was part of a Marie Skłodowska-Curie Actions Innovative Training Network involving training by partners AstraZeneca and Bruker. It also involved two secondments at the Institute of Physical Chemistry of the Albert-Ludwigs-Universität Freiburg, where the big majority of continuous-wave EPR experiments were carried out.

This work involved collaborations with several researchers from the University of Manchester and University of Freiburg. Their roles on each of the research articles are described below.

1.1.1 Manuscript titles, publication status and roles of authors

Manuscript 1, Chapter 2: "Direct evidence of an excited-state triplet species upon photoactivation of the chlorophyll precursor protochlorophyllide"

G. Brandariz-de-Pedro, D. J. Heyes, S. J. O. Hardman, M. Shanmugam, A. R. Jones, S. Weber, D. Nohr, N. S. Scrutton, A. J. Fielding, *J. Phys. Chem. Lett.*, 2017, 8, 1219.

This letter provides direct evidence of the triplet-state formed upon photoexcitation of Pchlide and compares the excited-state dynamics at room and cryogenic temperatures.

This manuscript was written by GBP with guidance from DJH, SJOH and AJF. Sample preparation was carried out by GBP. Ultrafast time-resolved measurements were conducted by SJOH. Laser flash-photolysis measurements were conducted by GBP with help from DJH. EPR measurements except the trEPR laser flash wavelength comparison were carried out by GBP with help from AJF and MS. The trEPR laser flash wavelength comparison measurements were carried out by DN with help from GBP. DFT calculations were carried out by GBP. All time-resolved spectroscopy data was analysed by GBP with guidance from DJH and SJOH. All EPR data was analysed by GBP with guidance from AJF. SW supervised the work carried out at the University of Freiburg. NSS helped supply initial funding. ARJ assisted GBP with experiment planning.

Manuscript 2, Chapter 3: "Excited-state dynamics of POR-bound protochlorophyllide at cryogenic temperatures"

Guillem Brandariz-de-Pedro, Derren J. Heyes, Samantha J. O. Hardman, Michiyo Sakuma, Muralidharan Shanmugam, Stefan Weber, Daniel Nohr, David Collison, Nigel S. Scrutton, Alistair J. Fielding

This manuscript pending submission provides a direct comparison of EPR and time-resolved spectral changes of free and POR-bound Pchlide, as well as the characterisation of a cryo-trapped hydride-transfer reaction intermediate.

This manuscript draft was written by GBP with guidance from DJH, SJOH and AJF. Purification of Pchlide was carried out by GBP with help from DJH. Purification of POR was carried out by GBP with help from Sakuma. Sample preparation was carried out by GBP. Ultrafast time-resolved measurements were conducted by SJOH. Laser flash-photolysis measurements were conducted by GBP with help from DJH. Pulse EPR measurements were conducted by GBP. trEPR measurements were carried out by DN with help from GBP. All time-resolved spectroscopy data was analysed by GBP with guidance from DJH and SJOH. All EPR data was analysed by GBP with guidance from AJF. Shanmugam supervised the work carried out at the MIB EPR facility. SW

supervised the work carried out at the University of Freiburg. DC supervised GBP. NSS helped supply initial funding.

Manuscript 3, Chapter 4: "Excited-state studies on the triplet state of protochlorophyllide analogues at cryogenic temperatures"

Guillem Brandariz-de-Pedro, Derren J. Heyes, Samantha J. O. Hardman, Nicholas F. Chilton, Stefan Weber, Daniel Nohr, David Collison, Nigel S. Scrutton, Alistair J. Fielding

This manuscript pending submission provides a direct comparison of EPR and time-resolved spectral changes of a range of Pchlide analogues.

This manuscript draft was written by GBP with guidance from DJH, SJOH and AJF. Final CASSCF calculations are pending to be added to the main text. Sample preparation was carried out by GBP. Laser flash-photolysis measurements were conducted by GBP. trEPR measurements were conducted by DN with help from GBP. DFT calculations were carried out by GBP. CASSCF calculations on compound A were conducted by NFC. CASSCF calculations on compounds B-H are being conducted by GBP. All time-resolved spectroscopy data was analysed by GBP with guidance from DJH and SJOH. All EPR data was analysed by GBP with guidance from AJF. SW supervised the work carried out at the University of Freiburg. DC supervised GBP. NSS helped supply initial funding.

1.2 Photochemistry

Life on Earth depends on photochemistry. In photosynthesis, light energy from the sun is fixated by living organisms, producing carbohydrates in the process, which then serve as an energy source to other living species. Another product of photosynthesis is molecular oxygen, which makes up 20% of our atmosphere and is essential for respiration. This amount of oxygen was not available in such high concentrations prior to the advent of photosynthetic organisms. Thus, photochemical reactions contributed to the evolution of the atmosphere's composition from the early times of life on Earth, allowing for more advanced, aerobic organisms to appear later.[1] The atmosphere, apart from having a composition dictated by photochemistry, also hosts crucial photochemical processes itself. By filtering harmful, high-energy UV-A and UV-B radiation, the atmosphere acts as a radiation shield to all beings on the planet's surface.[1] Photochemical processes in nature have played a main role in shaping the biosphere as we know it. Light absorption is involved in processes that have allowed life to exist on planet Earth and continue to be crucial to perpetuate its existence.

Apart from this, photochemistry is also present in plenty of man-made processes in our daily lives such as photography, light-activated medical treatments, photodegradable products and solar cells.[1,2] The behaviour of molecules can drastically change upon light absorption, displaying chemical properties distinct from the ground state compound. Thus, photochemistry can give access to energy states, reactions and analytical techniques that are not accessible in dark chemistry. Dark chemistry can be defined as that which is independent of the interaction of light with matter.[1,3]

Moreover, chemical processes can as well generate light, of which fireflies are a living example. Some photochemical processes do not involve an overall chemical change. In the case of fluorescence and phosphorescence, compounds emit radiation after having absorbed photons previously.[1,4,5]

1.2.1 Electromagnetic radiation

Light is an energy form that exhibits both wave-like and particle-like properties. It propagates in a straight line, although it can be refracted or reflected, at a speed of $3 \cdot 10^8$ m/s in a vacuum. Electromagnetic radiation waves can be described as a combination of

an oscillating magnetic field and an oscillating electric field. These fields are perpendicular to each other and to their direction of propagation. While wave theory explains phenomena like the propagation, reflection, refraction, diffraction, interference and polarisation of light, some other light properties, such as the photoelectric effect and black-body radiation can only be accounted for by treating light like a stream of particles, the photons. Ultraviolet (UV) and visible light comprise a relatively small region of the whole electromagnetic radiation spectrum (see Figure 1.1). Electromagnetic radiation is usually classified according to its wavelength or frequency, which are related according to:

Equation 1

$$\lambda = \frac{c}{\upsilon}$$

where λ is the wavelength of the radiation, corresponding to the distance between two consecutive maxima of the sinusoidal wave composing a monochromatic light beam, c is the speed of light in a vacuum and ν is the frequency of the monochromatic light beam in question.

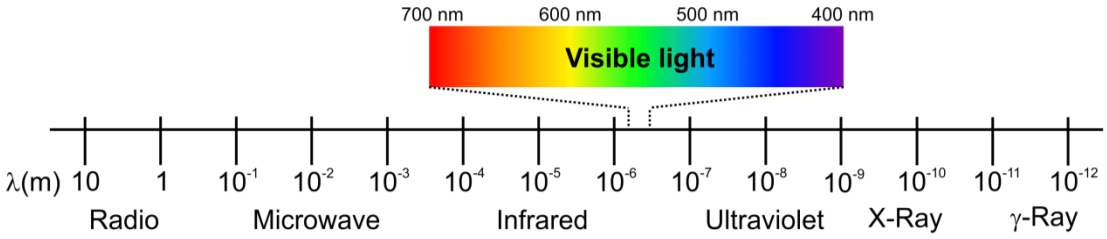

Figure 1.1. Representation of the electromagnetic spectrum displaying various radiation types according to their wavelength.

In order to understand photochemistry, a quantum mechanical approach to study light is necessary. Light absorption and emission events take place involving discrete quanta, the photons. The energy of a photon is given by:

Equation 2

$$E = h\upsilon = hc\tilde{\upsilon}$$

where *h* is Planck's constant (6.62607004×10^{-34} $m^2 \cdot kg \cdot s^{-1}$) and $\tilde{\nu}$, expressed in m^{-1}, is the wavenumber and equals $1/\lambda$.

The fact that the wavenumber is linearly related to the energy of a photon makes this unit particularly useful in photochemistry.[1,4]

1.2.2 Absorption

Light absorption takes place when a molecule (or atom) absorbs energy from the electromagnetic field. Conversely, when energy is provided to the electromagnetic field by a molecule, emission takes place.[6] In photoexcitation, a molecule (or atom) is promoted to a higher energy state by absorbing light. Photons can only be absorbed when their energy matches the energy difference between the initial and excited states of the molecule.[4,6]

When monochromatic light is absorbed by a sample its intensity becomes attenuated. The loss of intensity is proportional to the thickness of the absorbing material, the initial light intensity and the absorption coefficient of the medium for that specific wavelength. The optical density of a sample, also called absorbance, is dimensionless and described by $A=\log(I_0/I)$. The relationship between the intensity of light absorbed by a homogeneous absorbing isotropic sample, its concentration and thickness of the light path is described by the Beer-Lambert law (Equation 3):

Equation 3

$$\log_{10}\frac{I_0}{I} = A = \varepsilon \cdot c \cdot l$$

where ε is the molar extinction coefficient of the sample ($L \cdot mol^{-1} \cdot cm^{-1}$), c the concentration ($mol \cdot L^{-1}$) and l the path length of the light beam (cm).

This law is generally accurate in the case of liquid and frozen solutions, with the exception of cases when the composition varies with concentration, when absorption of light causes significant temperature shifts in the sample and in cases where very long-lived excited states are formed.[3,4]

1.2.3 Molecular orbitals, energy levels and selection rules

The concept of atomic orbitals is an approximation providing a structure-like visual representation of the electronic portion of an atomic wave function. A molecular orbital (MO) consists of a sum of the individual atomic orbitals composing it.[4,6] The list of electron-occupied MOs for a given molecular state describes its electronic configuration. This configuration describes how electrons are distributed among the different MOs.[6] The sum of all occupied MOs is an approximation of the electronic distribution of that particular electron configuration. When an electronic configuration has the lowest-energy orbitals filled it is defined as the ground state configuration for that particular molecular geometry. Any other possible configuration corresponds to an excited-state.[2]

The most relevant configurations for the study of photochemical processes of organic compounds are the ground state and the first few excited states. The highest-energy occupied MO for a ground state configuration is defined as HOMO, while the first higher energy MO, which is unoccupied in the ground state, is defined as the lowest-energy unoccupied MO (LUMO). These two orbitals are the most important MOs in organic photochemistry as transitions between them involve small amounts of energy for a given system.[2]

Atomic absorption transitions appear as sharp lines in UV-Vis absorption spectra while molecules display broad bands. This is due to the presence of additional closely spaced energy levels in molecules as a result of vibrational and rotational fine structures.[4] Multiple transitions between different energy levels that are very closely spaced give rise to the broadening characteristic of molecular UV-Vis spectra.[2]

In the relaxation pathway of photoexcited species we can differentiate between singlet and triplet species. Excited singlet states consist of two unpaired electrons of opposite spin, usually one of them remaining in the HOMO and the other one in a molecular orbital of higher energy.[4] In excited triplet states, the two unpaired electrons display the same spin orientation. This kind of excited state, as opposed to singlets, is usually not generated directly by absorption of light but rather by decaying from a higher energy excited state. In order for an excited singlet state to decay into a triplet species, intersystem crossing needs to take place, which will be explained later on.[4]

The nomenclature employed to describe excited states generally depends on the relevant properties to be emphasised about a particular system (*e.g.* symmetry, involved orbitals or ordering of energy states).[7]

One of the most commonly used notation schemes in photochemistry is the Enumerative system. In this system the singlet ground state is represented as S_0, while the excited singlet states are represented as S_1, S_2, S_3 and so on in ascending order of energy. The triplet states are accordingly represented as T_1, T_2, T_3, etc. This notation scheme is particularly useful to work with in cases where the ordering of energy states is a highly relevant property.[2]

Another notation scheme commonly used to describe electronic transitions is Group Theory, which emphasises the symmetry of the studied states. The Kasha notation scheme, on the other hand, focuses on the bonding characteristics of the system orbitals. The Clar notation emphasises the visible features of a particular transition in a recorded spectrum. The Platt and Mulliken notation schemes are based on the electronic structure of the molecular orbitals involved in a transition.[2,4]

A summary of different notation schemes and their corresponding nomenclature can be found in Table 1.1, which was adapted from reference 4.

Table 1.1. Notation schemes used to describe electronic configurations and transitions in photochemistry.[4]

system	state symbols		examples
enumerative	S_0	Singlet ground state	$S_0 \rightarrow S_1$
	S_1, S_2, S_3, S_n	Excited singlet states	$S_0 \rightarrow S_2$
	T_1, T_2, T_3, T_n	Triplet states	$T_1 \rightarrow T_2$
group theory	A, B, E, T (g, u, 1, 2, ', '')	Irreductible representations of molecule group point	$^1A_1 \rightarrow {}^1B_2$
			$^1A_{1g} \rightarrow {}^1B_{2u}$
			$^1A_{1g} \rightarrow {}^3E_{1u}$
Kasha	σ, π, n	Ground state orbitals	π→π*
	σ*, π*	Excited state orbitals	n→π*
Platt	A	Ground state	$^1A \rightarrow {}^1B_a$
	B, L (a, b)	Excited states	$^1A \rightarrow {}^1L_b$
Mulliken	N	Ground state	V←N
	Q, V, R	Excited states	Q←N
Clar	α, p, β	Intensity and band shape	

Transitions can be classified as allowed or forbidden according to selection rules derived from the theoretical expression of the transition moment. The spin selection rule dictates that in order for an electronic transition to be allowed, the two states involved must have the same multiplicity, thus implying that transitions between singlet and triplet states are forbidden. Therefore, forbidden transitions should not take place. However, perturbations from the solvent or vibronically induced transitions can result in relaxation of a selection rule, allowing forbidden transitions to be observed in practice.[3–5]

1.2.4 Chromophores

The word chromophore stems from the Greek words χρῶμα (khrôma), meaning colour and -φόρος (-phóros), meaning –bearing or -carrying. A chromophore is an atom or moiety in which an electronic transition corresponding to an absorbance band in the UV or visible region of the electromagnetic radiation spectrum occurs.[8] With the exception of chromophores absorbing only in the UV region, they are responsible for coloration of a compound. This definition has been extended to include moieties responsible for vibrational transitions responsible for absorption of infrared light. Moreover, the word chromophore is also often used to refer to a compound that absorbs in the UV and visible region instead of just the moiety within the compound responsible for absorption.[8]

Absorption spectra of organic compounds heavily depend on the structural characteristics of a molecule and different families of compounds show common traits. Because of this, most saturated organic compounds are colourless. Organic chromophores generally owe their absorptive properties in the UV-Vis region to π electrons. Light absorption in this region corresponds to transitions from bonding π or nonbonding n orbitals into an antibonding π* orbital. These transitions are represented as π→π* and n→π*.[2]

For linear conjugated π systems, the main absorption band shifts to longer wavelengths the longer the conjugated system is. Once this absorption reaches the visible region of light, a compound will become coloured.[2]

When it comes to cyclic conjugated π systems, their absorption properties depend on the number of π electrons. The most important compounds of this kind are aromatic hydrocarbons (4N+2 π electrons), which display bands denominated ^1L_b, ^1L_a (also called ^1B_a) and ^1B_b depending on their intensity being low ($\varepsilon=10^2$-10^3), moderately intense ($\varepsilon\approx10^4$) or very strong ($\varepsilon>10^5$), respectively.[2,4]

Low intensity bands display a lot more complex vibrational structure than the very strong ones. In the case of nitrogen heterocycles, a bigger number of nitrogen atoms introduced into a molecule will lead to a shift of the n→π band to longer wavelengths, partially because of the lowering in energy of the π* orbital.[2,4]

Absorption spectra of some organic compounds also depend heavily on solvent effects. The interaction between the solvent and the solute upon excitation has to be taken into account in these cases. Some of the factors accountable for solvent effects are: dispersion, polarisation, charge-transfer interactions and electrostatic forces.[4]

1.2.5 Jablonski diagrams

The various unimolecular processes involved in the generation and relaxation of photoexcited states are often represented by means of Jablonski diagrams. This type of diagram can be used to describe the different species involved, relaxation pathways available to each species and their lifetimes.[5]

In a Jablonski diagram, the singlet ground state is normally represented at the bottom as S_0, while the excited singlet and triplet states are represented above it in ascending order of energy following the enumerative notation scheme.[4,5] Generally, excited triplet states are of lower energy than their corresponding singlet state. A frequently used explanation for this phenomenon is a presumed higher repulsion between electrons in singlet states due to their wave function symmetry allowing electrons to be close together.[9] Quantum mechanical calculations on excited states of the Helium atom have suggested that the lower energy of triplet states is not due to reduced electron-electron repulsion but higher electron-nucleus attraction.[10,11]

In most organic photochemical reactions, only the lowest excited states S_1 and T_1 are reactive. Jablonski diagrams only represent unimolecular processes. Vertical arrows

between states indicate a fast, spin allowed transition while oblique arrows indicate a spin conversion. By convention, straight lines represent absorption and emission processes, while radiationless processes are represented by wavy arrows.[4,5] Vibrational energy levels are often displayed as horizontal lines within potential energy wells for each species (Figure 1.2A). In simplified Jablonski diagrams, only the lowest vibrational state of each species is represented and vibrational relaxation processes are not displayed (Figure 1.2B).

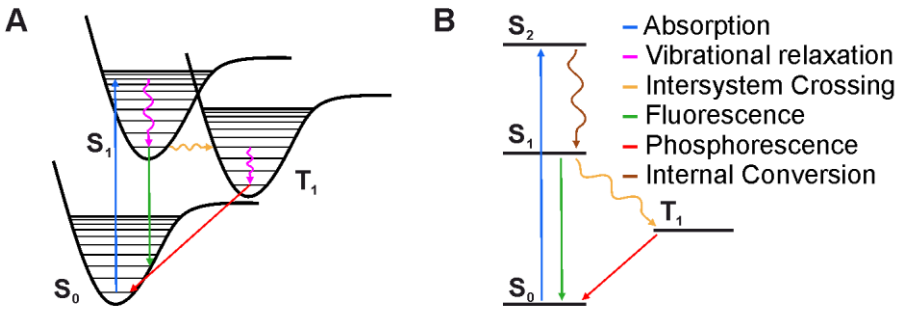

Figure 1.2. Jablonski diagrams representing absorption, luminescence and radiationless processes. (A) Diagram representing vibrational energy levels with horizontal lines. (B) Simplified diagram omitting vibrational relaxation processes and displaying only the lowest vibrational level for each species.

1.2.6 Photophysical processes

Photoexcited species experience a redistribution of their electronic density. When an electron is promoted from a bonding orbital to an antibonding one, the bonding situation of the molecule is altered, which will have an impact on its equilibrium geometry. The larger the differences in bonding or antibonding contribution from the affected orbitals to individual bonds, the bigger the impact on geometry.[4,5]

Extended, highly delocalised π systems generally experience smaller changes in bond length. Changes in electronic density can also have an effect on a molecule's dipole moment, solubility and, most notably, reactivity. Hence, molecules behave differently than when in the ground state and can lead to physical and chemical transformations otherwise unattainable.[4,5]

The energy originating from light absorption can be dissipated through unimolecular processes involving luminescence or through a radiationless process. Bimolecular processes allow for transferring this energy to other molecules. These processes depend on the molecular structure and their surroundings.[6]

Excess energy absorbed by the molecule can imply excitation of molecular vibrations of the final excited states. Vibrational energy is quickly distributed among the molecule's various normal vibrations or to neighbouring molecules. This process is called vibrational relaxation (VR). Vibrational energy can be dissipated very fast, especially in condensed phases, and will generally take place before other relaxation mechanisms.[4]

Radiationless transitions are differentiated depending on the involved levels being of the same multiplicity or different and are known as internal conversion (IC) and intersystem crossing (ISC) respectively.[2,5] Internal conversion involves a transition between two isoenergetic vibrational levels of different electronic states of the same multiplicity, which often have different energies when in equilibrium.[4] This description often is extended to include the vibrational relaxation of the final electronic state. In that case, the transition is expressed as $S_n \rightsquigarrow S_1$ or $T_n \rightsquigarrow T_1$, with S_n and T_n being higher energy excited states. These transitions are generally much faster than $S_1 \rightsquigarrow S_0$.[4]

Intersystem crossing transitions between a singlet and a triplet state require spin inversion. The most important ones are the ones responsible for radiationless deactivation of the lowest lying excited single and triplet states $S_1 \rightsquigarrow T_1$ and $T_1 \rightsquigarrow S_0$.[4]

Emission in the UV-Vis region can be observed at room temperature if the equilibrium of the molecular system with its surroundings has been perturbed by external effects such as radiation, heat or a chemical reaction. Emission of light is referred to as luminescence and, similarly to radiationless processes, its subcategories are differentiated depending on the involved levels being of the same multiplicity or different.[2,6]

Fluorescence takes place when luminiscence originates from a spin-allowed transition as a result of an electron from an excited singlet state returning to the ground state. This spin-allowed transition happens on a fast timescale (typically $\leq$10 ns lifetimes) and involves the emission of a photon. As part of the initially absorbed energy is usually dissipated through very fast radiationless processes, the energy of the emitted radiation

is lower than the absorbed one, which results in emission taking place at longer wavelengths than the absorbed light. The shift between the absorption and emission band is called the Stokes shift, which becomes larger with increasing difference between the equilibrium geometries of excited and the ground state.[4,5]

When luminescence takes place from an excited triplet state, the electron transitioning to the ground state undergoes an inversion of spin orientation in order to become a singlet again. This kind of light emission is called phosphorescence and takes place at relatively longer timescales than fluorescence because it is forbidden by the spin selection rule (typically ms to s lifetimes).[5] For this reason, generally, excited-state triplet species are longer lived than excited-state singlet species and radiationless mechanisms, such as collision-induced bimolecular processes, can compete with deactivating T_1. Triplet oxygen is often responsible for T_1 deactivation and will be discussed later in this section.

Since IC and VR are very fast processes, phosphorescence takes place from the thermally equilibrated, lowest triplet state T_1 into the ground state S_0. Phosphorescence emits light at longer wavelength than fluorescence as T_1 is generally energetically below S_1.[4,5]

Kasha's rule says that luminescence can be observed exclusively from the lowest excited state in the majority of cases. The reasoning behind this is that radiationless processes ($S_n \rightsquigarrow S_1$ and $T_n \rightsquigarrow T_1$) are usually so fast that lifetimes of higher excited states become extremely short and quantum yields of emission from higher excited states are very small. This rule is, however, relative and other luminescent transitions might be observed for some molecules depending on the sensitivity of the detector.

Some transition metal complexes with organic ligands exhibit phosphorescence and virtually no fluorescence. This can take place in compounds such as tris(2,2′-bipyridine)ruthenium(II), where a metal-to-ligand charge-transfer state is populated upon photoexcitation and ISC takes place on a subpicosecond timescale, making the triplet state the only appreciable photoexcitation product.[12–14]

In addition to the already discussed deactivation mechanisms, bimolecular processes provide important relaxation pathways for excited-state species in which energy is transferred from one molecule to another.[1,6] These mechanisms are generally referred

to as quenching. However, when the main interest of a bimolecular interaction is focussed on the energy-accepting molecule, this energy-transfer interaction is often referred to as sensitisation or sensitised excitation.[6]

One form of quenching would include chemical reactions originating from an excited-state species. When photophysical quenching does not involve a chemical reaction it can be represented as:

Equation 4

$$M^* \xrightarrow{Q} M'$$

where M' is a lower energy state of M. When Q is another M molecule, this mechanism is known as self-quenching or concentration quenching.

Most types of quenching involve collisions between the excited molecule and the quencher.[4] These collisions can involve an encounter complex $M^*\ldots Q$, where the molecule interacts weakly with the quencher, an exciplex MQ^*, where there is strong interaction, or an excimer MM^*, where strong interaction takes place between an excited and a ground-state molecule of the same kind.[4] In the cases of exciplex and excimer formation, a new species with a defined geometry is formed. These species can lose energy by IC, ISC, fluorescence, phosphorescence, an energy transfer leading to $M+Q^*$ or an electron transfer leading to either $M^+ + Q^-$ or $M^- + Q^+$.[4]

Energy transfer is also possible between two excited-state molecules.[2] This type of interaction is usually negligible due to concentration of excited-state species being generally too small. This phenomenon becomes more feasible in the case of two triplet states due to their lifetimes being longer.[2] Quenching between two triplet states is called triplet-triplet annihilation and the most common mechanism is:

Equation 5

$$^3D^* + {}^3A^* \rightarrow {}^1D + {}^1A^{**}$$

where the donor triplet *D* transfers energy to the acceptor species *A* producing a ground state singlet and a higher energy excited singlet state **. For most organic compounds, the combined triplet state energy is enough to promote one of them to a singlet state. This mechanism often takes place between two identical molecules, where the acceptor will undergo IC and reach the lowest excited singlet. In cases where this singlet state is

fluorescent, triplet-triplet annihilation produces delayed fluorescence.[2,4] Oxygen does quench triplet states in solution by acting as the acceptor triplet species in Equation 5 in a diffusion-controlled process. In this case the initial oxygen molecule is a ground state triplet accepting energy to become excited-state singlet oxygen.[2,6]

1.2.7 Quantum yield

The first law of photochemistry, formulated by Grotthus and Draper in the 19th century, states that only light that is absorbed by a molecule can bring about photochemical change. This is referred to as the principle of photochemical activation.[4]

The second law of photochemistry states that if a species absorbs radiation, one particle is excited for each quantum of radiation absorbed.[4]

As previously discussed, there may exist various mechanisms by which an excited species can react or lose energy and, on many occasions, more than one can coexist. The efficiencies of such processes are determined by their respective rate constants. The quantum yield is an efficiency parameter used to study photochemical reaction mechanisms.[2,4]

The quantum yield (Φ) of a specific process in a system is described as the amount of events taking place per photon absorbed by the system:[1,4,8]

Equation 6

$$\Phi = \frac{number\ of\ events}{number\ of\ absorbed\ photons}$$

And in the case of a light-activated reaction $\mathrm{A} \xrightarrow{hv} \mathrm{B}$:

Equation 7

$$\Phi_R = \frac{amount\ of\ reactant\ consumed\ or\ product\ formed}{amount\ of\ absorbed\ photons}$$

$$\Phi_{\mathrm{A}} = \frac{[\mathrm{A}]_t - [\mathrm{A}]_0}{\int_0^t \mathrm{I_a dt}} \qquad \Phi_{\mathrm{B}} = \frac{[\mathrm{B}]_t}{\int_0^t \mathrm{I_a dt}}$$

1.3 Time-resolved absorption spectroscopy

Sometimes, the concentration of atoms, radicals, excited species or other reactive intermediates in a stationary system is too low to be detected by analysis of the system's absorption spectra. Time-resolved experiments are a great tool to investigate the chemical nature of transient or reactive intermediates, determine their concentration and provide kinetic information about them[1].

1.3.1 Flash photolysis

The staple method and basis of time-resolved absorption spectroscopy techniques is flash photolysis. This method involves illuminating the sample with a high-power flash or laser pulse (Figure 1.3 blue pulse) in order to generate transient concentrations of intermediates that are high enough to be measured. In this kind of measurements, the concentration of reactants, intermediates or products can be followed by measuring absorption at a defined wavelength (Figure 1.3 red beam) as a function of delay after flash (DAF). This type of kinetic measurements is appropriate for measuring on μs-s timescales and is an invaluable tool to study photochemical processes.[1,15]

Figure 1.3. Schematic representation of a flash photolysis experiment where $h\nu_1$ represents the flash responsible for generating the transient species (blue) and $h\nu_2$ is the probe beam illumination (red).

In this kind of experiment, the sample is placed between the probe light source and a detector. The flash hits the sample perpendicularly to the probe beam so as not to reach the detector.[15,16] Absorption at the probe wavelength will reflect a change over time from DAF = 0, forming what is commonly referred to as a kinetic trace.

Kinetic traces can be fit, usually to exponential decay functions, to obtain information about the lifetime of species involved in the photochemical process of interest.[1] When kinetic traces are measured at multiple probe wavelengths, they can be combined in a three-dimensional dataset (wavelength, time, intensity) on which multivariate statistical

analysis can be performed. In this thesis, flash photolysis kinetic traces have been analysed to study triplet state decay times of different Pchlide samples in order to better understand which factors have an impact on its lifetime.

1.3.2 Ultrafast Pump-Probe Spectroscopy

Excited state dynamics of light-activated reactions on the fs-μs timescale can be followed by means of laser spectroscopy measurements. In a pump-probe setup, a first laser pulse (pump, Figure 1.4 blue pulse) results in light absorption from the sample, triggering the photolysis events of interest. This is then followed by a second light pulse (probe, Figure 1.4 red pulse) that allows for recording absorption at fixed DAF values. It is possible to measure differences in absorption at ultrafast timescales with time a time resolution of less than 200 fs.[17,18]

Figure 1.4. Schematic representation of a pump-probe experiment where $h\nu_1$ is the pump laser pulse (blue) and $h\nu_2$ is the probe laser pulse (red).

The main differences between this technique and flash photolysis are the shorter timescale at which it operates and that a full spectrum at a specific DAF is recorded with each measurement instead of recording a kinetic trace for a single wavelength. However, kinetic traces can be obtained by measuring spectra at many DAF values. In this type of experiment, the pump laser pulse can be parallel to the probe pulse.[17,18]

The resulting datasets from combining measurements can be analysed using multivariate statistics. The product of such analyses is a set of spectra with associated lifetimes. These spectra and lifetimes can be assigned to individual transient species and provide insight on the excited state dynamics of the studied system.[19] This technique has already been used to study the steps and species involved with photoexcitation of Pchlide on its own and complexed with POR.[20–23] In this thesis, ultrafast pump-probe spectroscopy has been used extensively to measure the excited state dynamics of a

series of Pchlide samples at cryogenic temperatures and to investigate a reaction intermediate.

1.4 **Electron Paramagnetic Resonance (EPR) spectroscopy**

1.4.1 Introduction to EPR

Electron paramagnetic resonance (EPR) spectroscopy is a technique that allows the study of paramagnetic compounds. It shares many theoretical and experimental aspects with nuclear magnetic resonance (NMR) spectroscopy.[24] The main difference between these techniques lies in the fact that rather than magnetic nuclei, EPR concerns the interactions of unpaired electrons, which have a magnetic moment more than two orders of magnitude larger than, for example, protons.[24] This limits the amount of compounds suitable as EPR samples, as there is a requirement for the samples to contain unpaired electrons, which are found much less often than magnetic nuclei, allowing NMR to be used to study a much larger range of compounds.[24]

The large magnetic moments imply a higher sensitivity for the same concentration of spins and the possibility to observe spin-spin interactions at longer distances. The stronger interactions in EPR also result in faster relaxation times and render the technique suitable for studies at shorter timescales. However, because the large magnetic moments of electrons result in signal observation times and radiation pulse lengths about two orders of magnitude shorter, EPR instrumentation generally needs to be more complex than that of NMR.[24–26]

EPR can provide information about electron spin density, structure, symmetry and lifetime of paramagnetic species thanks to the availability of several technique variations, such as continuous-wave (CW) EPR, time-resolved CW EPR, free induction decay, electron spin echo or hyperfine sublevel correlation spectroscopy.[27–29] The aforementioned EPR spectroscopy techniques differ in the nature and timing of the applied electromagnetic radiation and will be discussed later in this chapter.

Chemical bonding relies on the pairing and spin cancellation of electrons, while EPR-active substances need to be quite the opposite. A minority of pure compounds are paramagnetic and, therefore, accessible to EPR. Nitroxides and molecular oxygen are an example of this.[30,31] Certain solid-state materials like conducting polymers and semiconductors are also EPR active due to defects.[32,33]

Some of the most common EPR active species exhibit enhanced chemical activity due to having unpaired electrons. This would be the case for many excited-state species like the photoexcited singlet and triplet states discussed in section 1.2, which can lower their energy *via* physical or chemical processes. Transition metal complexes often contain multiple unpaired electrons and EPR has been used extensively to evaluate properties like the metal electronic configuration.[34,35]

Some reaction intermediates, especially in oxidation and reduction processes, display both high reactivity and EPR activity due to containing unpaired electrons prior to a complete rearrangement of chemical bonds. Biological reactions are a good example of this and some of them, including the main subject of this thesis, will be discussed in detail in this chapter.[36]

In the case of reaction intermediates or unstable free radicals with an extremely short lifetime, it is possible to use a technique called spin trapping. This technique allows for trapping such reactive species with a diamagnetic compound, the spin trap, furnishing a more stable free radical that can be studied and the properties of which can indirectly provide information on the original radical.[37] However, short-lived species can also be detected using transient EPR methods,[29] as will be described later.

1.4.2 Electron spin Hamiltonian

The electron spin Hamiltonian describes the energies of the different states found in the ground state of a given paramagnetic species.[27] The terms of the static spin Hamiltonian are related to various types of interactions like the electron Zeeman interaction, zero-field splitting, hyperfine couplings, nuclear Zeeman interactions, nuclear quadrupole interactions and spin-spin interactions between pairs of nuclear spins.[27] Considering the most relevant interactions in EPR spectroscopy, the static spin Hamiltonian for a system with an electron spin vector operator $\boldsymbol{S}$ and m nuclei with a spin operator $\boldsymbol{I}_k$ can be described as:[27,35,38]

Equation 8

$$H_0 = H_{EZ} + H_{ZFS} + H_{HF} + H_{NQ} = \frac{\beta_e \boldsymbol{B}_0 \boldsymbol{g} \boldsymbol{S}}{\hbar} + \boldsymbol{S}\boldsymbol{D}\boldsymbol{S} + \sum_{k=1}^{m} \boldsymbol{S}\boldsymbol{A}_k\boldsymbol{I}_k + \sum_{I_k>\frac{1}{2}} \boldsymbol{I}_k\boldsymbol{P}_k\boldsymbol{I}_k$$

where H_{EZ}, H_{ZFS}, H_{HF} and H_{NQ} are the electron Zeeman, zero-field, hyperfine and nuclear quadrupole interactions respectively, which will be discussed in this section.[27]

1.4.3 The Zeeman effect

Electrons are negatively charged particles with spin angular momentum, which inherently makes them tiny magnets. An electron's magnetic moment is directly proportional to its spin angular momentum, which can only have two values.[26] Consequently, when an unpaired electron finds itself within a magnetic field (B_0), it will align its magnetic dipole moment either in a parallel or an antiparallel orientation with respect to the field, which corresponds to electrons with magnetic quantum numbers $m_s = -1/2$ and $m_s = +1/2$ respectively.[25,26]

Due to the electron Zeeman interaction, the $m_s = -1/2$ and $m_s = +1/2$ states become energetically distinct when in a magnetic field (Figure 1.5). The energy of the state aligned antiparallel with respect to the field is higher in energy than that of the state aligned parallel to B_0. The energy gap between the two levels increases with the intensity of the applied magnetic field.[26] The energy difference is usually smaller than thermal energy, which leads to a small population difference. EPR spectroscopy experiments are often carried out at low temperature to achieve higher population differences.[27]

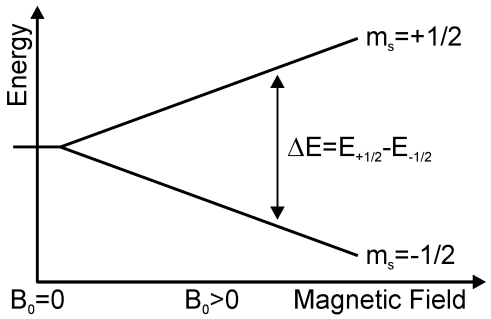

Figure 1.5. Energy level splitting of an unpaired electron in a magnetic field.[26]

These two energy levels allow spectroscopy to come into play. When microwave radiation is applied to a system of these characteristics and its energy matches that of the gap between the two electron spin orientations, the electron meets the resonance

condition and absorption of microwave radiation will cause a transition between the two spin orientations.[24]

The ratio between the two populations is defined by the Boltzmann distribution as follows:

Equation 9

$$\frac{N_+}{N_-} = e^{\frac{\Delta E}{-kT}}$$

where *k* is the Boltzmann constant and *T* the temperature of the system. N_+ and N_- relate to the upper state and lower state, respectively.

EPR transitions take place according to the selection rule:

Equation 10

$$\Delta M_S = \pm 1, \Delta M_I = 0$$

where M_S and M_I are the system's electronic and the nuclear spin quantum numbers respectively.

In EPR it is common practice to fix the microwave frequency and sweep the magnetic field to achieve the resonance condition. The most important equation of EPR, which derives from the H_{EZ} term of Equation 8, describes the resonance condition:

Equation 11

$$h\nu = g\mu_B B_0$$

where *h* is Planck's constant, *v* is the microwave frequency, *g* is the g-factor, μ_B is the Bohr magneton and B_0 is the magnetic field. The g-factor will be described in section 1.4.5. Transitions occur from the lower level to the upper and *vice versa* with equal probability. However, a higher population of the lower level results in a net radiation absorption. The most typically used frequency in EPR spectroscopy is ~9.5 GHz and is commonly denominated X-band. There is currently a range of microwave bands available for use in EPR spectroscopy, as presented in Table 1.2.

Table 1.2. Specifications of the standard EPR microwave bands.

band	frequency range (GHz)	typical EPR frequency (GHz)[25,39,40]	g_e center field (mT)[39]
L	1 - 2	1	35
S	2 - 4	3	130
X	8 - 12	9.8	340
K	12 - 18	24	850
Q	30 - 50	34	1220
V	50 -75	65	2320
W	75 - 110	94	3350
D	110 - 170	130	4640

1.4.4 Zero-field splitting and triplet states

When a system contains two unpaired electrons, its electronic state is defined by their alignment. When the electrons are aligned in an antiparallel manner there is only one possible spin state, a singlet, which implies that no EPR transition can take place. However, when the electrons are aligned in a parallel fashion, the electronic state is a triplet, which involves a strong interaction between two electrons taking place in an $S = 1$ system that contains three sublevels.[41] In the case of photoexcited triplet states, formation from and decay to a singlet state involves ISC, which contributes to making such transitions relatively slow. In the case of triplet states decaying to a singlet ground state, phosphorescence is often involved.[2,6]

Absorption of microwaves can trigger transitions between the triplet sublevels, which makes this electronic state EPR active. According to the EPR selection rule there are two allowed EPR transitions in triplet states (Equation 10, Figure 1.6). However, a third, forbidden transition with $\Delta M_s = 2$ can take place too, although with a much lower intensity. Due to its position in a field swept EPR spectrum, this is commonly referred to as the half-field transition.[42–45]

When the unpaired electrons find themselves in an environment of spherical symmetry, like in the case of atomic gaseous Hg, the triplet sublevels are degenerate in energy in the absence of an applied magnetic field.[41,46]

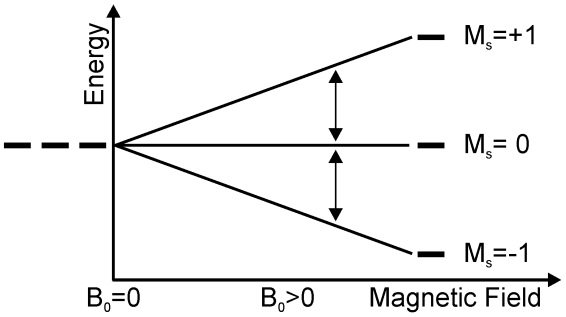

Figure 1.6. Sublevels of a triplet state with spherical symmetry in a magnetic field.[41]

However, as long as the system does not have spherical symmetry, the energy of triplet sublevels will be non-degenerate when no magnetic field is being applied. The lifting of degeneracy between triplet sublevels originates from dipolar interaction, as triplet state electrons are dipoles aligned in parallel inducing reciprocal repulsive dipole-dipole interactions between them, which translates into different effective magnetic fields for the various sublevels.[46–50] On the other hand, the energy splitting between singlet and triplet states, which tends to be two orders of magnitude larger, is caused by exchange interaction.[47]

The lifting of triplet sublevels degeneracy when the applied external field is null gives place to the phenomenon known as zero-field splitting (ZFS). Zero-field splitting takes place in systems with spin larger than ½.[26] It causes magnetic anisotropy, which allows for extracting geometry and structural information. For rhombic systems, two parameters, *D* and *E*, are used to define the zero-field splitting. *D* describes the axial component of the magnetic dipole-dipole interaction, and *E* is the transversal component. The energy of ZFS interactions and the values of *D* and *E* parameters can be extracted from the developed zero-field splitting term of Equation 8:[46,47]

Equation 12

$$\boldsymbol{H_{ZFS} = SDS = D_x S_x^2 + D_y S_y^2 + D_z S_z^2 = D\left[S_z^2 - \frac{1}{3}S(S+1)\right] + E\left(S_x^2 - S_y^2\right)}$$

Because the energy difference between the various sublevels is tightly bound to the symmetry of the system, when it comes to triplets, we can differentiate between three different states: T_Z, T_X and T_Y. Each one represents a state where the spin axes of both electrons are confined to the plane perpendicular to the Z, X or Y axis respectively. For

example, for *Tz*, the component of the spin angular momentum in the Z direction is zero and the spin axes are restricted to the XY plane.[50]

The energy of a triplet sublevel will generally be lower the more overlap there is between the system and the plane over which the electron spin axes are restricted. This can be understood in terms of a repulsive interaction between two parallel magnetic dipoles. For example, elongation of a system along the Z-direction will result in a relatively higher energy T_Z level than compression along the Z-axis, as the electrons, which in the case of T_Z are restricted to the XY plane, can stay further apart (less repulsion) in a system that has been flattened along Z in comparison to if it had been elongated. Usually, T_Z will be lower in energy than T_X and T_Y for planar systems in a strong magnetic field.[51,52]

The *D* and *E* parameters describe the energy separation of the triplet sublevels (Equation 12) and also reflect the symmetry of the species electronic distribution. *D* represents the energy difference between T_Z and the average of T_X and T_Y, while *E* is half the energy difference between T_X and T_Y.[42,43,48,52] As a general rule, higher values of the axial component *D* indicate a higher planarity of the electron distribution, while negative *D* values indicate an elongation in the Z-direction.[52]

It is worth pointing out that ZFS depends on the geometry of the electronic environment, which does not equal the structure of the studied species, although they are tightly related.[46,48] Because of this, one should aim at comparing chemically and structurally similar compounds in order to draw conclusions from changes in ZFS.[46,52] In the case of excited triplet states, which are the focus of this thesis, it is important to take into account that any structural information obtained regards the excited-state structure of the studied compound, which can differ from the ground state structure. In this thesis, the excited state structure of the compounds has been optimised prior to carrying out computational ZFS calculations.

When a triplet state is subjected to a magnetic field B_0, the zero field sublevels are transformed into three high field states: T_0, T_{+1} and T_{-1}. The T_0 state includes the electrons that are aligned perpendicular to the magnetic field, while T_{+1} contains the electrons that are aligned along the magnetic field and T_{-1} includes those that are aligned against it.[43,51] At high fields, the triplet sublevel corresponding to the axis aligned parallel to the magnetic field (*i.e.* T_Z if B_0 is parallel to the Z axis) will transform into

T_0. The energy of T_0 remains constant at increasing field values because the electrons it contains are confined to the plane perpendicular to the magnetic field. The other two zero field sublevels, which contain electrons aligned both along and against the magnetic field, intermix to give place to the T_{+1} and T_{-1} states, where all electrons are aligned either along the magnetic field (T_{+1}) or against it (T_{-1}) and experience Zeeman splitting (Figures 1.6 and 1.7). [6,43,48,51,52]

Two EPR transitions take place at different fields for each distinct orientation. The transitions are commonly described with a letter and a sign. The letter, Z, X or Y, is assigned according to the zero field sublevel corresponding to T_0 for that particular orientation. The + sign is chosen when the transition takes place between T_0 and T_{+1}, while the – sign is used when the transition takes place between T_0 and T-1. For example, the Z^+ transition corresponds to that between T_0 and T_{+1} for a triplet species aligned with its Z axis parallel to the magnetic field.[41,43,48]

EPR transitions for two orientations of the triplet state of naphthalene are represented in Figure 1.7, which was adapted from reference 41.

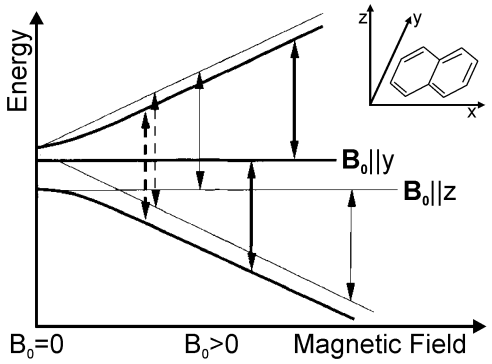

Figure 1.7. Zeeman splitting and EPR transitions of the S = 1 state of naphthalene.[41]

If all the spin systems in a sample are oriented the same way, which can be achieved with oriented lattices, each pair of transitions can be isolated by orienting the sample, accordingly.[51] When the magnetic field is not oriented with one of the system axes, EPR transitions take place at field positions in between those arising from the species main orientations.[42] Although the exact position of intermediate orientations can be calculated,[42] these are not directly relevant for the work in this thesis.

The EPR measurements in this thesis entail frozen solution samples, which, like powder samples, are randomly oriented solids. In randomly oriented solid samples, molecules are found in all possible orientations, as opposed to aligned in a certain direction, like in single crystals or oriented lattices. The EPR spectrum of a randomly oriented solid represents the sum of transitions corresponding to all possible orientations of the molecule.[42,43] This implies the overlap of a large number of features in the EPR spectrum and, as a result of this, spectra of this type of samples display broad features.[42,43,51,52]

Magnetically equivalent orientations (e.g. all orientations where the XY plane is parallel to B_0 for a system with axial symmetry) will experience an EPR transition at the same field position, resulting in more intense EPR features for that field position.[26] The turning points in frozen solution triplet state spectra are dictated by the fields at which transitions take place for each principal orientation and ZFS parameters can be inferred from the separation between such transitions with the help of computational simulations.[42,43]

As will be presented in the following chapters, frozen solution EPR spectra of Phclide and its analogue compounds display a broad, antisymmetric lineshape. This is to expect from triplet state EPR spectra, as they display a pair of equally intense features of opposite sign for each orientation (see Figure 1.7).

Comparison of ZFS parameters between samples of Pchlide in different protein complexes will help draw conclusions on how the molecule geometry and the electronic environment are affected in each scenario. Deviations in ZFS between Pchlide and analogue molecules can also be helpful to determine which groups have a greater impact on the molecular geometry, which is directly related to protein active-site binding suitability.[53]

1.4.5 The g-tensor

An unpaired electron will behave differently in a magnetic field depending on the configuration and symmetry of the molecular orbital it is occupying, as well as its specific orientation with respect to a local coordinate system.[47] Apart from the already discussed contribution to the magnetic moment from spin angular momentum S, there is

also an orbital angular momentum L. The two interact through the spin-orbital interaction.[47] The contribution from this interaction to the total magnetic moment increases with atomic number. The expression used to describe the effect of spin-orbital coupling on an unpaired electron is called the g tensor, which is present in Equation 11.[25] For an unbound electron, the quantitative prediction of this parameter is:

$$g_e = 2.002319304$$

In practice, the *g* value of an electron will deviate from that of g_e. Electrons with larger g values will appear at lower fields than those with a smaller *g* value. In magnetically anisotropic systems, the g tensor will have two components for axial systems: $g_{parallel}$ and $g_{perpendicular}$ (g_z and g_{xy}), and three for rhombic systems (g_x, g_y, g_z).

The interaction of unpaired electrons with the magnetic field is the source of the main features of an EPR spectrum. However, other interactions like hyperfine coupling also play a role in determining the features of an EPR lineshape.

1.4.6 The hyperfine interaction

The hyperfine coupling is the interaction between the magnetic moments of an electron spin and a nuclear spin as described by the hyperfine interaction term of Equation 8:

Equation 13

$$H_{HF} = \boldsymbol{SAI}$$

Where the hyperfine tensor $\boldsymbol{A}$ consists of two terms: the Fermi contact interaction (isotropic term) and the anisotropic term, derived from electron-nuclear dipole-dipole coupling and related to r^{-3}, with r being the distance between the atom containing the electron and the interacting nucleus. The Fermi contact interaction accounts for the non-zero probability of the electron spin and the nuclear spin to be in the same point in space when the electron spin finds itself in an s orbital. The reason behind the anisotropy of the electron-nuclear dipole-dipole coupling is due to the fact that p, d and f orbitals are not spherically symmetric, this interaction is orientation dependent.[24,54]

Hyperfine coupling results in further splitting of the electronic spin states in the magnetic field. When a hyperfine coupling is large enough, it will result in a multiplet

pattern in field sweep EPR spectra. The hyperfine splitting can be directly read in these cases. Smaller, unresolved splittings contribute to the linewidth of EPR spectra.[55] However, there are advanced pulsed EPR techniques that allow determination of small couplings.[27] These pulsed EPR techniques will be described in this section and some of them have been used to measure hyperfine couplings of the POR system in chapter 3. Hyperfine couplings are commonly expressed in field or frequency units.

1.4.7 Nuclear quadrupole interaction

In nuclei with spin ≥1, the charge distribution is non-spherical and described by the nuclear electric quadrupole moment Q. Neighbouring electrons and magnetic nuclei generate an electric field gradient (EFG). Nuclear quadrupole interactions can induce shifts on the position of EPR transitions. Moreover, they can contribute to the appearance of forbidden transitions.[25,26]

These interactions are relatively small in EPR spectra, as they are second order contributions to the spectrum. However, in experiments like electron spin echo envelope modulation (ESEEM) and electron nuclear double resonance (ENDOR) spectroscopy they appear as first order splittings (more on these techniques in Section 1.4.11).[27] Investigating nuclear quadrupole interactions can provide information on the identity and chemical nature of the different nuclei coupled to the paramagnetic centre of interest.[56] The interaction between a nuclei and the EFG is described by the Hamiltonian:

Equation 14

$$H_{NQ} = \mathbf{IPI}$$

where **P** is the nuclear quadrupole tensor. This tensor is traceless in its principal axes system and the Hamiltonian can be written as:

Equation 15

$$H_{NQ} = P_x I_x^2 + P_y I_y^2 + P_z I_z^2 = \frac{e^2 qQ}{4I(2I-1)\hbar}\left[(3I_z^2 - I(I+1)^2) + \eta(I_x^2 - I_y^2)\right]$$

where eq is the EFG and $\eta = (P_x\text{-}P_y)/P_z$ is the asymmetry parameter, for which $|P_z| \geq |P_y| \geq |P_x|$ and $1 \geq \eta \geq 0$ apply. P_z is defined as $P_z = e^2qQI(2I(2I\text{-}1)\hbar)$.

The most common way to express nuclear quadrupole parameters in the literature is by stating η and $e^2qQ/\hbar$. Computational methods such as density functional theory (DFT) calculations can be used to determine the quadrupole tensor.[56]

1.4.8 Relaxation times

The population of energy levels of a sample returns to thermal equilibrium after being microwave-irradiated. The time it takes for the sample to achieve the equilibrium magnetisation after excitation is referred to as relaxation time.[24,27]

There are two distinct relaxations. Longitudinal relaxation, T_1, describes the relaxation along the direction of the external magnetic field B_0. Conversely, transverse relaxation, T_2, accounts for the relaxation time in the plane perpendicular to B_0. The longitudinal relaxation is a thermal process in which the spin system exchanges energy with its environment. T_1 is also commonly referred to as spin-lattice relaxation because it involves an interaction with the lattice. T_2, also called spin-spin relaxation, occurs without an energy exchange with the lattice. Instead, it takes place through an interaction between spins of the sample.[24,27]

Relaxation times have an effect on the lineshape of EPR spectra. When a sample is irradiated with too much microwave power, the magnetisation induced by the microwaves (B_1) can become too large and result in the transverse relaxation time not being fast enough for a full recovery of the magnetisation equilibrium. In these cases, the saturation phenomenon takes place. This effect results in lineshapes and ratios between peaks not being proportional to the relative amount of spins involved in the different EPR transitions of a compound.[24,54]

1.4.9 Continuous-wave (CW) EPR

In continuous-wave (CW) EPR the sample is irradiated with microwaves at a fixed frequency while the magnetic field is swept. The absorption of microwave radiation by the sample at resonance fields is recorded. This is the most basic EPR experiment.[26]

In order to achieve maximum sensitivity, the impedance of the EPR resonator needs to be tuned for each sample. To do this, EPR instruments have an iris tuning screw that changes the coupling between the microwave transmission line and the resonator. When the resonant enhancement of the resonator is maximum, the resonator is critically coupled.[26]

In standard CW EPR measurements the amplitude of the magnetic field is modulated at a certain frequency in order to increase the signal-to-noise ratio. A larger modulation amplitude results in an increased signal-to-noise ratio at the expense of spectral resolution (broadening of signals). For samples that display several peaks within a short field range it is often beneficial to use a small modulation amplitude.[26,47]

Field modulation and phase sensitive detection cause the output signal to be the derivative of the net microwave absorption by the sample instead of the absorption signal itself. The dependence of microwave absorption versus applied field represents the so-called EPR spectrum of a sample, which often is represented as the absorption derivative versus the field.[24,54]

1.4.10 Time-resolved CW EPR

In order to measure short-lived radicals and photoexcited paramagnetic species by CW EPR it is necessary to achieve time resolution. This can be achieved by means of pulsing the generation of the paramagnetic species, which often involves using a pulsed laser source, and gating the detection system.[29]

In time-resolved CW EPR (trEPR) the field is not modulated and the measured signal is the time-resolved microwave absorption at a series of magnetic field positions. Usually, transients are recorded from right before the laser pulse until up to a few microseconds after the laser flash, depending on the lifetime of the paramagnetic species. In this kind of experiment it is recommendable to measure some transients at an out-of-resonance

field position in order to carry out a baseline subtraction since the laser pulse itself can have an effect in the registered transients when it hits the walls of the EPR cavity.[25,29]

A trEPR spectrum can be obtained by plotting the EPR intensity at a certain delay after flash over the range of field positions. An often better alternative is to instead integrate over a time-range of the transient signals and plot the integration value versus field position.[29]

Hyperfine coupling interactions can take time to evolve and might not be apparent in trEPR measurements for the first few hundreds of nanoseconds. This is in part due to the spin states not being in a Boltzmann equilibrium at very early times. Microwave radiation being present during the photochemical events leading to the species of interest, rather than after, can also have a broadening effect on the EPR linewidth at times close to the laser flash. When this poses an issue, as could be the case with very short-lived species, pulsed EPR techniques can be better suited for analysis.[26,27,29]

Although a decay of the signal can be measured with trEPR, it is not always representative of the decay time of such species under normal conditions, as the constant microwave radiation triggers EPR transitions between levels that might differ in lifetime.[25,29]

In this thesis, trEPR measurements were conducted at the University of Freiburg to record the EPR signature of all samples, which enabled the use of spectral simulations to induce ZFS parameters of the studied systems.

1.4.11 Pulsed EPR

In pulsed EPR, electron spins are subjected to a constant magnetic field B_0 and the spectrometer setup and microwave pathway remain close to those in a CW EPR setup. However, in this case, microwaves are not applied to the system throughout the experiment. Instead, pulsed EPR techniques work by exciting electron spins with a series of microwave pulses of determined duration and intensity. These pulses generate an induced signal, which is, then, measured while no microwaves are being applied.[27]

There is a need for larger B_1 fields in pulsed experiments, which are achieved by using a microwave power amplifier.[24,54] Another distinctive characteristic of pulsed EPR,

directly related to the fact that excitation and detection take place at different points in time is that critical coupling of the resonator is not necessary. Overcoupling of the resonator allows for faster time resolution and an increased excitation bandwidth. The need for larger excitation bandwidths and shorter pulse lengths to carry out pulsed EPR techniques delayed its implementation in comparison to pulsed NMR.[27]

Initially, the net magnetisation vector (**M_0**) of the electron spins is aligned in a constant magnetic field. This alignment is perturbed when a short microwave pulse at a frequency meeting the resonance condition is applied.[27]

When in a magnetic field, the magnetic moment of electrons precesses around the magnetic field axis at the electron's Larmor frequency $\omega_L = -\gamma B_0$, with γ being the gyromagnetic ratio of the electron.[27] This frequency corresponds to the electron's EPR transition and equals $g\mu_B$ as per the resonance condition formula (Equation 11) and varies for each magnetically distinct electron in the system.[27]

Pulsed EPR induces the aforementioned tilts in order to generate measurable microwave signals. Because of this, it is easier to work with a frame which rotates around B_0 with a reference frequency ν_0. In such coordinate system (x', y', z'), the microwave magnetic field B_1 coincides with the x' axis, causing a precession of **M_0** around this axis with angular velocity $\omega_1 = -\gamma B_1 = 2\pi\nu_1$. This frequency is called the Rabi frequency.[27]

A microwave pulse of duration t_p rotates **M_0** by $\theta p = 2\pi\nu_1 t_p$. A microwave pulse of such duration that it rotates **M_0** by $\pi/2$, results in **M_0** aligning with the y'-axis, which implies an equalisation of populations in the two energy states. A pulse rotating the magnetisation vector by π results in a complete inversion of the initial vector, thus inverting the populations of the spin states, as represented in Figure 1.8. These are the two main types of pulses used in pulsed EPR techniques.[24,57]

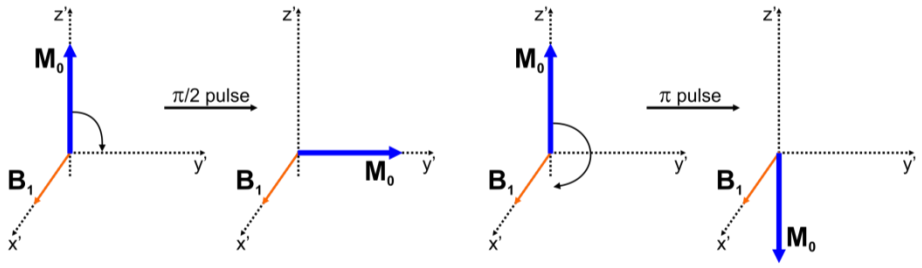

Figure 1.8. Schematic representation of the the net magnetisation vector rotation induced by π/2 and π pulses.

Realignment of the net magnetisation vector is responsible for the generation of a microwave signal that can be detected (echo, Section 1.4.11.2). By using certain pulse sequences and data processing operations, different properties can be studied.

1.4.11.1 Free Induction Decay

After tilting the magnetisation of a sample with a microwave pulse, the elementary magnetisation vectors with distinct rotational frequency values (slightly different from ν_1 depending on electronic environment) precess in the xy-plane.[27]

These elementary magnetisation vectors fan out with an offset from the reference frame rotation frequency $\nu r-\nu_0$, where νr are the rotational frequencies of the elementary magnetisation vectors. During realignment, the sample emits microwave radiation as the magnetisation rotates at the Larmor frequency. The intensity of this radiation is a monoexponential decay of a sum of sinusoidal waves, the frequencies of which correspond to each of the electrons' EPR transition.[27]

The decay time corresponds to the transversal relaxation time $T_2 \sim 1/\Delta\nu_r$, which allows an estimation of this parameter from this experiment. Free induction decay (FID) measurements can provide an EPR spectrum by applying a Fourier Transform (FT) operation on the measured signal and extracting the corresponding frequency information. However, since many spectrometers have a response time on the same timescale as the spectral features, the resulting spectra are not suitable for quantitative study in most cases.[24,27]

1.4.11.2 Electron Spin Echo

Elementary magnetisation vectors fan out completely after a single π/2-pulse, resulting in a defocusing of the magnetisation. However, when a π-pulse is applied at time t = τ after the initial pulse and this pulse is applied along the same axis, refocusing takes place. A refocusing pulse inverts all elementary magnetisation vectors, rotating them by 180º around the x-axis.[24,27] After inversion, elementary magnetisation vectors continue to rotate in the same direction, effectively coinciding at the y-axis instead of fanning out. When the magnetisation vectors refocus, a microwave pulse called an *electron spin-echo* (ESE) is generated. The maximum intensity of the ESE occurs at time 2τ after the initial π/2 pulse as depicted in Figure 1.9.[24,27]

When measuring species generated *in situ* by a laser flash, as is the case for the excited triplet states studied in this thesis, the delay after flash (DAF) at which the microwave sequence is triggered can become an important variable to optimise in order to maximise the signal intensity, as the EPR active species will be generated and then decay over a certain time range.[51]

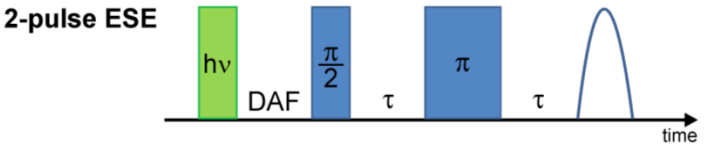

Figure 1.9. Schematic representation of a two-pulse electron spin-echo pulse sequence preceded by a laser flash.

By integrating the ESE over a range of field positions it is possible to obtain a two-pulse ESE field sweep which, in essence, reveals the EPR spectrum of the sample. This type of measurement provided the first EPR spectra of the compounds studied in this thesis.

ESE decay measurements can be a useful complementary tool to time-resolved absorption spectroscopy. In this thesis, results of both techniques were compared to evaluate the effect of solvents and oxygen concentration on the excited triplet state lifetimes.

1.4.11.3 Electron Spin Echo Envelope Modulation

The decay of an ESE takes place while the spin system experiences magnetic modulations from nearby nuclei. In electron spin echo envelope modulation (ESEEM), nuclear transition frequencies can be indirectly measured with EPR.[27] This time-domain technique is based on measuring the intensity decay of an echo generated after a sequence of pulses when varying an inter-pulse delay. There are two standard variants of this technique. One measures the primary-echo discussed in the previous section and the other measures a stimulated echo, which is generated using a sequence of three π/2 pulses as represented in Figure 1.10.[27]

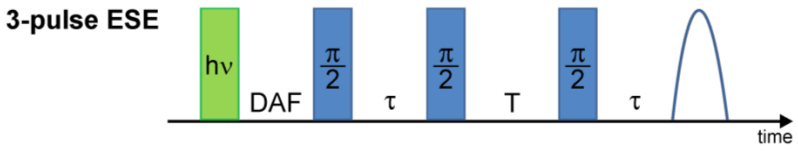

Figure 1.10. Schematic representation of a three-pulse electron spin-echo pulse sequence preceded by a laser flash.

In 2-pulse ESEEM, as τ is subsequently incremented, the echo intensity is modulated by the nuclear transition frequencies of the nuclei coupled to the electron spin. Moreover, the sum and difference of the nuclear frequencies are also observed as modulation in 2-pulse ESEEM.[27,58]

In 3-pulse ESEEM, the first two pulses are separated by a constant delay τ while the time T between the second and third pulses is incremented. The stimulated echo, which is measured at time τ after the third pulse, is modulated by the nuclear frequencies only.[24,27,58]

A frequency-domain spectrum can be obtained by carrying out a FT of processed time-domain ESEEM data. The revealed frequencies correspond to the aforementioned modulations.[58] An advantage of 3-pulse ESEEM, aside from revealing the pure nuclear frequencies without sum and difference frequencies interfering, is that envelope modulations of the stimulated echo are observable over longer times, contributing to narrower peaks in the frequency-domain spectra. An inconvenience of 3-pulse ESEEM occurs in situations where the τ of choice equals the periodicity of the Larmor frequency (or an integer multiple), the contribution from such nuclei can be supressed.[58]

In order to avoid missing data due to this suppression, 3-pulse ESEEM experiments are usually carried out at different τ values.[58]

In this work, ESEEM measurements and their simulations were used to characterise Nitrogen hyperfine couplings of the Pchlide substrate in different protein environments.

1.4.11.4 Hyperfine Sublevel Correlation Spectroscopy

The pulse sequence for HYperfine Sublevel COrRElation spectroscopy (HYSCORE) is achieved by introducing a π pulse between the second and last pulse of the 3-pulse ESEEM sequence. The delay between the second and third pulse, t_1, is varied in one dimension while the time between the third and fourth pulse, t_2, is varied in a second dimension. This pulse sequence is represented in Figure 1.11. This leads to a two-dimensional time-domain experimental output. The frequency-domain spectrum can be obtained *via* FT in both dimensions.[27]

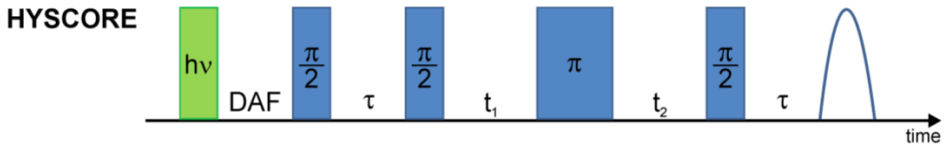

Figure 1.11. Schematic representation of a HYSCORE pulse sequence preceded by a laser flash.

An advantage of this two-dimensional technique is that it exposes cross-peaks which provide correlations between nuclear frequencies from opposite electron spin manifolds. HYSCORE also provides information about the relative signs of nuclear frequencies. The signs of hyperfine and nuclear quadrupole coupling constants reveal certain properties of a paramagnetic species. Generally, the (++)-quadrant shows peaks with weak hyperfine interaction, while peaks with strong interaction appear in the (+-)-quadrant. HYSCORE is also subject of the suppression effect and experiments are often carried out using multiple τ values.[24,27,58]

Matched HYSCORE is a commonly used variation of this technique that focuses on maximising the intensity of cross-peaks. In a system where two levels are very close in energy (a and b on Figure 1.12), promotion of an electron to either of them from a lower

energy level (c) could be possible with what is known as a semi-selective pulse. The pulse, in this case, would be resonant with the two transitions from the lower energy state to both higher energy levels (a-c, b-c) but not with the transition between the higher energy levels (a-b).[27]

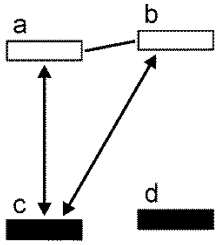

Figure 1.12. A semi-selective pulse excites an allowed transition (a-c) and a forbidden transition (b-c).

This kind of pulse is responsible for the correlations between nuclear frequencies on the transition between the higher states (a-b) observable on HYSCORE experiments. These depend on polarisation being transferred from electron to nuclear spins and the superposition of the nuclear spins axis orientations.[27] The optimum pulse length to maximise transfer depends on relaxation times and the contribution of off-resonance pulses to the signal for each particular experiment. Therefore, pulse length needs to be adjusted experimentally, achieving a matched pulse. Matched pulses can also be used in ESEEM and ENDOR experiments.[27]

HYSCORE has recently been used for the first time to study a photoexcited triplet state.[59] In this project, matched HYSCORE experiments were carried out on Pchlide samples to obtain more detailed information about the electronic couplings in its excited triplet state. The obtained experimental data will be included in a future publication after performing the appropriate data analysis and simulations.

1.4.11.5 Electron Nuclear Double Resonance Spectroscopy

Electron Nuclear DOuble Resonance spectroscopy (ENDOR), similarly to ESEEM, provides information about hyperfine coupling between an electron spin and coupled nuclei. In the case of ENDOR, both microwave and radiofrequency pulses are applied, resulting in a hybrid between EPR and NMR in which part of the electronic polarisation

is transferred to the nuclear transitions. As opposed to ESEEM, however, this technique is better suited to measure strong hyperfine couplings. Moreover, this is a frequency-domain experiment.[27]

The simplest ENDOR experiment is Davies-ENDOR. The pulse sequence starts with a π-pulse, which saturates an EPR transition. Posterior irradiation of the sample with radiofrequency excites NMR transitions and results in a desaturation of the EPR transition. Finally, a detection subsequence consisting of a π/2 and a π pulse is applied. Another standard variation of ENDOR is Mims ENDOR, in which the initial π pulse is split in two π/2 pulses separated by a delay τ.[27,58]

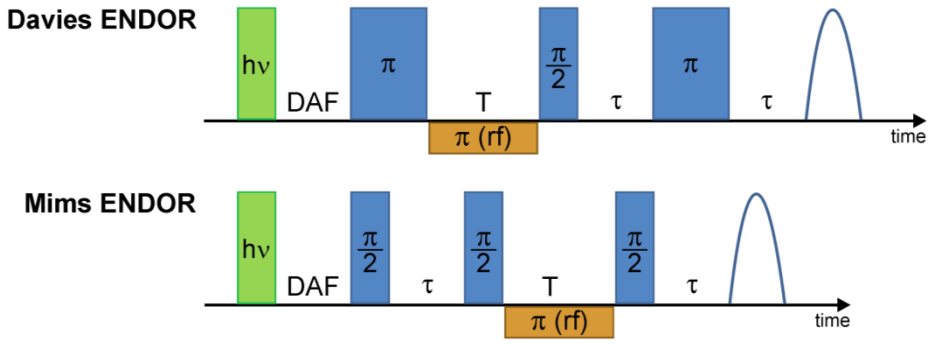

Figure 1.13. Representation of the pulse sequences in Davies and Mims ENDOR experiments. The brown rectangle represents the radio frequency mixing pulse characteristic of ENDOR experiments.

The sequences described in this section are currently standard. However, there are improved, newer variations of many of the pulsed EPR techniques which offer some advantages in terms of sensitivity and accuracy.[58,60–63]

ENDOR was used during this project but the signal-to-noise ratio of the experimental data obtained in that occasion was insufficient to draw conclusions from. Although the experimental conditions could be further optimised to achieve better results, a decision was made to focus on other experimental techniques for the duration of the project.

1.5 Light-activated enzymes

The initial activation of a photoreaction is mainly provided by the absorption of light, as opposed to the activation by heat in thermal reactions. Moreover, in a medium

containing a variety of compounds and systems, as would be the case in a biological environment, light allows for selectivity of activation, since only light-absorbing molecules are excited. Generally, light also allows activating reactions to occur at lower temperatures.[64–68]

Photoreactions can be divided into three different stages. First, absorption takes place, involving photon absorption by a certain molecule and the formation of an electronically excited molecule. Then, the primary photochemical processes take place, involving electronically excited molecules. Finally, the secondary or "dark" chemical processes occur from intermediate species previously produced in the primary photochemical processes. A full understanding of a light-activated process implies knowing the molecular changes taking place from the initial absorption until the formation of products.[6]

For most enzymatic systems, rapid mixing strategies are necessary in order to initiate catalysis, which usually limits the study of the chemical reactions to millisecond timescales or slower. In hydrogen transfer reactions this can be particularly challenging, as the rates are often very fast due to the reduced size of the atom.[69,70]

There are, however, several biological processes that involve light-activated reactions.[66] By studying light-activated systems, the limitations of rapid mixing techniques can be overcome by using a reaction trigger (*e.g.* laser pulse) that occurs on a faster timescale than the chemical steps of interest and allows measurements on ultrafast timescales.[71] Moreover, enzymatic studies over such timescales allow for an in-depth understanding of enzyme mechanisms and investigations into how protein motions might be coupled to chemical steps. The study of light-activated reactions is also particularly important in terms of expanding the scientific knowledge in the field of light harnessing, which is of growing interest.[71] Currently, there are three known light-dependent enzyme systems and one of these, protochlorophyllide oxidoreductase (POR), which is the main topic of this thesis, is discussed in detail below. The other two enzymes, DNA photolyase and a fatty acid photodecarboxylase, both use a flavin cofactor and are briefly discussed in the following section.

1.5.1 DNA photolyases

Solar UV-B wavelength (280-315 nm) and UV-C (100-280 nm)[72] wavelength radiation have mutagenic and lethal effects on living organisms.[73] When the damage inflicted is too large, cells are able to initiate apoptosis, a type of programmed cell death, eliminating themselves from a population that otherwise might suffer serious pathological consequences.[74]

Some organisms are able to repair part of this damage thanks to the DNA photolyase family of enzymes.[75,76] DNA photolyases are highly efficient DNA-repair enzymes that absorb blue light to carry out their activity, which involves repairing UV-damaged DNA by catalysing the splitting of cyclobutane pyrimidine dimers (CPDs). CPDs are formed by covalent cross-linking of neighbouring pyrimidine bases due to [2 + 2] photocyclisation of the C5–C6 double bonds of two bases, which is induced by UV light, and makes up for most UV-induced DNA lesions.[77]

There are two classes of DNA photolyases, both of which contain a flavin adenine dinucleotide (FAD) cofactor. The first one, class-I (see Figure 1.14, taken from reference 83), is mainly found in fungi and eubacteria, while class-II photolyases are widely present in plants and mammals.[78–81] The crystal structure of both apo-photolyase and in complex with DNA has provided an understanding of the way these systems work.[82,83]

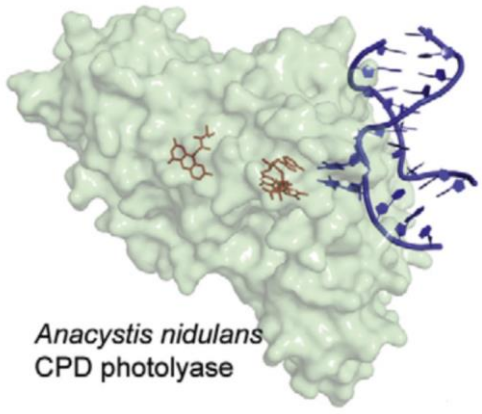

Figure 1.14. Structure of a substrate-bound class-I DNA photolyase protein.[83]

The first step in the repair reaction is the binding of the DNA lesion to the active site of the photolyase. It is crucial for these enzymes to distinguish these lesions from non-dimerised pyrimidine doublets in an efficient manner because the amount of photolyase

molecules per cell is small.[84] In this step, the dimer is flipped outside of the DNA into the active site of the enzyme.

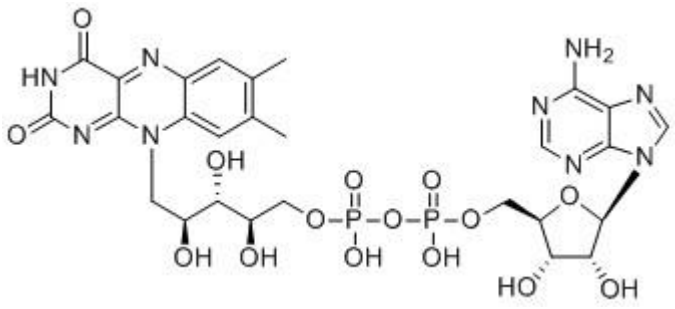

Figure 1.15. Schematic representation of flavin adenine dinucleotide (FAD). A cofactor found in photolyases.

In a subsequent step, absorption of a blue-light photon promotes the transfer of an electron from the flavin cofactor to the CPD. This absorption of light is enhanced by antenna pigments, which are enzyme-bound chromophores with absorption bands that do not overlap with the main pigment and contribute to extending the absorption range of the protein by absorbing energy that is subsequently transferred *via* dipole-dipole coupling.[85–88] Ultrafast spectroscopy studies have determined the lifetime of the transient flavin species, concluding that this depended not only on the presence of the substrate but also on the particular nucleobases forming the dimer.[89] Time-resolved EPR spectroscopy provided further evidence of such radical intermediates and showed that they appeared at field positions close to the neutral radical of FAD (Figure 1.16, taken from reference 90).[89,90]

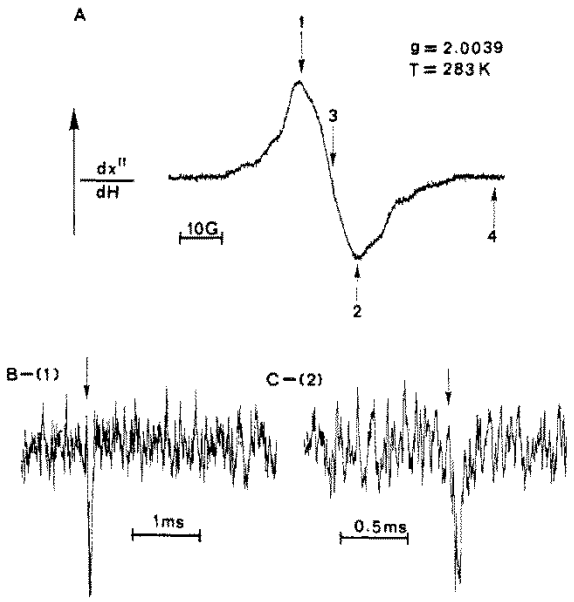

Figure 1.16. EPR spectrum of the dark-stable neutral E-FADH· radical in DNA photolyase (A) with marked field positions (1-4). Transient E-FADH2 radical species registered at field position 1 (B) and at field position 2 (C).[90]

Posteriorly, the cyclobutane ring is split open, breaking the two bonds in a sequential manner.[91] The electron is then captured back by the catalytic flavin, although there is little mechanistic information regarding the cyclobutane ring opening.[92]

Finally, the DNA reanneals correctly and relaxation of the photoexcited enzyme takes place.[77] A general overview of the different states of pyrimidine bases and the radical steps involved in DNA repair can be seen in Figure 1.17. The quantum yield of photoactivated DNA repair is very efficient, with yields of more than 90%.[90,93,94]

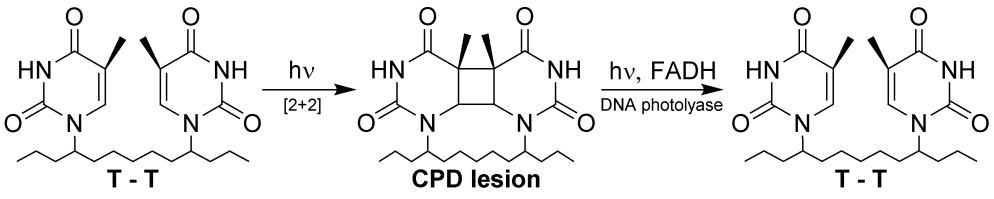

Figure 1.17. Scheme representing formation and repair of DNA UV-lesions by DNA photolyase.[94]

1.5.2 Fatty acid decarboxylase

Very recently, some microalgae have been found to synthesise *n*-alkanes and –alkenes by means of a photoenzyme that catalyses the decarboxylation of fatty acids in response to blue light.[95] This fatty acid decarboxylase (FAP) contains a tightly bound FAD cofactor. FAP is a photoenzyme and requires a constant input of light in order to carry out the reaction. The enzyme is active when irradiated with light of a wavelength between 400 and 520 nm due to the fact that the FAD acts as the light-harvesting moiety of the protein. In the protein, fatty acids are bound in a tunnel-shaped active site placed close to the FAD (see Figure 1.18, taken from Reference 95).[95,96]

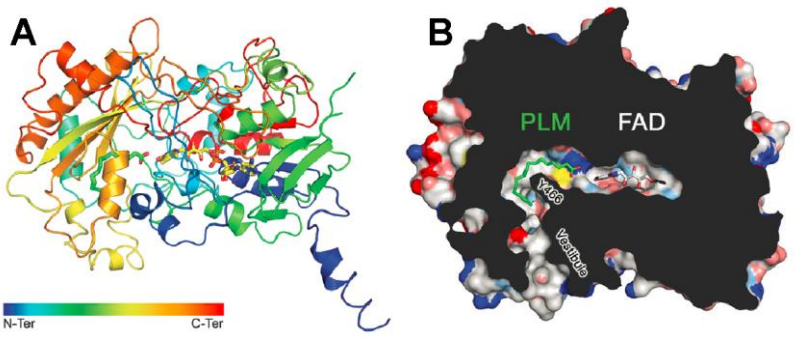

Figure 1.18. (A) Overall architecture of the FAP enzyme in complex with palmitate (PLM) and FAD. (B) Slice through the surface representation of FAP.[95]

Light absorption leads to a radical-based reaction in FAP that starts with FAD capturing an electron from the carboxylic group after photoexcitation. The crystal structure of FAP revealed that the protein is related to the glucose-methanol-coline oxidoreductase family, which are a group of thermally activated enzymes.[95,96]

1.5.3 Magnetic studies on light-activated proteins

The fact that light-activated enzymatic reactions involve paramagnetic species like the FAD radical makes them suitable for electron paramagnetic resonance (EPR) spectroscopy studies. In the past, EPR techniques have been used with great success to study light-activated biological systems such as DNA photolyases.[90]

For studies of this kind, it is important to prepare samples in an aqueous buffer to maintain enzymatic activity. Addition of glycerol to the buffer is common practice for

measurements at cryogenic temperatures,[97] as it contributes to achieving optically transparent frozen samples by reducing the amount of cracks that appear upon freezing.

By using the FAD cofactor in its neutral radical form as a natural spin-probe, the binding of DNA photolyases to the target CPD lesions has been studied using EPR and electron-nuclear double resonance (ENDOR) measurements.[97,98]

Evidence of the radical intermediates involved in this reaction was first provided by time-resolved EPR.[89] ENDOR spectra were used to characterise the hyperfine couplings of the FAD protons in *E. coli* DNA photolyase.[98] Moreover, this technique, in accordance with previous calculations,[99] confirmed a large distance between the flavin and the CPD,[97,100] which refuted a more recently proposed model.[101]

EPR studies have not yet been carried out on the very recently discovered FAP enzyme.[95,96] However, the fact that it contains an FAD cofactor like DNA photolyases could make FAP suitable for magnetic studies.

The work of this thesis focuses on the use of EPR to study the only other known light-driven enzyme, protochlorophyllide oxidoreductase.

1.6 Protochlorophyllide oxidoreductase

1.6.1 The biological role of protochlorophyllide oxidoreductase (POR)

Chlorophyll (Chl) is a green pigment responsible for capturing light energy and acts as the cofactor for the photosynthetic proteins that are responsible for transforming sunlight into chemical energy in the photosystems of phototropic organisms.[86] It is the most abundant natural pigment on Earth and it is present in photosynthetic bacteria, green algae and plants. In plant biosynthesis, the final reaction leading to the conjugated π-system in Chl involves the reduction of a double bond in protochlorophyllide (Pchlide), which gives rise to chlorophyllide (Chlide).[102,103] This reaction is crucial for the assembly of the photosynthetic apparatus as the product undergoes a further reaction to produce Chl.[103,104] The reduction from Pchlide to Chlide can be catalysed by two different types of POR: light-dependent POR (POR) and dark-operative POR (DPOR), as represented in Figure 1.19. Both of them can be found in cyanobacteria, algae, bryophytes, pteridophytes and gymnosperms, whereas angiosperms (or higher plants)

rely entirely on light-dependent POR and anoxygenic photosynthetic bacteria only use DPOR.[105,106]

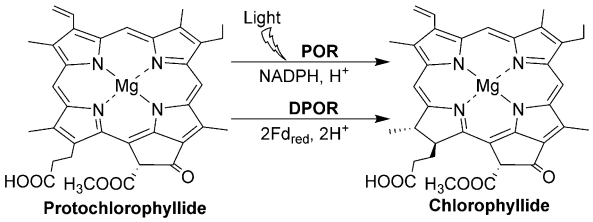

Figure 1.19. Schematic representation of the reduction of protochlorophyllide.

These two forms of POR are structurally distinct and catalyse the reduction of Pchlide by using a different mechanism. POR has not been successfully crystallised yet, as opposed to DPOR.[107,108] The light-driven reaction is responsible for major changes in plant morphology.[71,109] POR is the main component of etioplast membranes, where it forms organised networks.[104] The POR-pigment complexes disintegrate upon illumination, leading to the production of Chl, the reorganisation of plastid membranes and the development of chloroplasts.[71,104] The work in this thesis focuses on the light-dependent POR enzyme, which unlike most enzymatic systems, can be studied at ultrafast timescales and cryogenic temperatures, making it a unique study model.[109]

1.6.2 Reaction mechanism of POR

In the reaction catalysed by POR, a *trans* hydrogenation takes place across the C17-C18 double bond of Pchlide, generating Chlide as a product.[71,104,110] The protein requires NADPH as a cofactor and, in the dark, the ternary complex consisting of POR, Pchlide and NADPH can be found.[111] The formation of this ternary complex has been found to be the overall rate-limiting step of the enzymatic catalytic cycle and it involves various steps dominated by conformational changes in POR.[71,112] The substrate initially absorbs light and the reaction involves Pchlide excited states, which undergo hydride and proton additions.

Since the POR-catalysed photoreduction of Pchlide can be triggered precisely at low temperatures and on fast timescales, and its substrate is rich in optical signals that can be followed by a range of spectroscopic techniques, POR is a good model for studying enzyme catalysis and associated protein dynamics in conditions that are often not

accessible for other enzymes.[71,109] POR is also a good model to study how light energy can be transformed into chemical energy. Hence, there have been numerous spectroscopic and kinetic studies to elucidate the catalytic mechanism of POR.[21,105,110,113–115] As observed in low temperature absorption and emission visible spectroscopy studies, the reduction of Pchlide involves a light-dependent step[113] followed by a series of slower, light-independent reactions.[116,117] The overall reaction of POR can be represented as: Pchlide-POR-NADPH + H^+ → POR + $NADP^+$ + Chlide. The catalytic cycle of POR is represented in Figure 1.20.

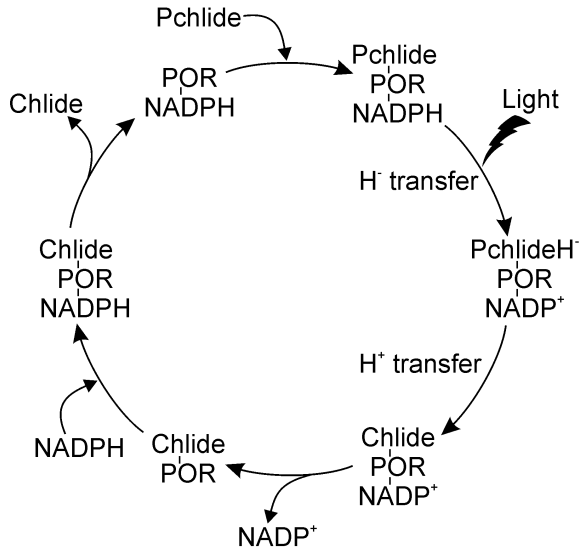

Figure 1.20. Scheme of the catalytic cycle of POR representing the overall reaction and various intermediates.[118]

First, a light-driven hydride transfer occurs from the pro-*S* face of NADPH to the C17 position of Pchlide, forming a negatively charged intermediate.[71,119,120] This in turn facilitates the following light-independent proton transfer from a proposed Tyr residue to the C18 position.[71,121] These two sequential H-transfer reactions have been shown to occur on the microsecond timescale by means of quantum tunneling.[122] It is important to note that in a POR variant (C226S), hydrogen and proton transfers were shown to occur in a one-step mechanism, where Pchlide took the hydride from NADPH and the proton from Tyr 193 simultaneously.[67] Alternative hydrogenation mechanisms have been proposed for POR based on experimental observations on similar systems.[123] It was recently discovered that the initial hydride transfer step itself can proceed in a stepwise manner with an initial electron transfer from NADPH followed by a subsequent proton-coupled electron transfer.[110] This study provided the first experimental evidence that stepwise mechanisms for hydride transfer may exist in a

biological system.[110] The subsequent light-independent steps involve a series of product release and cofactor binding steps necessary to regenerate the initial ternary complex.[116,117,124]

After hydrogenation, POR remains as a ternary complex with the oxidised coenzyme $NADP^+$ and Chlide, the product. Firstly, $NADP^+$ is released from the ternary complex, followed by binding of reduced coenzyme, NADPH. After that, Chlide is released from the complex and a new molecule of substrate is bound to regenerate the starting ternary complex. In order for the regeneration of the complex to take place, the protein needs to undergo conformational changes to aid the release and binding events.[71,117,124]

As discussed in the previous section, a full understanding of a light-activation process involves knowing the molecular changes that take place from the initial absorption until the formation of products.[6] Although the chemical steps in the POR reaction cycle have been well established and shown to occur on the microsecond timescale the reaction chemistry is completely dependent on excited-state processes in the Pchlide molecule, which occur on a picosecond timescale. Although the exact photochemical mechanisms in POR have not been fully elucidated yet there have been several transient spectroscopy studies on the standalone substrate and analogue compounds, protein variants and combinations thereof, which have provided more details of the excited-state processes that are necessary for catalysis.[20,22,23,123,125–134]

1.6.3 Excited state studies of Pchlide alone

There have been several photochemical studies of Pchlide in isolation, including both time-resolved UV-Vis and IR spectroscopy as well as fluorescence lifetime measurements.[22,129–132] The isolated Pchlide pigment shows complex excited-state dynamics involving a series of species and multi-exponential dynamics. Both a branched and a sequential model have been proposed to describe the relaxation pathways from the excited state(s) of Pchlide (see Figure 1.21).[22,129–133]

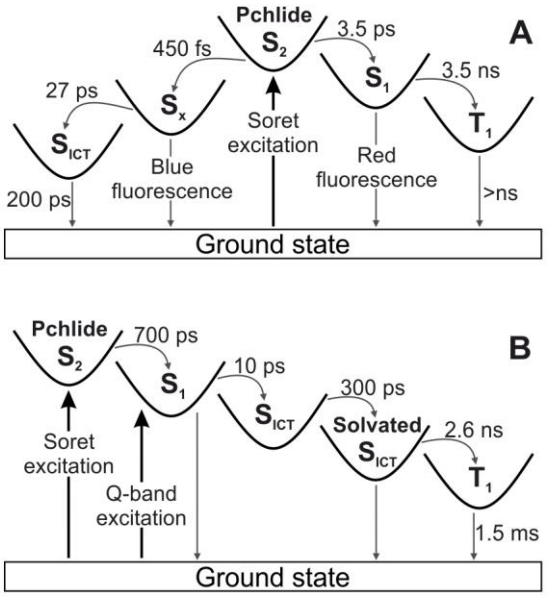

Figure 1.21. Diagram displaying the (A) branched[22,130,131,133] and (B) sequential[132] models proposed to describe the relaxation pathways of photoexcited Pchlide.[71]

In the branched model (Figure 1.21A), the highest singlet-state is suggested to decay *via* two pathways, a reactive and a non-reactive one. In the non-reactive pathway, the thermally equilibrated S_1 state is reached after the initial high-energy singlet undergoes VR and vibrational energy redistribution with a lifetime of a few picoseconds.[130,132] This S_1 state then decays *via* ISC, forming the lowest-lying triplet state T_1 within a few nanoseconds.[133] This triplet-state is relatively long-lived and displays absorption bands at 530 and 890 nm.[22] The longer wavelength feature has been assigned to a $^3(\pi\text{-}\pi^*)$ absorption.[22,135] In the reactive decay pathway of the branched model, the initial singlet-state is suggested to decay first into an intermediate Sx state, which then decays into an intramolecular charge transfer (ICT) with a lifetime of around thirty picoseconds. Formation of this excited-state was originally only observed in polar solvents.[130,131,134] The S_{ICT} state decays into the singlet ground state with a lifetime of a few hundred picoseconds.

Subsequent time-resolved studies revealed the formation of the S_{ICT} state was independent of solvent polarity. It was suggested that the S_{ICT} state was an intrinsic step of the decay pathway of Pchlide.[132] This gave some more weight to the proposed sequential decay model (Figure 1.21B), in which the initial excited-state upon blue light absorption would correspond to the S_2 state. The S_2 state displayed a displacement of the spectrum to shorter wavelengths, referred to as blue-shift, in fluorescence and

decayed over several hundred femtoseconds into the S_1 state, which very rapidly formed the S_{ICT}.[131] The ICT state was shown to form a less energetic, solvent-stabilised $S_{ICT\text{-}solv}$ over a few hundred picoseconds. Lastly, the solvated ICT state undergoes ISC with a lifetime of a few nanoseconds to give rise to the long-lived T_1 triplet.[132]

The photophysical steps of the sequential model are represented in Figure 1.22.

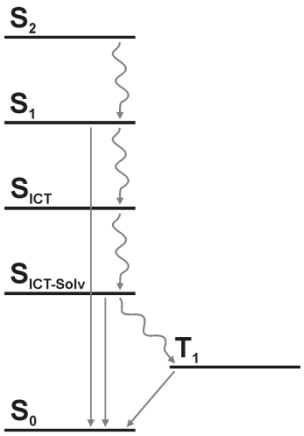

Figure 1.22. Jablonski diagram representing the sequential model of Pchlide excited-state dynamics.[132]

The interactions of Pchlide and the excited ICT state with solvent (a methanol solution) have also been studied by time-dependent density functional theory.[136] Theoretical calculations indicated the presence of intermolecular site-specific coordination and hydrogen-bonding interactions, involving Pchlide and the methanol molecules. Calculations also revealed that such interactions could be strengthened in the Pchlide S_1 excited states. These interactions were found to be strong enough to have an effect on the absorbance properties of Pchlide from steady-state and time-resolved absorption spectroscopy measurements. Moreover, the S_1 state was found to exhibit ICT characteristics for both isolated Pchlide and the methanol hydrogen-bound complex.[136]

Time-resolved infrared measurements have also been used to study the vibrational frequencies related to these excited state processes. The vibrational frequencies of the C=O keto group on ring E (see Figure 1.23) of Pchlide displayed significant shifts that suggest the involvement of a dynamic hydrogen-bond of this group in the ICT state. The charge transfer characteristics could arise from the tendency of this ring to withdraw electron density. Other delocalised C=C and C=N bonds within Pchlide are also likely

to present structural deviations.[129,132] In another study, it was shown that, in fact, the aforementioned keto group is essential for POR activity.[137]

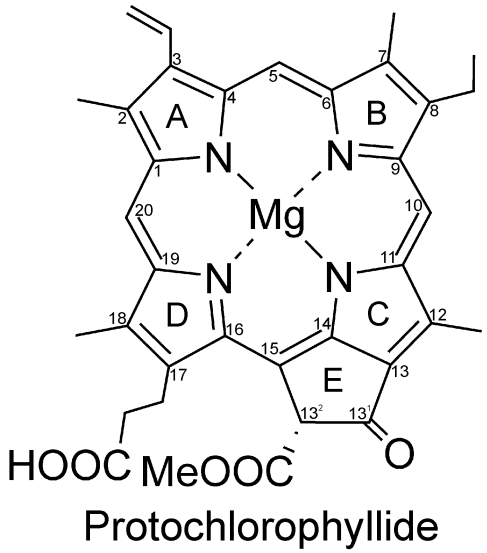

Figure 1.23. Schematic representation of the protochlorophyllide pigment displaying the main ring and Carbon atom labels.[137]

Using an analogue compound where this group had been removed resulted in a considerable loss of enzymatic activity and rendered Pchlide unable to form states with strong hydrogen bonds.[137] It was suggested that this C=O group could undergo protonation in the reduction mechanism to favour the reduction of the C17-C18 double bond.[125,129,132] All of this is in agreement with an initial nucleophilic attack from NADPH, as this step would benefit from a lower electron density at the double bond, either because of the effect of protonating the keto group in C13 or from the excited-state charge delocalisation in Pchlide.[71,126] Studies carried out to date have focussed on the subnanosecond excited state dynamics of Pchlide and, currently, it is completely unknown what role, if any, the excited state triplet of Pchlide plays in the photochemical mechanism.[22,129–133]

1.6.4 Excited state studies of protein-bound Pchlide

Multiple photochemical studies have also been carried out on POR-bound Pchlide.[20,21,23,110,113–117,123,127] Time-resolved spectroscopy measurements have been carried out on a range of active and inactive protein complexes. The inactive, pseudo-ternary complex consisting of POR, Pchlide and the oxidised cofactor $NADP^+$ was

measured by time-resolved fluorescence and pump-probe spectroscopy in order to study the effects the protein has on the excited-state dynamics of bound Pchlide. These measurements confirmed that formation of the singlet ICT state still ocurred when the Pchlide was bound to the enzyme upon excitation.[20] A significant blue shift in the absorption spectra indicated that the enzyme's active site stabilised this species. Moreover, POR-bound Pchlide displayed longer S_1 lifetimes and a reduced probablity of ISC into the triplet state, which has been suggested to be related to a photoprotective role of POR as a lower amount of generated triplets would minimise potentially harmful photosensitation reactions.[20]

The more recent finding that the rate of quenching of the triplet by O_2 is five times less for protein-bound than unbound Pchlide suggests another mechanism for the photoprotective role of the enzyme.[110] It is likely that the enzyme prevents the dangerous build-up of reactive oxygen species as O_2 is occluded from the active site and is unable to react with the Pchlide triplet state. However, further studies are necessary to confirm this, which will require direct detection of the triplet state in time-resolved studies.

Ultrafast pump-probe spectroscopy studies on the active ternary POR complex have revealed intermediate species with characteristic differences in their associated spectra.[23,110,115,125,127,128] An increase in the hydrogen-bonding interactions between POR and the substrate was observed in the active complex, which also displayed a change in energy of the ICT singlet state of Pchlide, presumably due to stabilisation.[127] Moreover, the formation of a hydride transfer reaction intermediate has also been identified.[113,114,122,127]

IR spectroscopy studies display more spectral differences between unbound Pchlide and the active POR ternary complex in comparison to UV-Vis and it was through IR studies that an additional reactive pathway leading to the hydride transfer intermediate was revealed.[127] The excited state dynamics were found to branch from the ICT state of Pchlide, leading to a reactive pathway (40% quantum yield) and a non-reactive one. Along the reactive pathway, spectral features revealed a loss of double bond character of the C17-C18 bond, which becomes more susceptible to a nucleophilic attack due to polarisation.[127,138]

Several POR variants with modifications in active site residues have been studied. This strategy provides information about which residues are important in terms of substrate binding affinity, stabilisation of excited states and catalytic efficiency which, due to the unavailability of a protein crystal structure, would otherwise be difficult to infer.[110,128] By means of both static and time-resolved spectroscopy measurements, it was possible to identify a series of residues important for photochemistry. The photochemistry is impaired in POR upon removal of the Tyr residue, where studies revealed the absence of the hydride transfer intermediate.[127]

A study on the C226S POR variant revealed an alternative reaction mechanism where the initial hydride was transferred to the C18 position instead of C17. In this POR variant, which furnishes the same Chlide steroisomer, the substrate appeared to bind in the active site with a 180º rotation in comparison to wild type POR.[110,123] Changes to active site residues can have a big impact on interactions between the active site, NADPH and Pchlide, as well as on the electron withdrawing properties of other residues, the acidity of their protons, the conformational stability of the active site, the affinity for substrate and coenzyme binding and, ultimately, photochemistry.[67,127,128]

1.7 Project objectives

1.7.1 Probing excited-state triplet species

The formation of a long-lived triplet state during the excited-state relaxation of Pchlide has been previously implied from time-resolved absorption spectroscopy studies. However, there has been no direct evidence of such excited-state species.[22,132] This project aims to provide such evidence and to characterise the triplet-state by combining EPR spectroscopy and time-resolved absorption spectroscopy measurements, as well as probing the effect of temperature, oxygen concentration and solvent changes on the various excited-state species' lifetimes.

1.7.2 Effect of POR binding on excited state dynamics and electron delocalisation

Although the discrete reaction steps involved in the photoreduction of Pchlide have been described,[110,113,114,116,117,121] there are no studies on the electron delocalisation of photoexcited Pchlide. By cooling down active and inactive POR complexes at cryogenic temperatures and measuring them using both EPR and absorption spectroscopy techniques, this project aims to reveal some of the effects the enzyme has on the photoexcited substrate such as electronic coupling to different atoms and protein-induced spectral differences of the long-lived excited state. This should provide a better understanding of the electronic environment and the potential involvement of this long-lived excited state in POR catalysis.

1.7.3 Effect of structural changes on triplet-state lifetime and electron delocalisation

Previous infrared (IR) and visible absorption spectroscopy studies on Pchlide structural analogues have revealed the importance of certain groups in the substrate when it comes to facilitating light harvesting and reactivity.[137] In this work, we aim to expand on the current knowledge by carrying out CASSCF calculations to predict differences in molecular orbital occupation (electron delocalisation) within different analogues. Structure-induced differences in triplet-state lifetimes will also be evaluated.

2 Direct evidence of an excited-state triplet species upon photoactivation of the chlorophyll precursor protochlorophyllide

J. Phys. Chem. Lett., 2017, 8, 1219.

Published in: The Journal of Physical Chemistry Letters

First published: 28th February 2017

Authors: Guillem Brandariz-de-Pedro, Derren J. Heyes, Samantha J. O. Hardman, Muralidharan Shanmugam, Alex R. Jones, Stefan Weber, Daniel Nohr, Nigel S. Scrutton, Alistair J. Fielding

DOI: 10.1021/acs.jpclett.7b00200

Contributions: Chapter 2 is a published letter written by GBP with guidance from DJH, SJOH and AJF. Sample preparation was carried out by GBP. Ultrafast time-resolved measurements were conducted by SJOH with help from GBP. Laser flash-photolysis measurements were conducted by GBP with help from DJH. EPR measurements except the trEPR laser flash wavelength comparison were carried out by GBP with help from AJF and MS. The trEPR laser flash wavelength comparison measurements were carried out by DN with help from GBP. DFT calculations were carried out by GBP. All time-resolved spectroscopy data was analysed by GBP with guidance from DJH and SJOH. All EPR data was analysed by GBP with guidance from AJF.

Direct evidence of an excited-state triplet species upon photoactivation of the chlorophyll precursor protochlorophyllide

Guillem Brandariz-de-Pedro,[†,‡] *Derren J. Heyes,**[,‡] *Samantha J. O. Hardman,*[‡] *Muralidharan Shanmugam,*[‡] *Alex R. Jones,*[†,‡] *Stefan Weber,*[§] *Daniel Nohr,*[§] *Nigel S. Scrutton,*[‡] *Alistair J. Fielding**[,†]

[†]School of Chemistry and the Photon Science Institute, University of Manchester, Oxford Road, Manchester M13 9PL, U.K.

[‡]Manchester Institute of Biotechnology, University of Manchester, 131 Princess Street, Manchester M1 7DN, U.K.

[§]Institute of Physical Chemistry, Albert-Ludwigs-Universität Freiburg, 79104 Freiburg, Germany

Corresponding Author

*E-mail: Alistair.Fielding@manchester.ac.uk

*E-mail: Derren.Heyes@manchester.ac.uk

2.1 ABSTRACT:

The chlorophyll precursor protochlorophyllide (Pchlide), which is the substrate for the light-driven enzyme protochlorophyllide oxidoreductase, has unique excited-state properties that facilitate photocatalysis. Previous time-resolved spectroscopy measurements have implied that a long-lived triplet state is formed during the excited-state relaxation of Pchlide, although direct evidence for its existence is still lacking. Here, we use time-resolved electron paramagnetic resonance (EPR) in combination with time-resolved absorption measurements at a range of temperatures (10-290 K), solvents, and oxygen concentrations to provide a detailed characterisation of the triplet state of Pchlide. The triplet decays in a biphasic, oxygen-dependent manner, whilst the first reported EPR signature of a Pchlide triplet displays both emissive and absorptive features and an antisymmetric spectrum similar to other porphyrin triplet states. This work demonstrates that the Pchlide triplet is accessible to various cryogenic spectroscopic probes over a range of timescales and paves the way for understanding its potential role in catalysis.

KEYWORDS electron paramagnetic resonance, protochlorophyllide, triplet state, photochemistry, time-resolved spectroscopy, excited state

2.2 INTRODUCTION:

Protochlorophyllide (Pchlide) (Figure 2.1), a crucial intermediate in the biosynthesis of chlorophyll, is the predominant pigment found in seedlings and dark-grown plants.[71,108,109] As the substrate for the light-driven enzyme protochlorophyllide oxidoreductase (POR) Pchlide has unique excited state properties that allow it to capture sunlight and trigger the subsequent formation of chlorophyll and development of the plant.[71] The reaction catalyzed by POR involves a light-driven hydride transfer from NADPH to the C17 position of Pchlide,[114,122] followed by a thermally-activated proton transfer from a conserved Tyr residue to the C18 position.[67] Catalysis is dependent on excited-state processes in the Pchlide molecule, which occur on an ultrafast, picosecond, timescale. Previous time-resolved absorption and fluorescence spectroscopy measurements on the isolated Pchlide substrate have shown that it is an intrinsically reactive molecule with multi-phasic excited-state dynamics.[20,22,71,126,129–134]

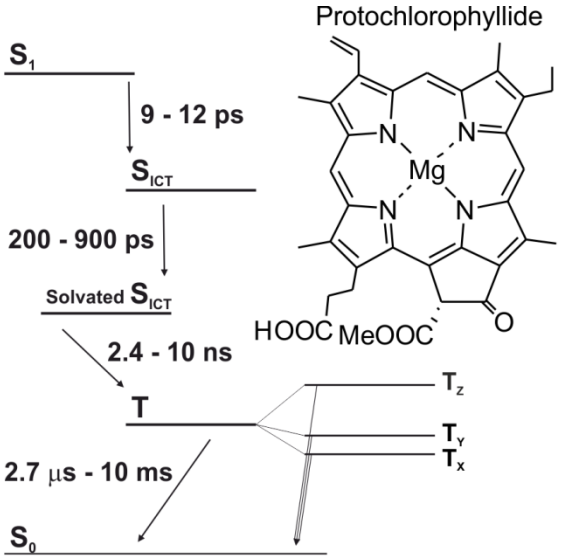

Figure 2.1. Decay lifetimes of protochlorophyllide's excited states.

The excited-state dynamics depend strongly on solvent polarity[130,132,134] and have been interpreted by using both a branched model[22,126,130,131,133,134] and a sequential model[132] (Figure 2.1). However, both models involve the formation of an excited-state intramolecular charge transfer (ICT) state[20,22,126,129–134] and formation of a putative long-lived triplet state by intersystem crossing on a nanosecond timescale.[22,132] The triplet state has absorption bands at approximately 530 and 890 nm and is formed with a significant quantum yield (0.23-0.34).[22,132] However, the existence of this triplet

species has only been based on circumstantial evidence, such as the long lifetime and absorption features in the near infra-red region.[22] Moreover, it is unclear whether the triplet state is directly involved in the reaction mechanism of POR[67,71,127] or if the enzyme has a photoprotective role in preventing non-productive side reactions of the highly reactive triplet intermediate.[22] As triplet states are paramagnetic we have used time-resolved electron paramagnetic resonance (EPR) spectroscopy to provide the first reported direct characterisation of the excited-state Pchlide triplet species. These measurements have been combined with cryogenic time-resolved absorption measurements to investigate the thermodynamic properties and oxygen-dependence of triplet formation and decay.

2.3 RESULTS AND DISCUSSION:

Using EPR spectroscopy it is only possible to observe the triplet state at cryogenic temperatures. Hence, initially it was important to provide a direct comparison of the excited-state dynamics of Pchlide at both cryogenic and room temperatures by using time-resolved absorption measurements after laser excitation at 450 nm (ps to µs timescale) as described in the Supporting Information. The time-resolved difference spectra from these measurements (Figures S2.1-S2.8) were fitted to a sequential kinetic model by global analysis to yield evolution associated difference spectra (EADS) (Figure 2.2).[127] The time-resolved spectral changes at a range of temperatures between 10 K (Figure 2.2) and room temperature (Figure 2.2), and in the presence and absence of oxygen could all be fitted to four components with only minor differences in the lifetimes of the various excited state species (Table 2.1). The first three excited-state components have been described previously and correspond to the formation of an ICT state from the S_1 excited state (~5 ps), solvation of the ICT state (~200 ps) and decay of the S_1/S_{ICT} excited state into the long-lived triplet state on the nanosecond timescale (~4 ns).[22,126,130–134] Hence, it appears that temperature and presence of oxygen only have a minimal effect on these three excited-state processes, which are directly related to the formation of the triplet state. Although there are only minor differences in the electronic spectra of the different Pchlide excited singlet states, these species have previously been confirmed by corresponding time-resolved fluorescence and infra-red measurements. In contrast, the triplet state has a distinctly blue-shifted bleach at ~629 nm and less intense excited state absorption features.[127,137]

The remaining long-lived component (τ_4), which relates to the decay of the triplet state, occurs on longer timescales than the 80 µs time window of the pump-probe measurements.

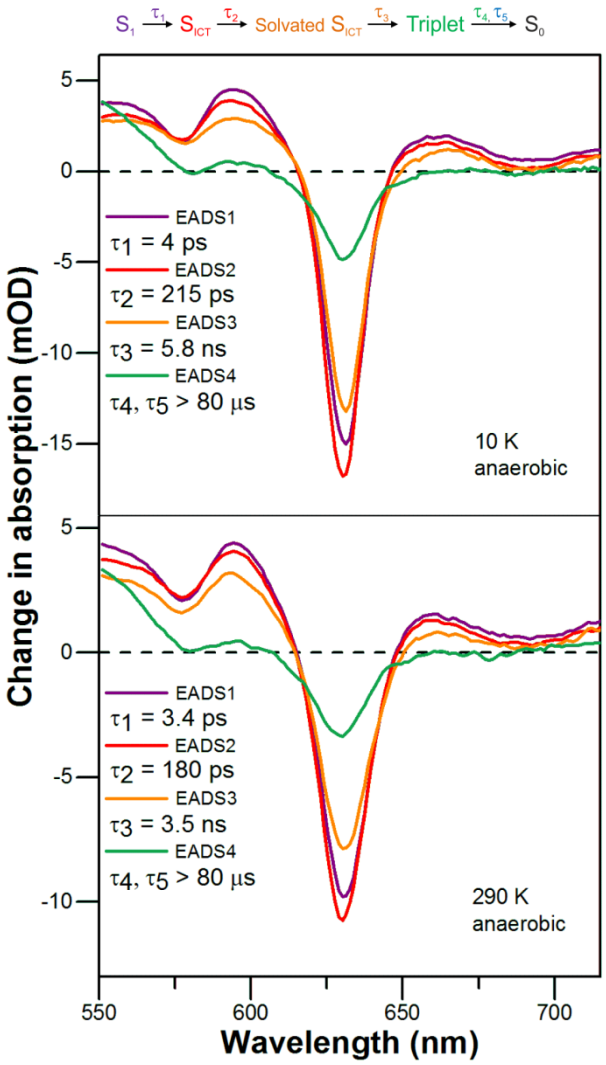

Figure 2.2. Evolution associated difference spectra (EADS) resulting from a global analysis of the time-resolved absorption data for an aqueous, anaerobic Pchlide sample after excitation at 450 nm at 10 K and 290 K. The EADS were obtained from fitting the time-resolved absorption data to a sequential exponential model as described in the supplementary information. The triplet decay lifetime was set to infinity on the 80 µs timeframe of the measurement.

Table 2.1. Lifetimes of the S_1 (τ_1), S_{ICT} (τ_2), solvated S_{ICT} (τ_3) and triplet excited states of Pchlide (τ_4 and τ_5) measured in both aerobic and anaerobic aqueous buffer solutions at 10, 80, 150 and 290 K. For experimental conditions see Supporting Information.

	T (K)	τ_1 (ps)	τ_2 (ps)	τ_3 (ns)	τ_4 (ms)	τ_5 (ms)
anaerobic	**10**	4.0 ± 0.2	215 ± 5	5.8 ± 0.1	6.9 ± 0.1	24.9 ± 0.2
	80	6.3 ± 0.3	276 ± 5	4.9 ± 0.1	7.5 ±0.1	22.3 ± 0.2
	150	5.0 ± 0.2	170 ± 3	4.1 ± 0.1	6.4 ± 0.1	19.4 ± 0.1
	290	3.4 ± 0.4	180 ± 6	3.5 ± 0.1	0.35 ± 0.01	1.82 ± 0.01
aerobic	**10**	4.6 ± 0.2	205 ± 8	5.9 ± 0.1	3.1 ± 0.2	-
	80	4.7 ± 0.2	597 ± 20	6.0 ± 0.1	3.6 ± 0.1	-
	150	5.6 ± 0.2	278 ± 9	5.5 ± 0.1	3.7 ± 0.2	-
	290	3.8 ± 0.2	364 ± 26	4.9 ± 0.2	0.11 ± 0.01	-

In order to investigate the kinetics of triplet decay in more detail the time-resolved absorption measurements were extended to the ms timescale by using laser flash photolysis experiments (Figures 2.3 and S2.9-S2.16). Consequently, the triplet state of Pchlide was found to decay in a biphasic process under anaerobic conditions with τ_4 values of approximately 7 ms and τ_5 values of approximately 22 ms at cryogenic temperatures, with τ_4 and τ_5 values of approximately 350 µs and 1.8 ms at room temperature (Figure 2.3A, Table 2.1). However, in the presence of oxygen the triplet decay kinetics become faster and more monoexponential in nature, displaying τ_4 values of ~3.5 ms at cryogenic temperatures. The oxygen dependence was investigated further by following the recovery of the Pchlide ground state (absorbance at 630 nm) over a range of oxygen concentrations at room temperature (Figure 2.3B). The triplet decay kinetics show a strong dependence on oxygen concentration, confirming that the triplet excited-state of Pchlide can interact with molecular oxygen, presumably to yield singlet oxygen or other reactive oxygen species *via* triplet-triplet energy transfer.[139,140] In addition, the observed lifetimes show no dependence on temperature at cryogenic temperatures (Figure S2.33) suggesting that the decay of the triplet state is an adiabatic process in frozen samples.

As previous studies have shown that the excited-state dynamics of Pchlide depend strongly on solvent polarity[130,132,134] the transient absorption measurements were repeated in alcohol solutions. The ultrafast steps leading to the formation of the triplet state are very similar to those in water and show no noticeable dependence on oxygen or temperature (Figures S2.17-S2.24, Table S2.1). However, the decay

of the Pchlide triplet state now appears to follow single, monoexponential kinetics under both aerobic and anaerobic conditions with a lifetime of ~3 ms at cryogenic temperatures. Moreover, at higher temperatures the triplet excited state decays much more rapidly in polar solvent (lifetime of ~2μs) than in water (lifetime of ~0.1 ms). It has previously been shown that dimers/aggregates of Pchlide, formed in water-based buffers, display different excited state dynamics to monosolvated Pchlide found in polar solvents.[21,141] Hence, it is possible that the differences in aggregation state of Pchlide may also explain the changes in triplet decay kinetics observed in the present work.

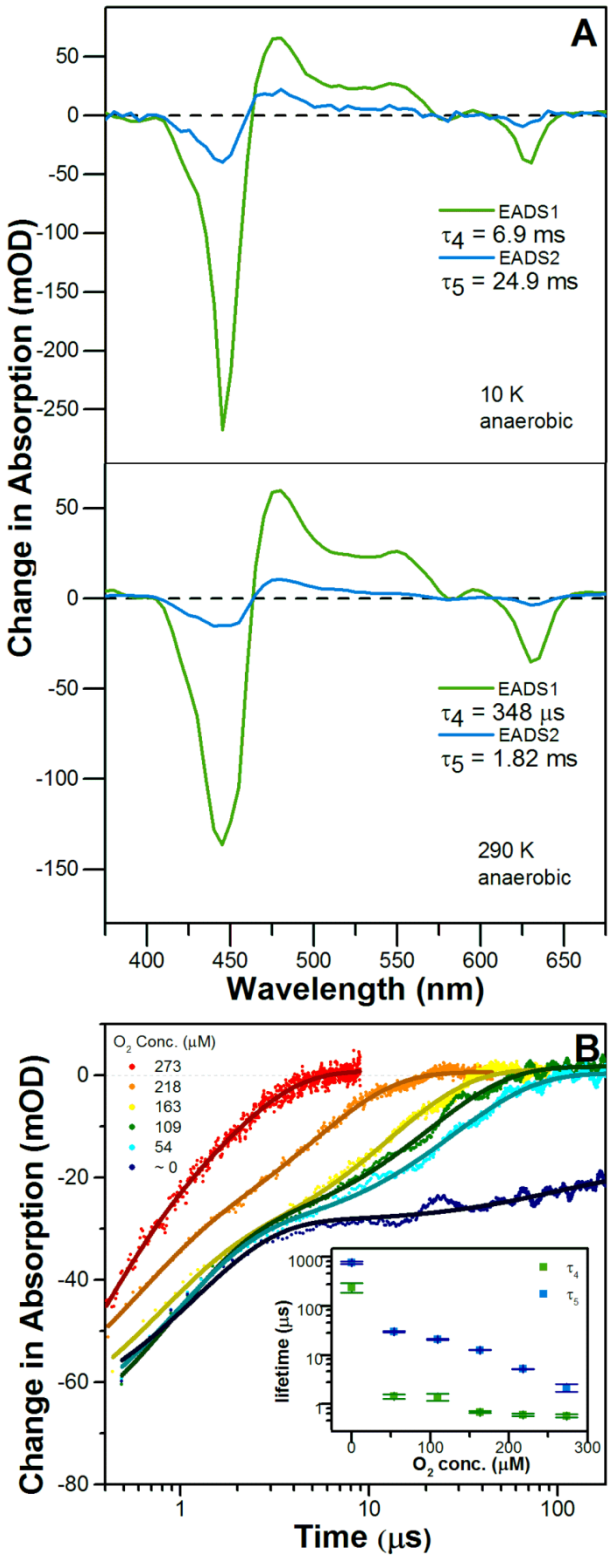

Figure 2.3. (A) EADS resulting from a global analysis of the laser flash photolysis data for an aqueous, anaerobic Pchlide sample after excitation at 450 nm at 10 K and 290 K. The EADS were obtained from fitting the data to a sequential exponential model as described in the supplementary information. (B) Lifetime values (τ_4 and τ_5) obtained from fitting a double exponential decay to ground state recovery (630 nm) flash photolysis time traces. Samples consisted of Pchlide dissolved in mixtures of anaerobic and aerobic aqueous buffer at room temperature.

In order to provide direct experimental evidence of the existence of an excited-state triplet of Pchlide time-resolved continuous wave EPR (trEPR) has been used after photoexcitation with laser pulses at 532 nm and 460 nm (Figures S2.35 and S2.36). The EPR signature of the photoexcited triplet state Pchlide was obtained from integrating trEPR time traces over a range of magnetic field positions. The EPR spectrum displays both emissive and absorptive features and an antisymmetric lineshape (Figure 2.4A), which are all features that are characteristic of a triplet state.[41,142,143] The lifting of the degeneracy of spin states in the absence of an applied magnetic field is referred to as zero-field splitting (ZFS). The value of the ZFS parameter is usually defined *via D* and *E* parameters. *D* describes the axial component of the magnetic dipole-dipole interaction, and E the transversal component. The values of the ZFS splitting parameters obtained from a simulation of the spectrum (Figure S2.36) are of a rhombic symmetry and were found to be $|D| = 860 \pm 8$ and $|E| = 182 \pm 5$ MHz. These values are comparable to those of chlorophyll *a* ($|D| = 818 \pm 24$ and $|E| = 120 \pm 6$ MHz) and chlorophyll *b* ($|D| = 878 \pm 27$ and $|E| = 156 \pm 3$ MHz)[144], suggesting that the energy states of the triplet state of Pchlide are similar to those found in the chlorophylls. Changes in the *E* value reflect some differences in asymmetry. Density functional theory calculations incorrectly predicted ZFS parameters as $|D| = 648$ and $|E| = 166$ MHz, although this error might be due to the inability of the method to accurately take into account various molecular orbitals in highly delocalized systems, such as photoexcited Pchlide.[145]

Electron spin echo (ESE) field-swept spectra (Figure 2.4A) measured at different delay-after-flash (DAF) values reflect the anisotropic decay of the triplet sub-levels of the Pchlide triplet state, as previously observed in other organic triplets.[51,146,147] Triplet sub-level decay rates were calculated from measuring the intensity of the two-pulse spin echo EPR signal at increasing DAF values. A representation of the ESE intensity vs the DAF is shown in Figure 2.4B. A double exponential decay with a positive and a negative component was fit to the time evolution traces. These were measured at the high-field Z^+ orientation of the triplet state EPR spectrum for Pchlide samples in aerobic and anaerobic aqueous and alcohol solutions, providing the decay constants from T_0 for that orientation as per the following formula:

Equation 16

$$I = A_1 e^{(-t/\tau_1)} + A_0 e^{(-t/\tau_0)}$$

with *I* being the ESE intensity, *t* the DAF, $|A_1|$ and $|A_0|$ being the initial relative populations of T_{+1}/T_{-1} and T_0, with τ_1 and τ_0 as their respective decay lifetimes. A_0 is positive for the "+" canonical orientations and negative for the "-" orientations, representing absorption and emission from T_0 respectively. The opposite is true for A_1 and T_{+1}/T_{-1}. The triplet EPR decay lifetimes in different solvents show the same trends as the optical experiments, with faster decays in the alcohol solutions and in the presence of oxygen. However, it should be noted that the EPR signal intensity for the aerobic aqueous sample was too weak to measure accurately.

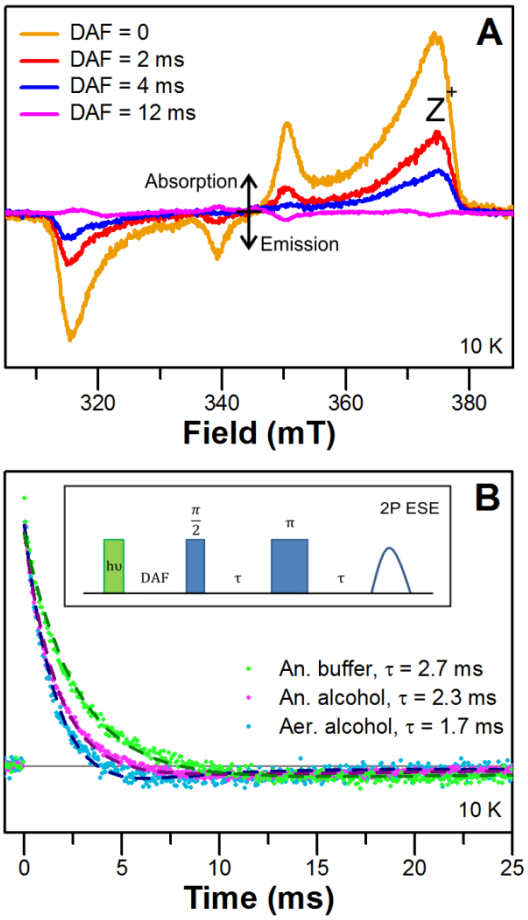

Figure 2.4. (A) ESE field-swept spectra of Pchlide recorded at 10 K in anaerobic aqueous buffer at different DAF values displaying an anisotropic decay of the triplet state spectrum features. (B) ESE-detected kinetics of the Pchlide triplet in anaerobic aqueous buffer and both anaerobic and aerobic alcohol solutions at 10 K at the high-field Z^+ canonical orientation. Lifetimes correspond to the decay from T_0. Inset: Pulse sequence for the EPR two-pulse electron spin echo (ESE) experiment consisting of a laser pulse (in green), microwave pulses (in blue at a delay after flash DAF and separated by a delay τ) and the generated spin echo signal.

This work provides the first direct evidence that a long-lived triplet state is formed during the excited-state relaxation of Pchlide. trEPR measurements confirm that the Pchlide triplet, which forms on the nanosecond timescale and decays on the millisecond timescale, is similar to other porphyrin triplet states. The Pchlide excited-state triplet species has been shown to react with oxygen, suggesting that highly reactive oxygen species could be formed, which may lead to photo-damage in the cell. Hence, it is likely that specific chromophore-protein interactions occur when Pchlide is bound to the enzyme, which would help to minimize any undesirable effects of Pchlide triplet formation. These findings open up an exciting new range of pulsed EPR spectroscopy studies such as ESE envelope modulation (ESEEM), hyperfine sublevel correlation (HYSCORE) or electron nuclear double resonance (ENDOR), which will be essential to gain further information on the electronic couplings of Pchlide in the excited triplet state. In addition, measurements on POR-bound Pchlide will provide important insights into how the enzyme active site affects such electronic properties and the potential role of the triplet state in POR catalysis.

ASSOCIATED CONTENT

Supporting Information. The following files are available free of charge. Detailed experimental methods, raw transient absorption data, thermodynamic data, EPR data (PDF).

AUTHOR INFORMATION

Notes

The authors declare no competing financial interests.

ACKNOWLEDGMENTS

G.B.-P. acknowledges Early Stage Researcher funding from the European Union's Seventh Framework Programme FP7-PEOPLE-2013-ITN through the 'MAGnetic Innovation in Catalysis' (MAGIC) Initial Training Network (Grant agreement no. 606831). We would like to acknowledge the use of the EPSRC EPR National Service in carrying out this work. NSS is an Engineering and Physical Sciences Research Council (EPSRC) Established Career Fellow (EP/J020192/1). Ultrafast spectroscopy was performed at the Ultrafast Biophysics Facility, Manchester Institute of Biotechnology, as funded by BBSRC Alert14 Award BB/M011658/1.

2.4 Supporting Information:

Direct evidence of an excited-state triplet species upon photoactivation of the chlorophyll precursor protochlorophyllide

Guillem Brandariz-de-Pedro,[†,‡] Derren J. Heyes,*[,‡] Samantha J. O. Hardman,[‡] Muralidharan Shanmugam,[‡] Alex R. Jones,[†,‡] Stefan Weber,[§] Daniel Nohr,[§] Nigel S. Scrutton,[‡] Alistair J. Fielding,*[,†]

[†]*School of Chemistry and the Photon Science Institute, University of Manchester, Oxford Road, Manchester M13 9PL, U.K.*

[‡]*Manchester Institute of Biotechnology, University of Manchester, 131 Princess Street, Manchester M1 7DN, U.K.*

[§]*Institute of Physical Chemistry, Albert-Ludwigs-Universität Freiburg, 79104 Freiburg, Germany*

Corresponding Authors

*E-mail: Alistair.Fielding@manchester.ac.uk

*E-mail: Derren.Heyes@manchester.ac.uk

Contents

2.4.1 Ultrafast Pump-Probe Spectroscopy

Pchlide samples were contained in a 2 mm path length sample holder in an Optistat cryogen-free cryostat (Oxford Instruments). A Ti-sapphire amplifier system (Spectra Physics Solstice Ace) was used to generate 800 nm pulses at 1 kHz, which were used to pump an OPA (Topas Prime) with an associated Nir UVis unit to achieve the pump pulses centered at 450 nm (~10 nm full width at half-maximum, 100 fs, 250 nJ). A sapphire crystal-generated white light continuum was used as a probe and changes in absorption were measured between 500 and 750 nm. Ultrafast broadband transient absorption measurements were carried out (at randomly ordered time points) in a Helios (Ultrafast Systems LLC) spectrometer (1 ps to 2.6 ns, ~0.2 ps resolution) and in an Eos (Ultrafast Systems LLC) spectrometer (0.5 ns to 80 µs, and 5 ns to 8.3 ms, ~0.5 ns resolution). The 1 ps – 2.6 ns, and 0.5 ns to 80 µs datasets were collected on samples of anaerobic and aerobic Pchlide in aqueous buffer (50 µM Pchlide, 40 v% glycerol, 20 m/v% sucrose, 50 mM Tris-HCl, pH 7.5, 1 v% Genapol) and in an alcohol solution (50 µM Pchlide, MeOH 1:4 EtOH). The two datasets were then merged for each sample, as described previously[127] and global analysis was performed on the complete datasets obtained at a range of temperatures. Using a laser repetition rate of 100 Hz, 5 ns to 8.3 ms datasets were collected for an aerobic Pchlide sample in aqueous buffer (50 µM Pchlide, 40 v% glycerol, 20 m/v% sucrose, 50 mM Tris-HCl, pH 7.5, 1 v% Genapol) and for both aerobic and anaerobic Pchlide samples in alcohol solution (50 µM Pchlide, MeOH 1:4 EtOH).

2.4.2 Flash Photolysis

Pchlide samples were contained in a 1 cm path length cuvette in an Oxford instruments prototype cryogen-free cryostat. An Nd:YAG laser (Brilliant B, Quantel) was used to generate 1064 nm pulses, which were guided through two harmonics to double the frequency to 355 nm and finally tuned by an OPO to achieve the 450 nm pulses (~8 ns, ~20 mJ). Single-wavelength absorption transients were measured using an Applied Photophysics LKS spectrometer (up to 85 ms, ~10 µs resolution). The single-wavelength detection system consisted of a probe beam from a xenon arc flash lamp that could be pulsed for measurements <1ms, which was passed through a monochromator, the cryostat sample windows, another monochromator after the sample

to eliminate scattered light from the pump pulse and a photomultiplier. Ground-state recovery lifetimes were calculated from the average of ten time-resolved absorption measurements at 630 nm by fitting to a single (alcohol solution samples) or double (buffer samples) exponential function. Global analysis was performed on datasets containing transient measurements at a range of wavelengths from 300 to 680 nm. For this setup, Pchlide samples in anaerobic aqueous buffer (20 µM Pchlide, 40 % (v/v) glycerol, 20 % (wt/v) sucrose, 50 mM Tris-HCl, pH 7.5, 1 % (v/v) Genapol) were used.

2.4.3 Global Analysis

In order to reduce the matrix of change in absorbance as a function of time and wavelength to an exponential decay model, the data sets were analysed using Glotaran, an open-source software package.[148] Datasets were fitted to a simple sequential model, where the decays were associated to transitions between evolution-associated difference spectra. The lifetime errors quoted correspond to the standard error derived from the fitting procedure.

2.4.4 Electron Paramagnetic Resonance Spectroscopy

Laser pulses from a Nd:YAG laser (Minilite, Continuum) frequency doubled to 532 nm (~5 ns, ~6 mJ) were used to generate the photoexcited triplet state of Pchlide. X-band (9 GHz) direct detection and two-pulse spin echo decay measurements were performed on an X-band Bruker Elexsys E580 spectrometer equipped with an Oxford Instruments gas-flow cryostat. Transient direct detection measurements were performed using a Bruker MS5 resonator at a temperature of 10 K and integrating the signal over 1 µs across a range of magnetic field intensities. Two-pulse electron spin echo (ESE) decay measurements were performed using a Bruker MD5 resonator at a temperature of 10 K, using the pulse sequence shown as an inset in Figure 2.4B with mw pulses of lengths $t_{\pi/2}$ = 16 ns, t_{π} = 32 ns and τ = 300 ns at fixed field positions and increasing the delay after flash (DAF) over time. Generally, anaerobic Pchlide samples were used for EPR measurements in aqueous buffer (50 µM Pchlide, 40 v% glycerol, 20 m/v% sucrose, 50 mM Tris-HCl, pH 7.5, 1 v% Genapol) and alcohol solution (MeOH 1:4 EtOH) since the presence of oxygen accelerates the spin relaxation time independently of the excited

state lifetime. Experimental zero-field splitting (ZFS) parameters were acquired from simulating the triplet's field sweep spectrum using the Easyspin software extension for Matlab.[149] Additionally, a DFT calculation of the ZFS parameters of the triplet state of Pchlide was performed in ORCA using the B3LYP hybrid functional and the EPR-II basis set as previously described by Sinnecker.[150,151]

2.4.5 Supporting Data

Raw time-resolved absorption spectroscopy data (aqueous buffer)

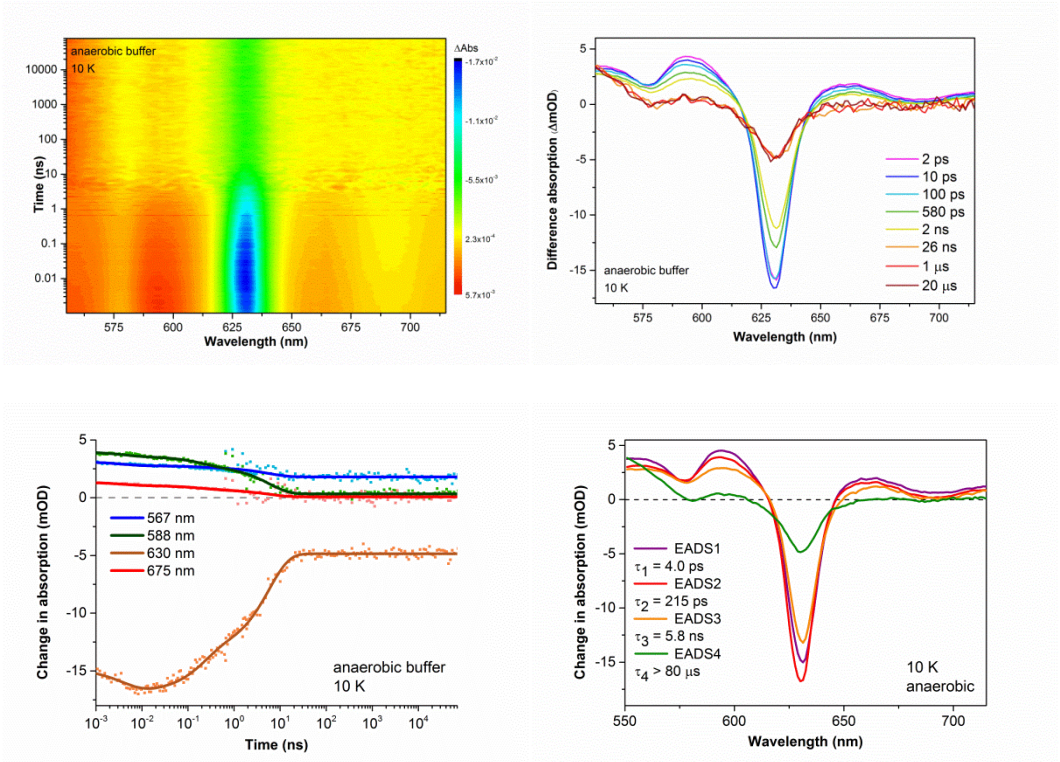

Figure S2.1. Time-resolved visible spectroscopy data for Pchlide in anaerobic buffer at 10 K after photoexcitation at ~450 nm and corresponding fits. Time-resolved difference spectra were recorded between 1 ps and 80 µs as described in the experimental section.

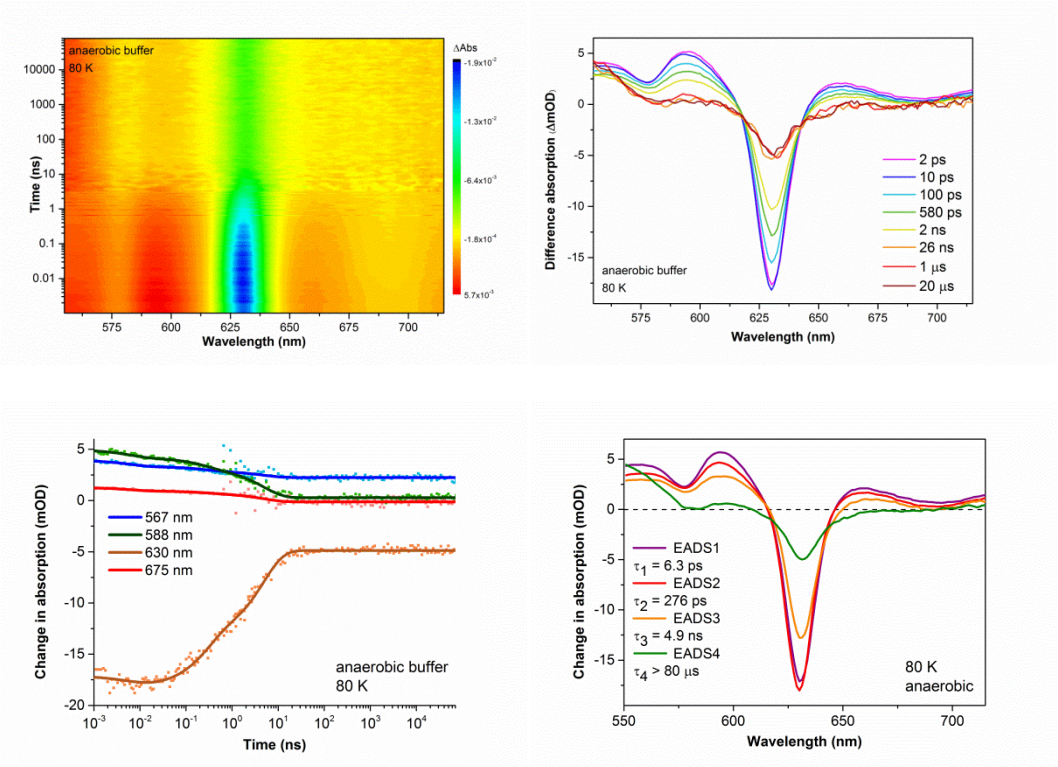

Figure S2.2. Time-resolved visible spectroscopy data for Pchlide in anaerobic buffer at 80 K after photoexcitation at ~450 nm and corresponding fits. Time-resolved difference spectra were recorded between 1 ps and 80 µs as described in the experimental section.

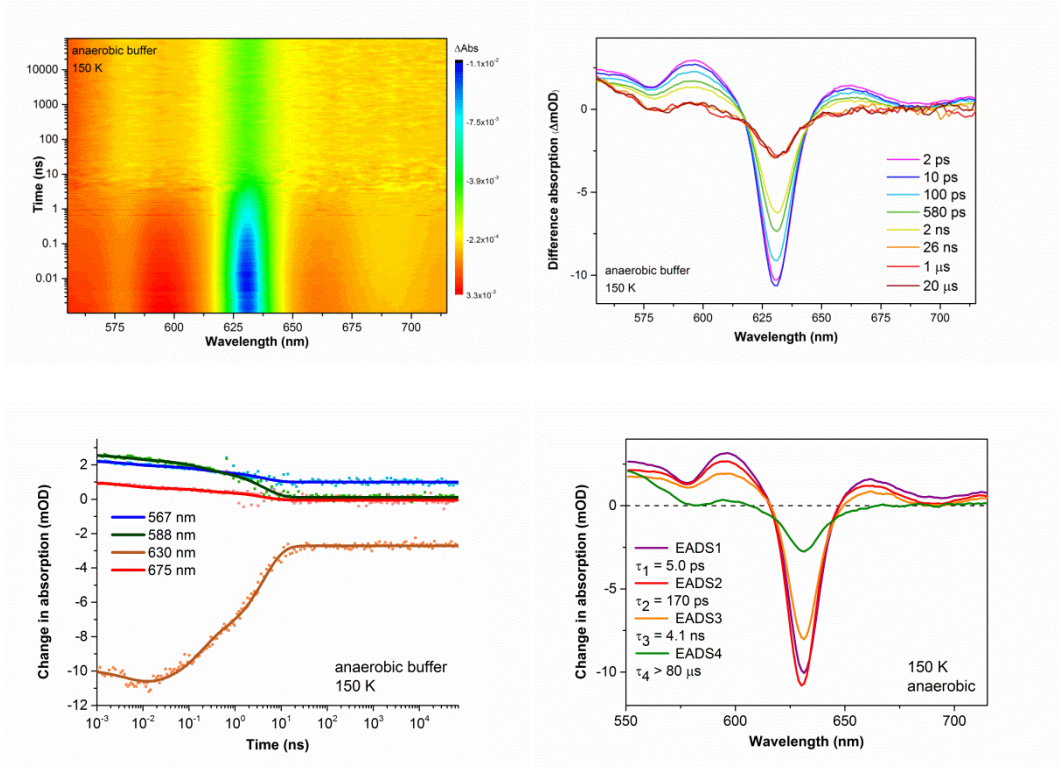

Figure S2.3. Time-resolved visible spectroscopy data for Pchlide in anaerobic buffer at 150 K after photoexcitation at ~450 nm and corresponding fits. Time-resolved difference spectra were recorded between 1 ps and 80 µs as described in the experimental section.

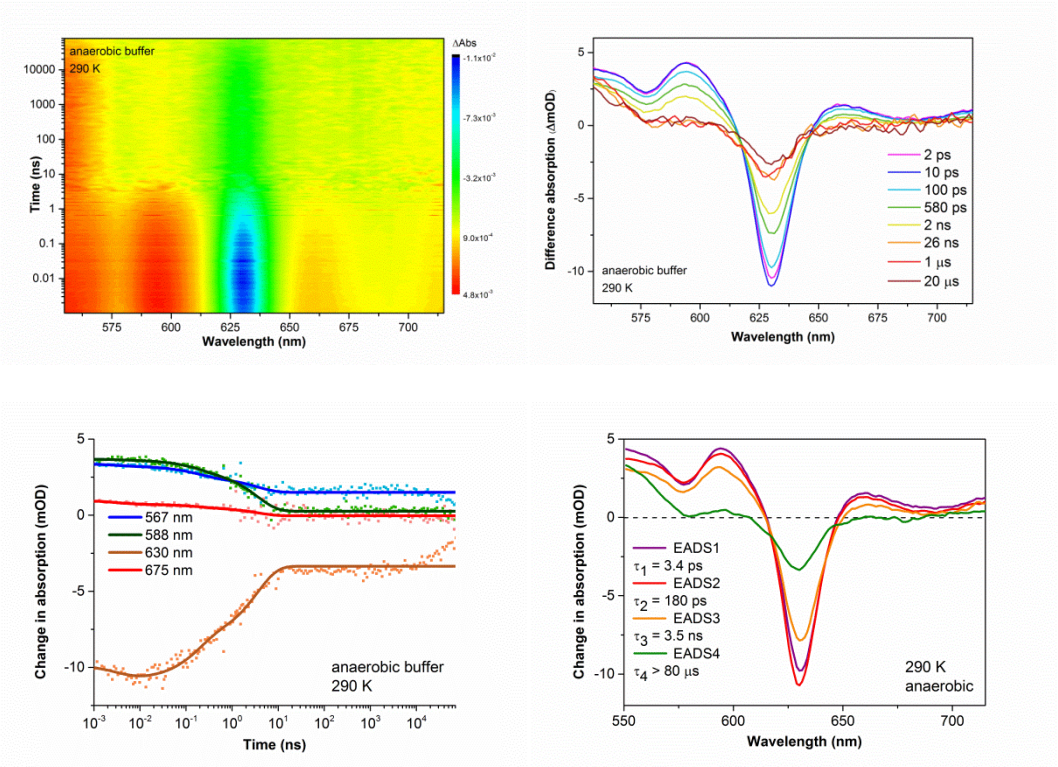

Figure S2.4. Time-resolved visible spectroscopy data for Pchlide in anaerobic buffer at room temperature after photoexcitation at ~450 nm and corresponding fits. Time-resolved difference spectra were recorded between 1 ps and 80 µs as described in the experimental section.

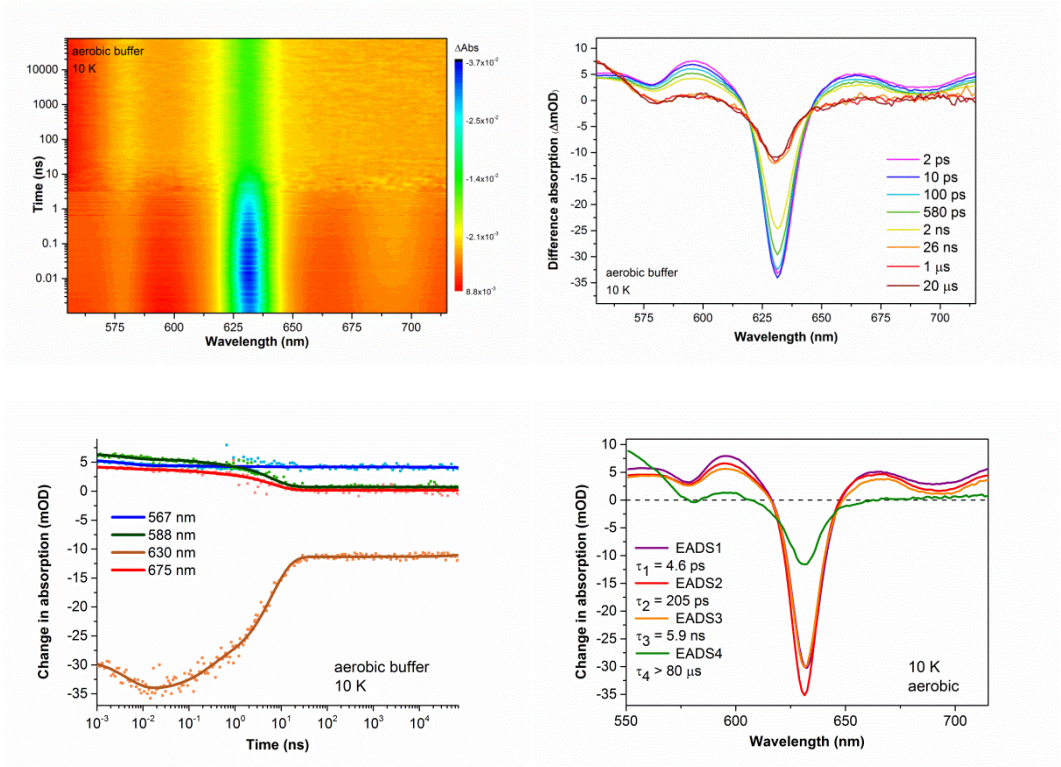

Figure S2.5. Time-resolved visible spectroscopy data for Pchlide in aerobic buffer at 10 K after photoexcitation at ~450 nm and corresponding fits. Time-resolved difference spectra were recorded between 1 ps and 80 µs as described in the experimental section.

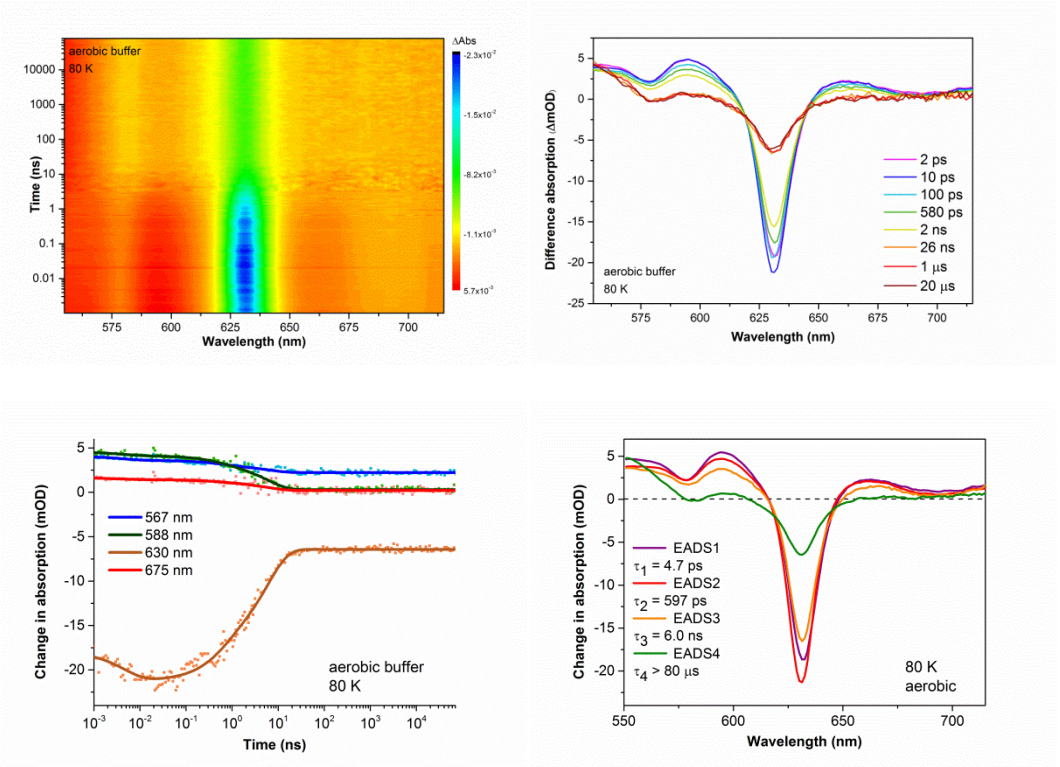

Figure S2.6. Time-resolved visible spectroscopy data for Pchlide in aerobic buffer at 80 K after photoexcitation at ~450 nm and corresponding fits. Time-resolved difference spectra were recorded between 1 ps and 80 µs as described in the experimental section.

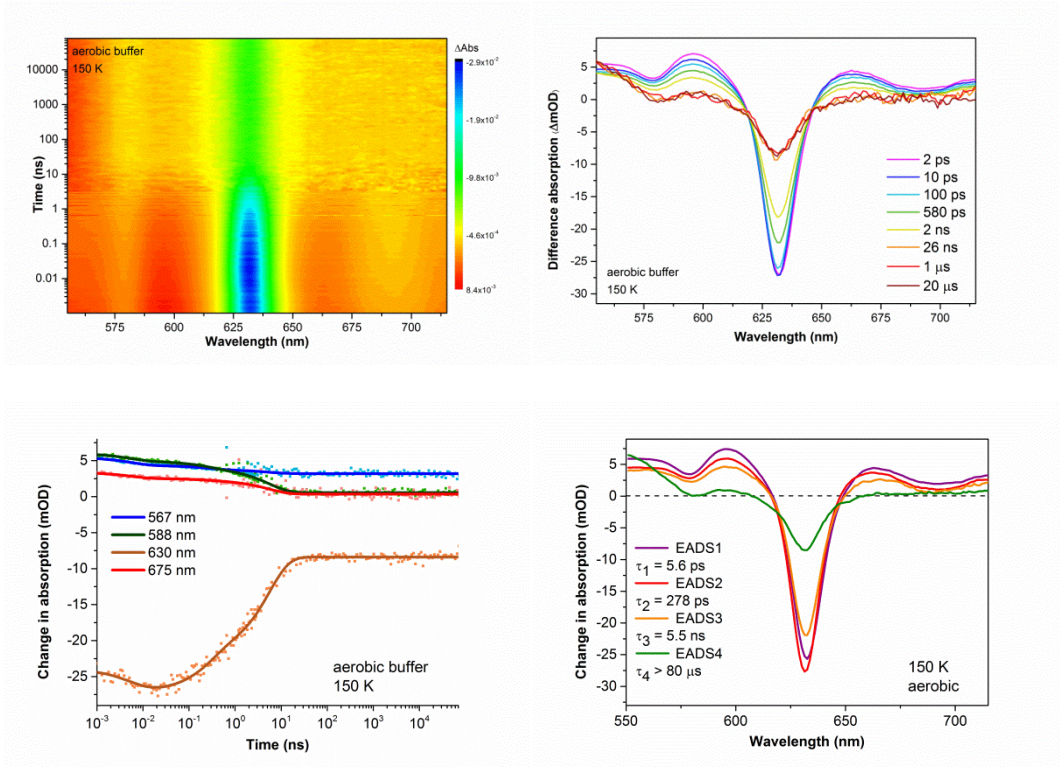

Figure S2.7. Time-resolved visible spectroscopy data for Pchlide in aerobic buffer at 150 K after photoexcitation at ~450 nm and corresponding fits. Time-resolved difference spectra were recorded between 1 ps and 80 µs as described in the experimental section.

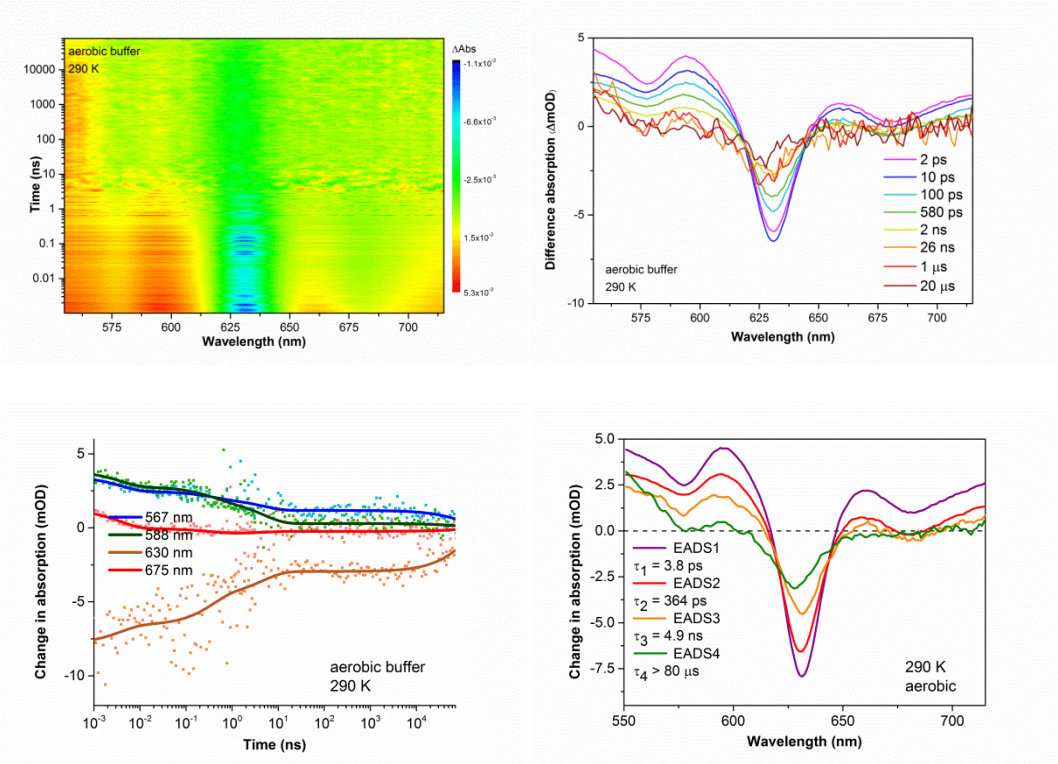

Figure S2.8. Time-resolved visible spectroscopy data for Pchlide in aerobic buffer at room temperature after photoexcitation at ~450 nm and corresponding fits. Time-resolved difference spectra were recorded between 1 ps and 80 µs as described in the experimental section.

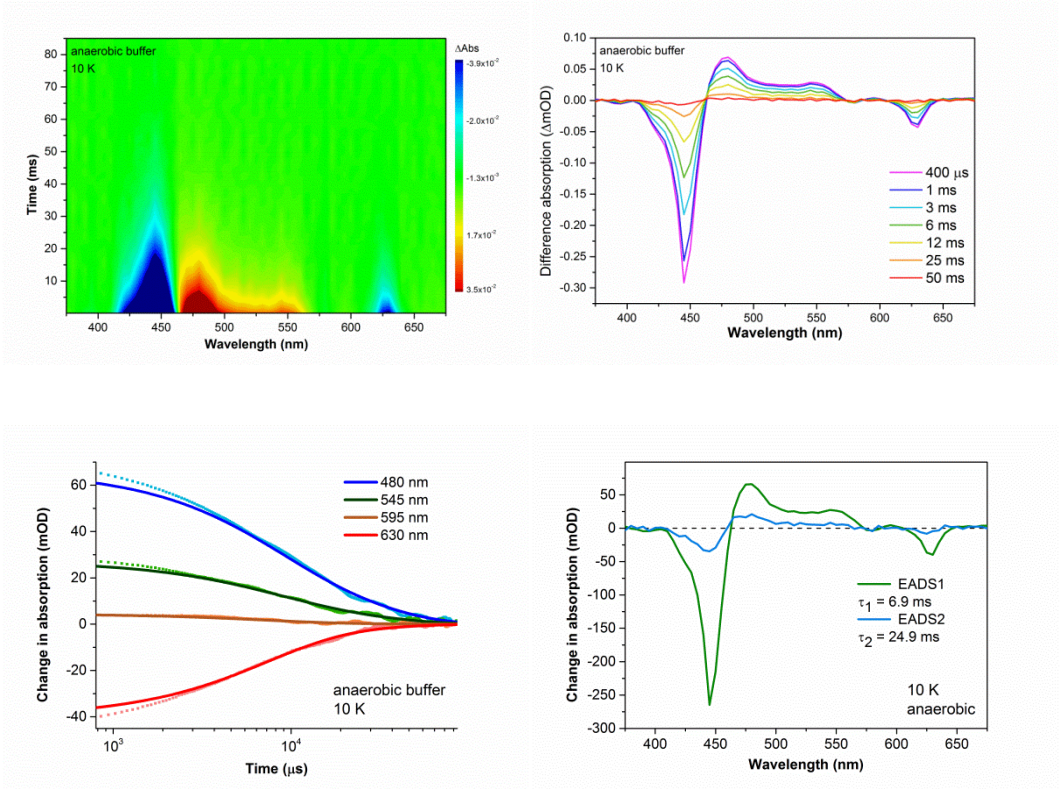

Figure S2.9. Time-resolved visible spectroscopy data for Pchlide in anaerobic buffer at 10 K after photoexcitation at 450 nm and corresponding fits. 85 ms single-wavelength transients were recorded between 305 and 680 nm as described in the experimental section.

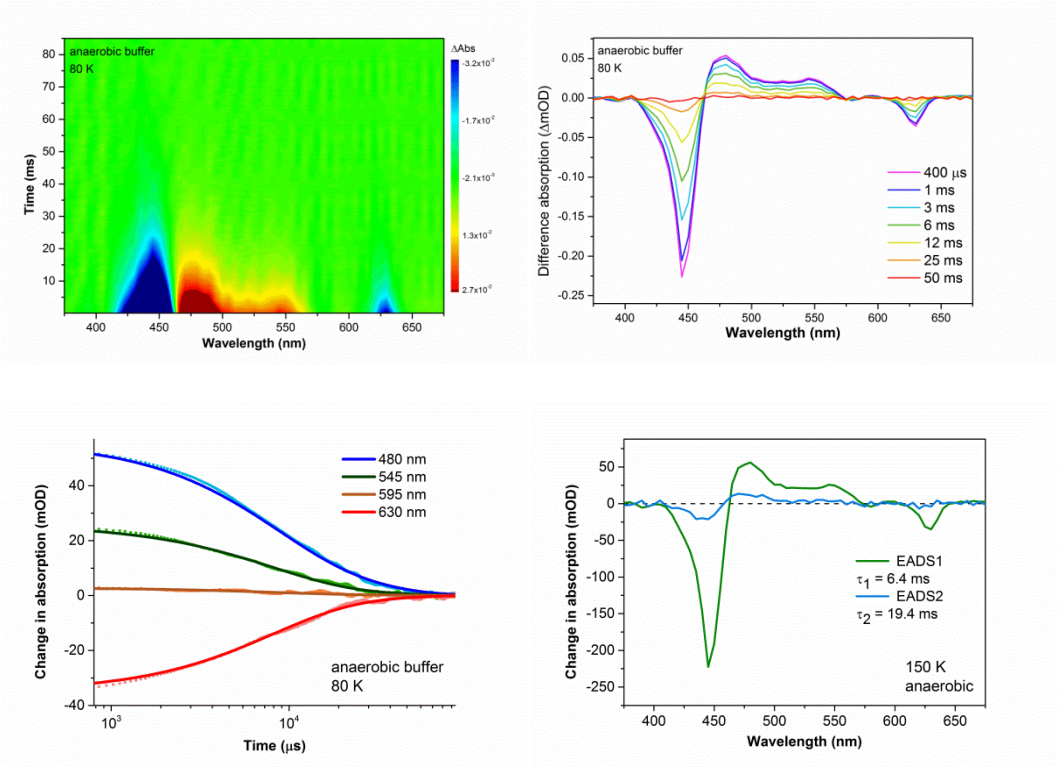

Figure S2.10. Time-resolved visible spectroscopy data for Pchlide in anaerobic buffer at 80 K after photoexcitation at 450 nm and corresponding fits. 85 ms single-wavelength transients were recorded between 305 and 680 nm as described in the experimental section.

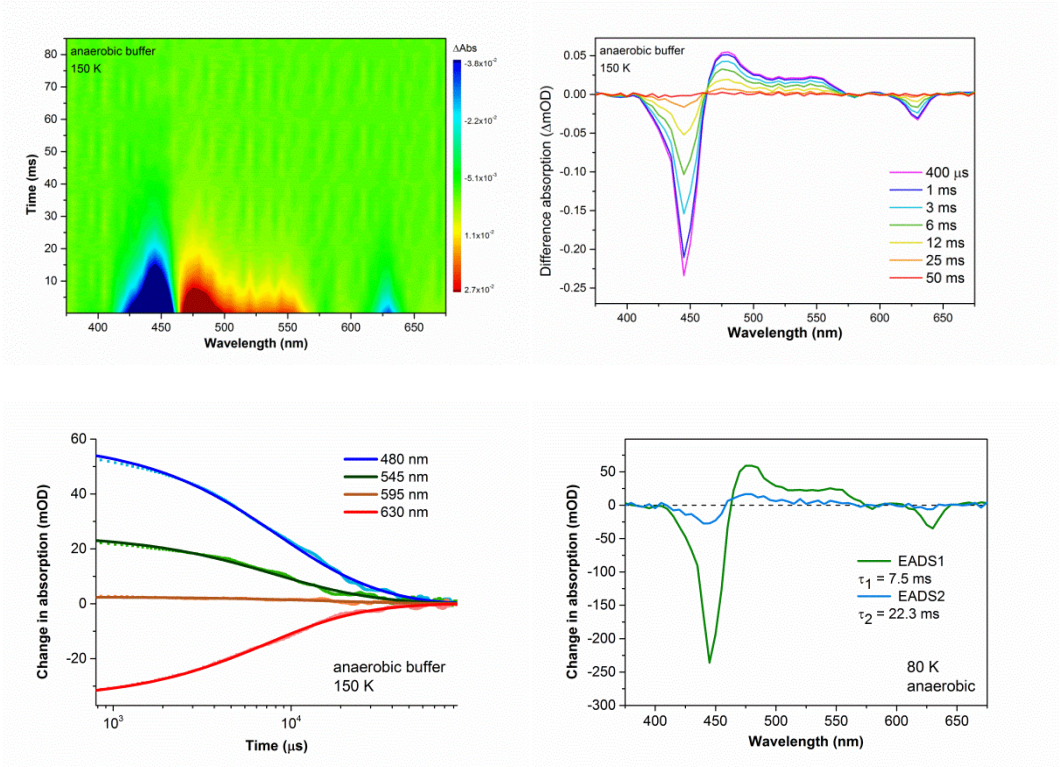

Figure S2.11. Time-resolved visible spectroscopy data for Pchlide in anaerobic buffer at 150 K after photoexcitation at 450 nm and corresponding fits. 85 ms single-wavelength transients were recorded between 305 and 680 nm as described in the experimental section.

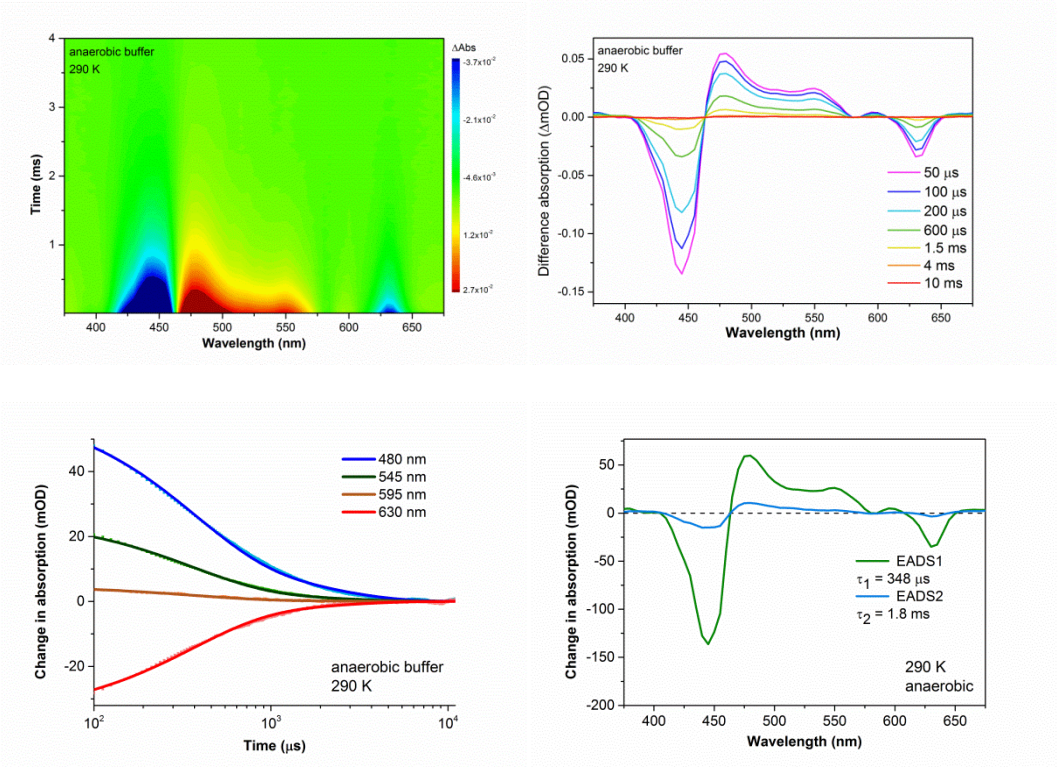

Figure S2.12. Time-resolved visible spectroscopy data for Pchlide in anaerobic buffer at room temperature after photoexcitation at 450 nm and corresponding fits. 10 ms single-wavelength transients were recorded between 305 and 680 nm as described in the experimental section.

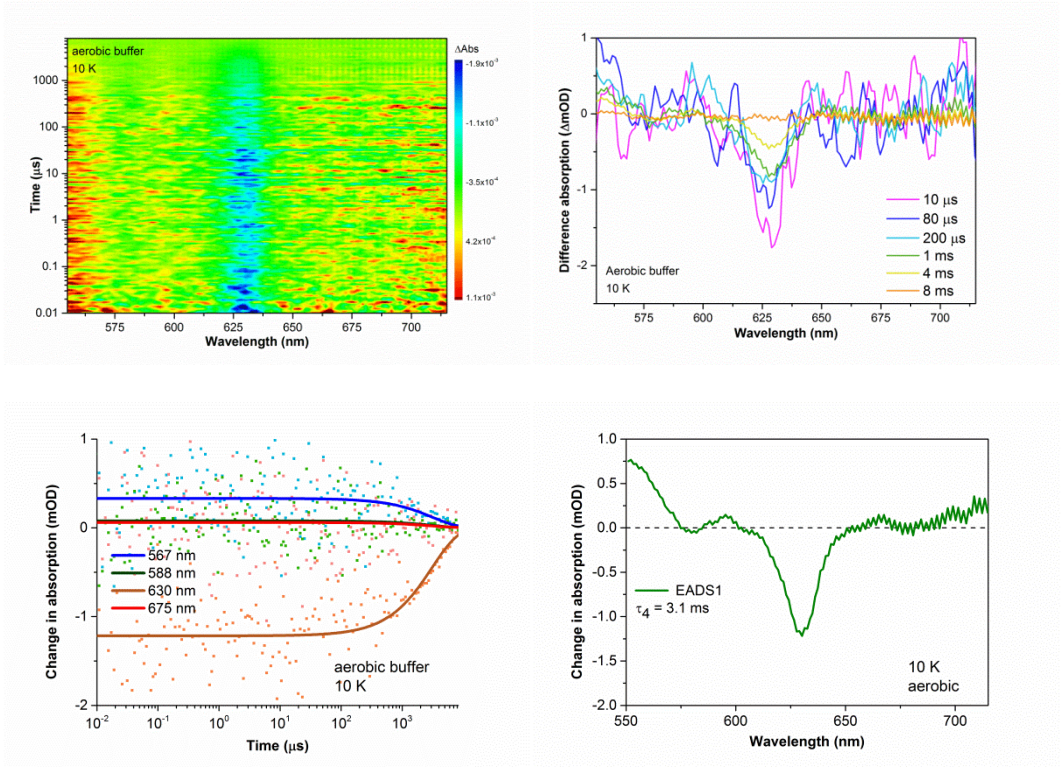

Figure S2.13. Time-resolved visible spectroscopy data for Pchlide in aerobic buffer at 10 K after photoexcitation at ~450 nm and corresponding fits. Time-resolved difference spectra were recorded between 10 ns and 8.3 ms as described in the experimental section.

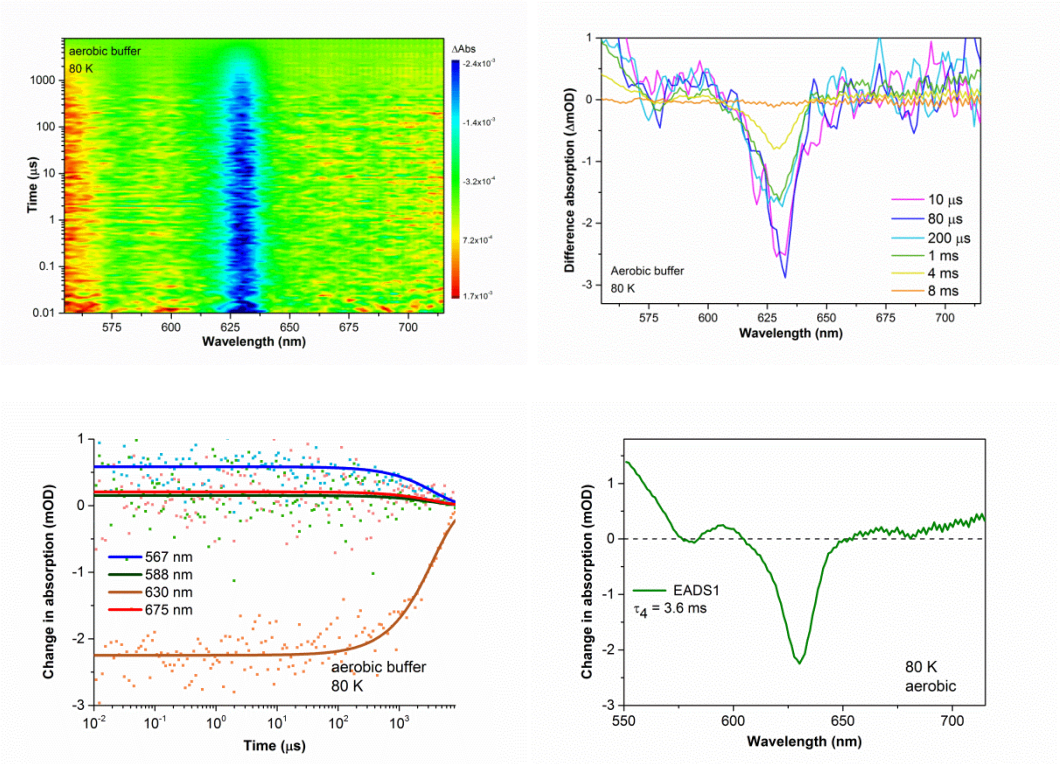

Figure S2.14. Time-resolved visible spectroscopy data for Pchlide in aerobic buffer at 80 K after photoexcitation at ~450 nm and corresponding fits. Time-resolved difference spectra were recorded between 10 ns and 8.3 ms as described in the experimental section.

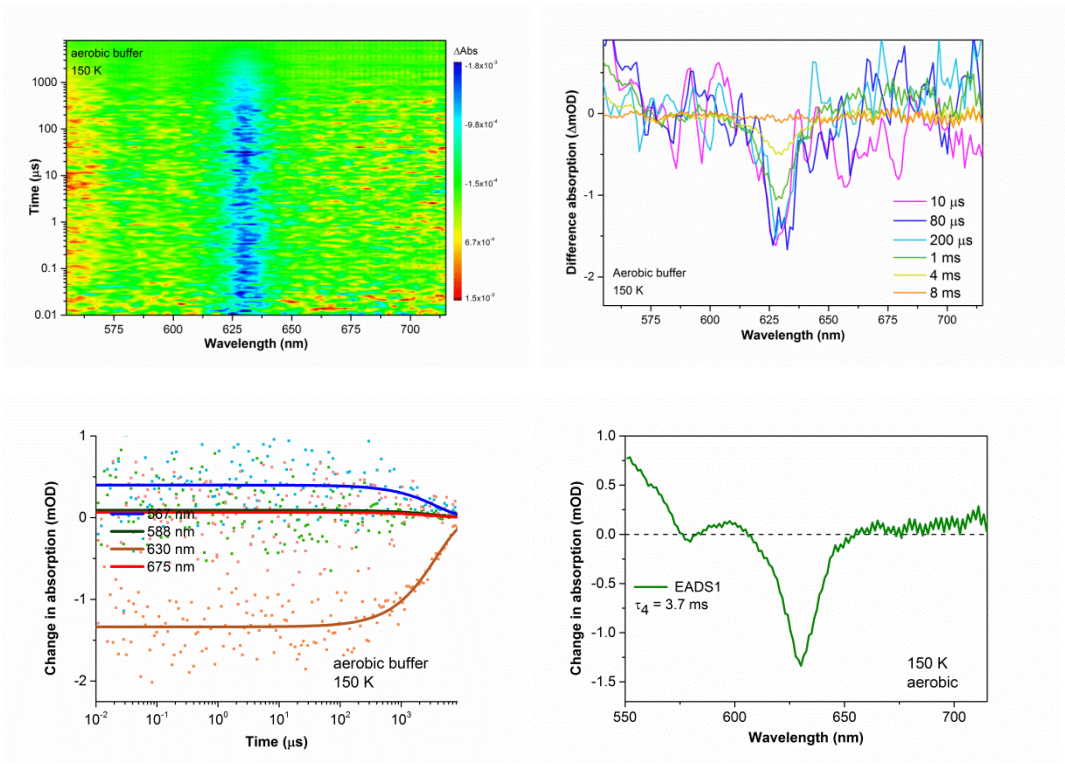

Figure S2.15. Time-resolved visible spectroscopy data for Pchlide in aerobic buffer at 150 K after photoexcitation at ~450 nm and corresponding fits. Time-resolved difference spectra were recorded between 10 ns and 8.3 ms as described in the experimental section.

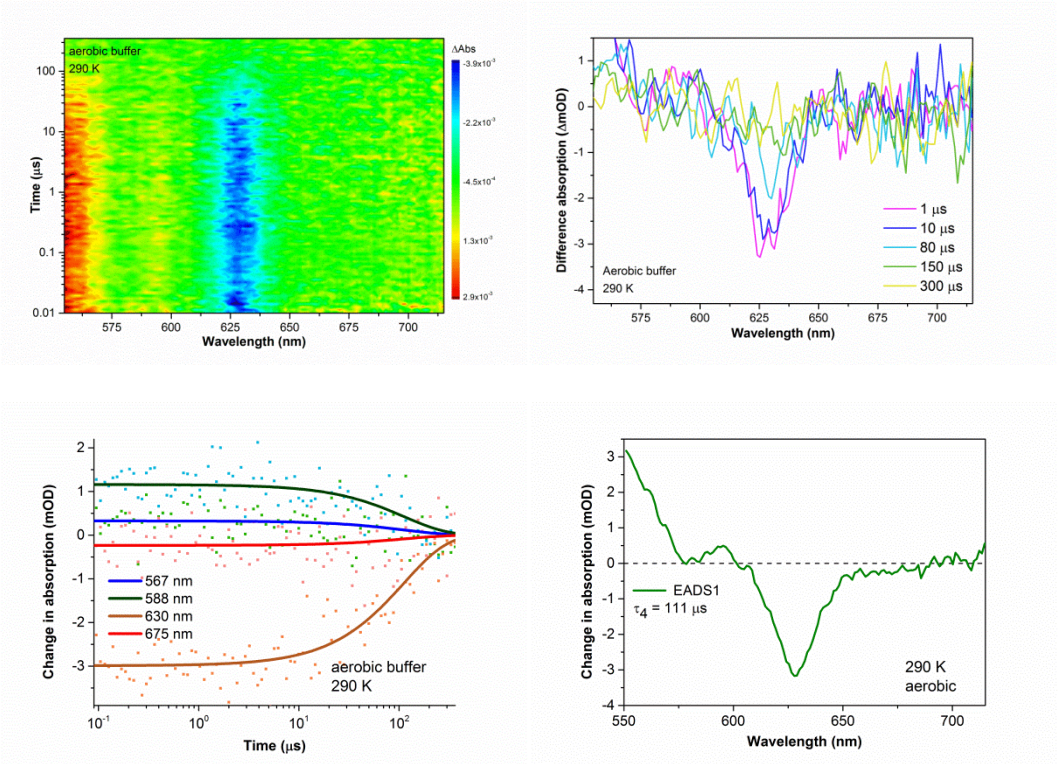

Figure S2.16. Time-resolved visible spectroscopy data for Pchlide in aerobic buffer at room temperature after photoexcitation at ~450 nm and corresponding fits. Time-resolved difference spectra were recorded between 10 ns and 8.3 ms as described in the experimental section.

Raw time-resolved absorption spectroscopy data (alcohol solution)

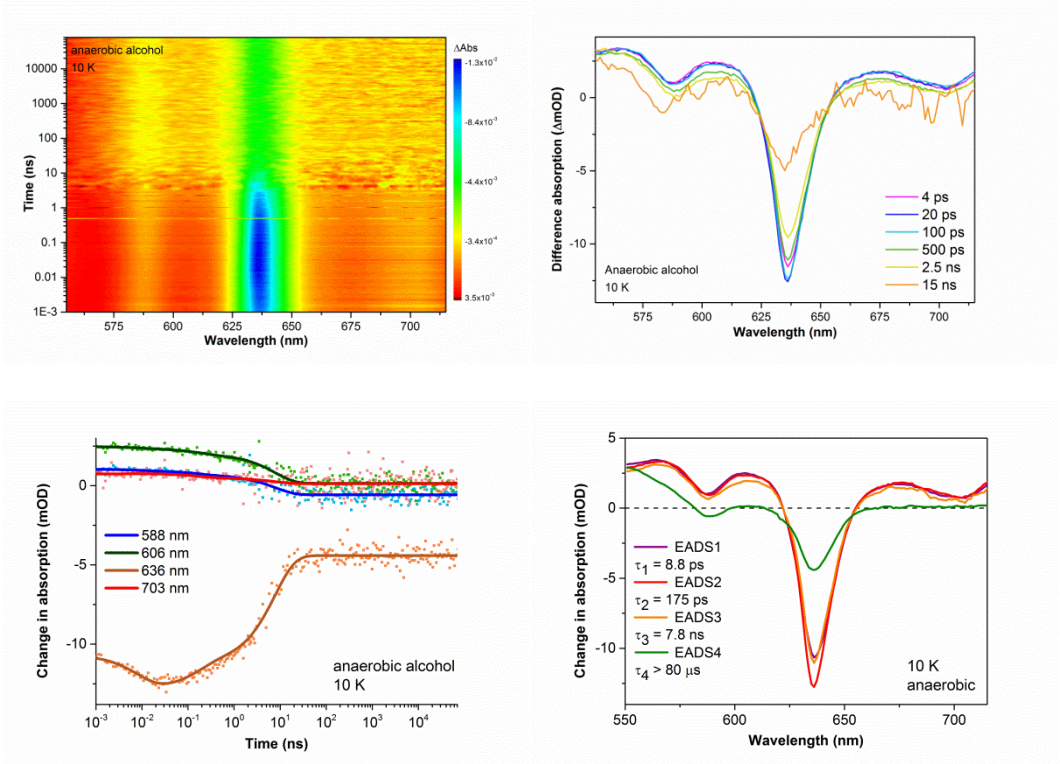

Figure S2.17. Time-resolved visible spectroscopy data for Pchlide in anaerobic alcohol solution at 10 K after photoexcitation at ~450 nm and corresponding fits. Time-resolved difference spectra were recorded between 1 ps and 80 μs as described in the experimental section.

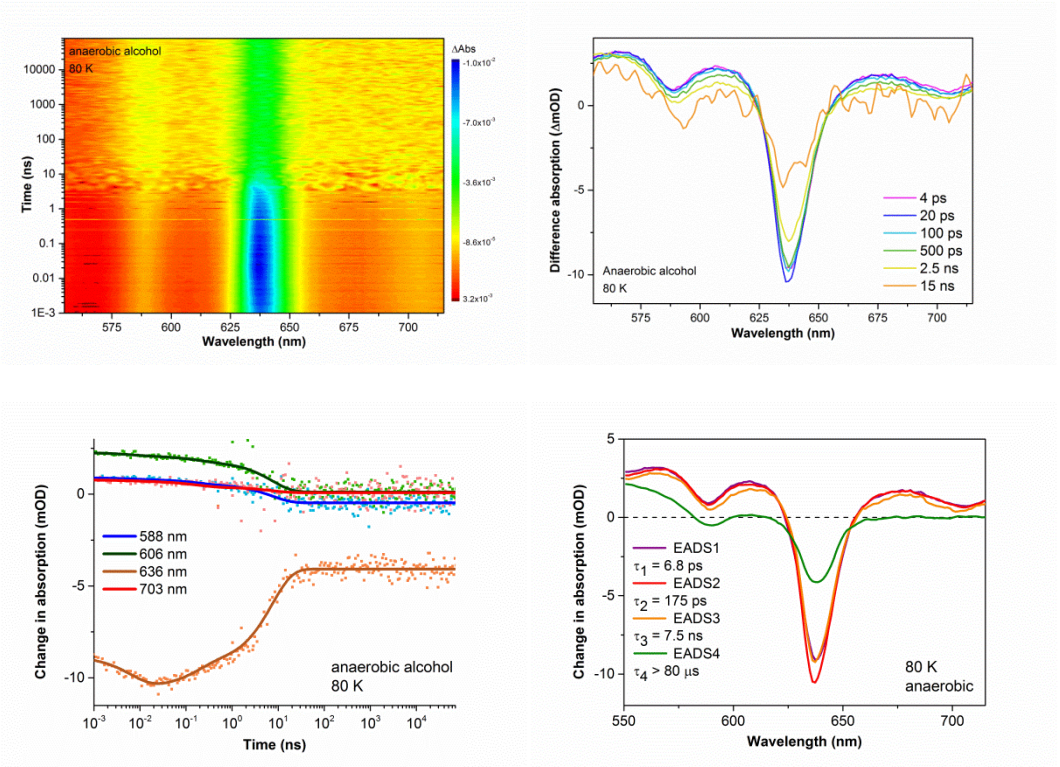

Figure S2.18. Time-resolved visible spectroscopy data for Pchlide in anaerobic alcohol solution at 80 K after photoexcitation at ~450 nm and corresponding fits. Time-resolved difference spectra were recorded between 1 ps and 80 μs as described in the experimental section.

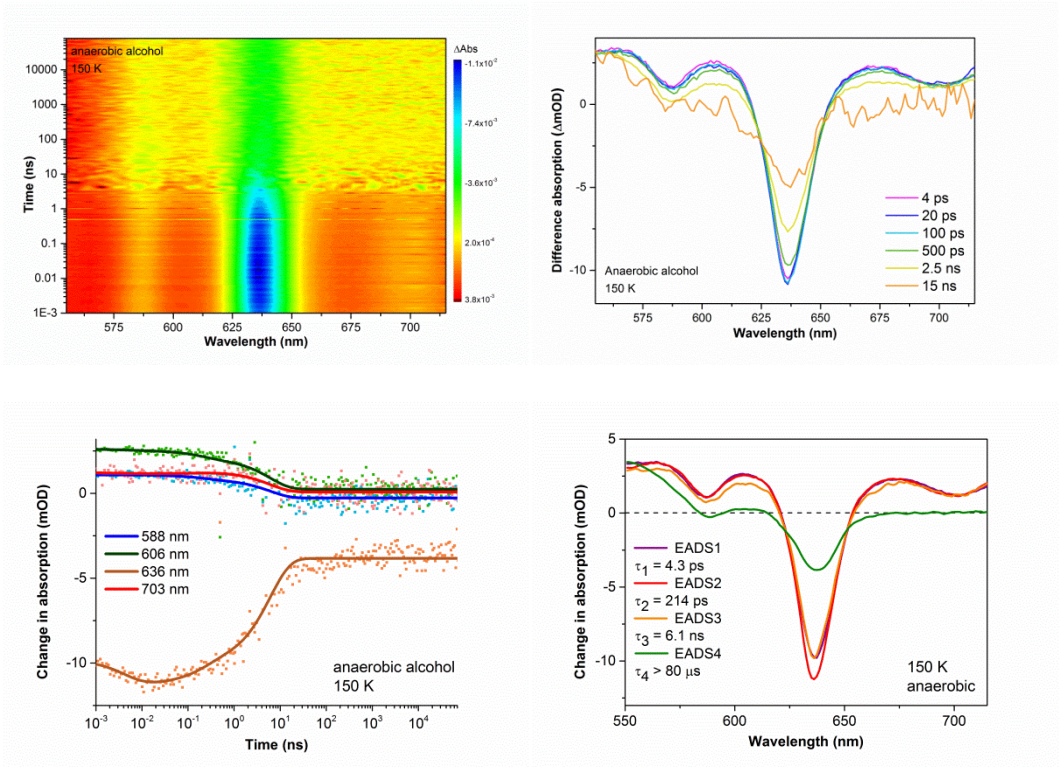

Figure S2.19. Time-resolved visible spectroscopy data for Pchlide in anaerobic alcohol solution at 150 K after photoexcitation at ~450 nm and corresponding fits. Time-resolved difference spectra were recorded between 1 ps and 80 μs as described in the experimental section.

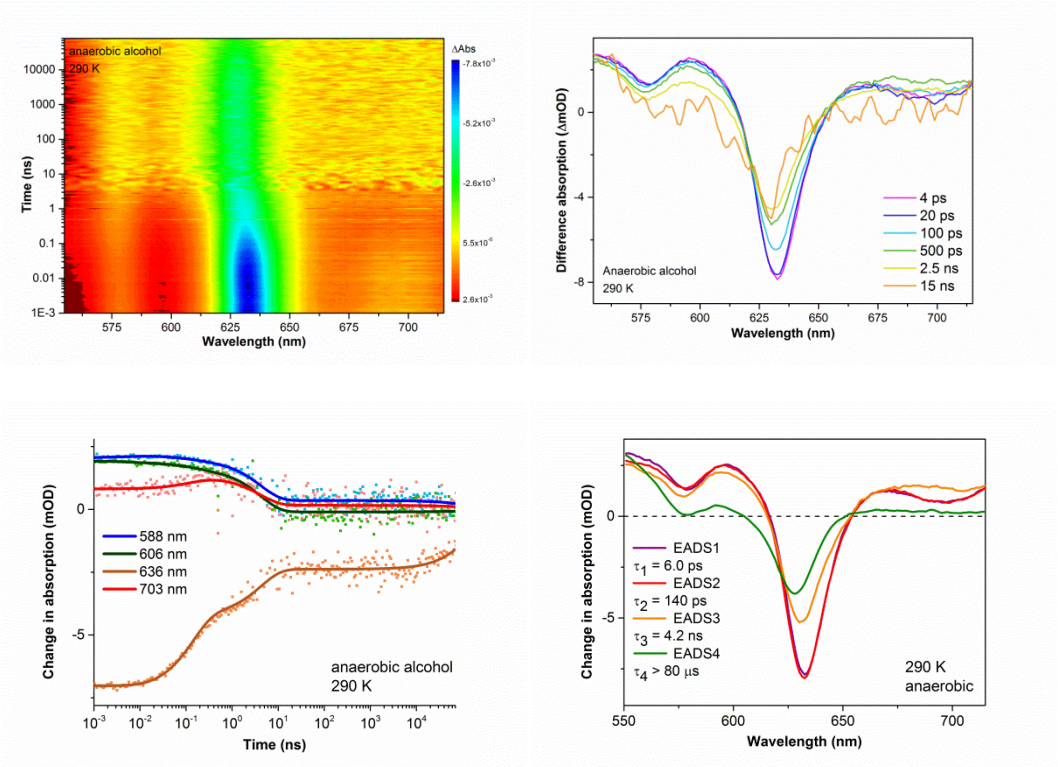

Figure S2.20. Time-resolved visible spectroscopy data for Pchlide in anaerobic alcohol solution at room temperature after photoexcitation at ~450 nm and corresponding fits. Time-resolved difference spectra were recorded between 1 ps and 80 μs as described in the experimental section.

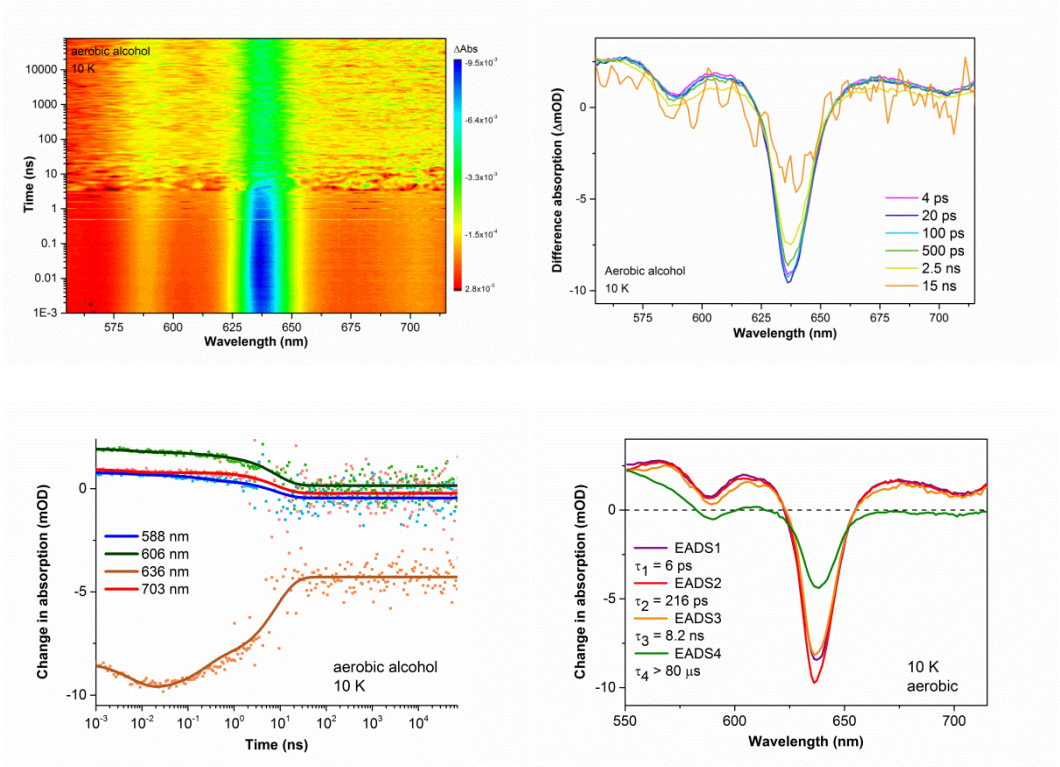

Figure S2.21. Time-resolved visible spectroscopy data for Pchlide in aerobic alcohol solution at 10 K after photoexcitation at ~450 nm and corresponding fits. Time-resolved difference spectra were recorded between 1 ps and 80 μs as described in the experimental section.

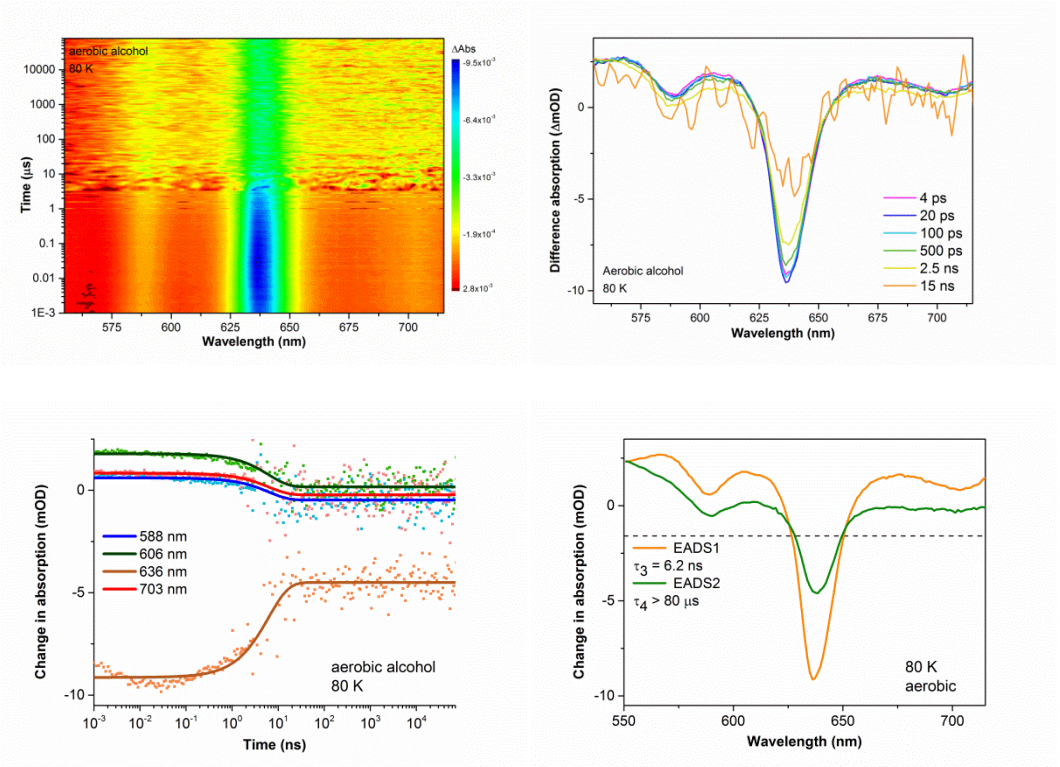

Figure S2.22. Time-resolved visible spectroscopy data for Pchlide in aerobic alcohol solution at 80 K after photoexcitation at ~450 nm and corresponding fits. Time-resolved difference spectra were recorded between 1 ps and 80 µs as described in the experimental section.

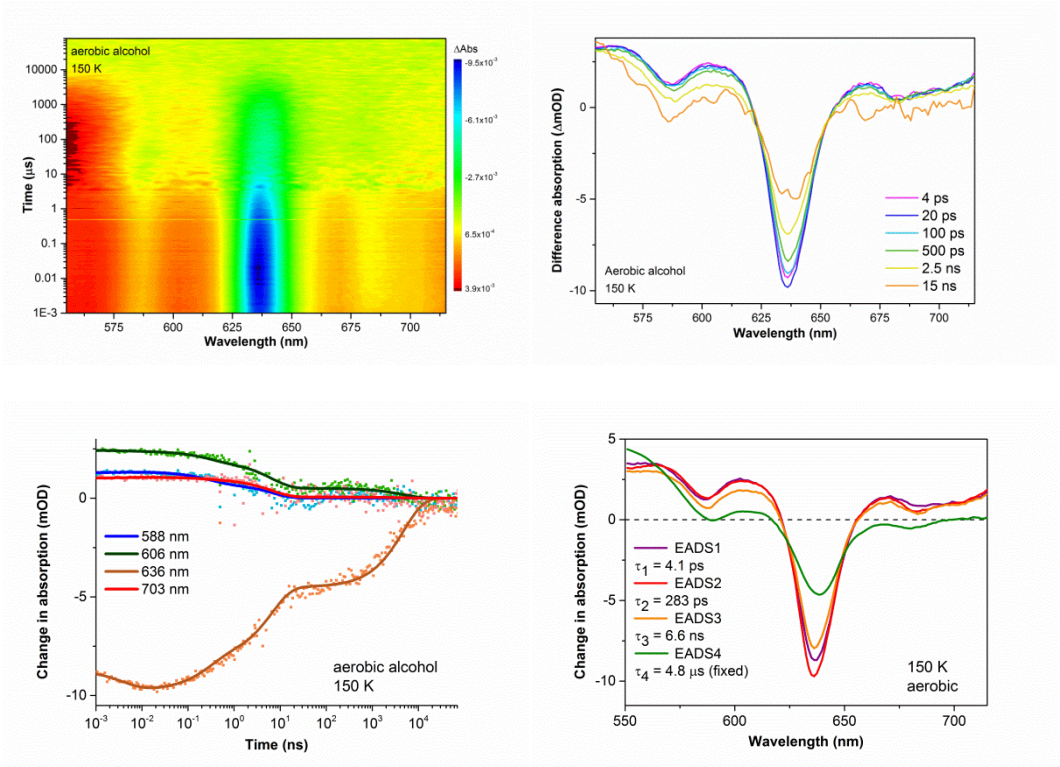

Figure S2.23. Time-resolved visible spectroscopy data for Pchlide in aerobic alcohol solution at 150 K after photoexcitation at ~450 nm and corresponding fits. Time-resolved difference spectra were recorded between 1 ps and 80 µs as described in the experimental section.

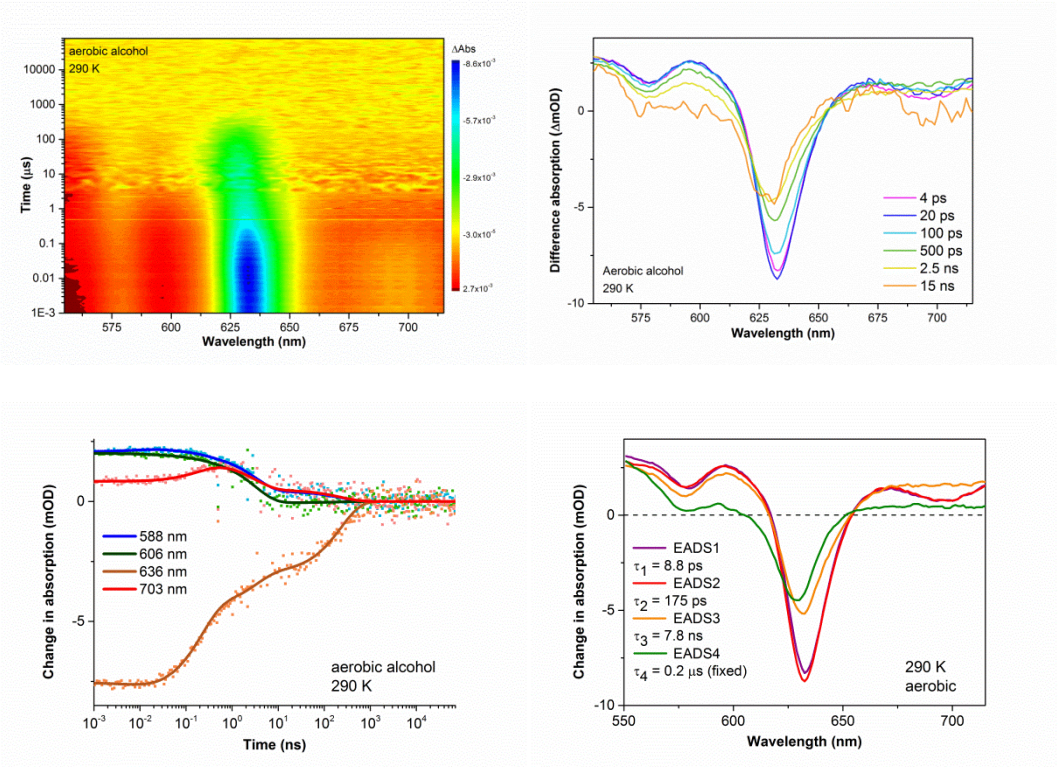

Figure S2.24. Time-resolved visible spectroscopy data for Pchlide in aerobic alcohol solution at room temperature after photoexcitation at ~450 nm and corresponding fits. Time-resolved difference spectra were recorded between 1 ps and 80 µs as described in the experimental section.

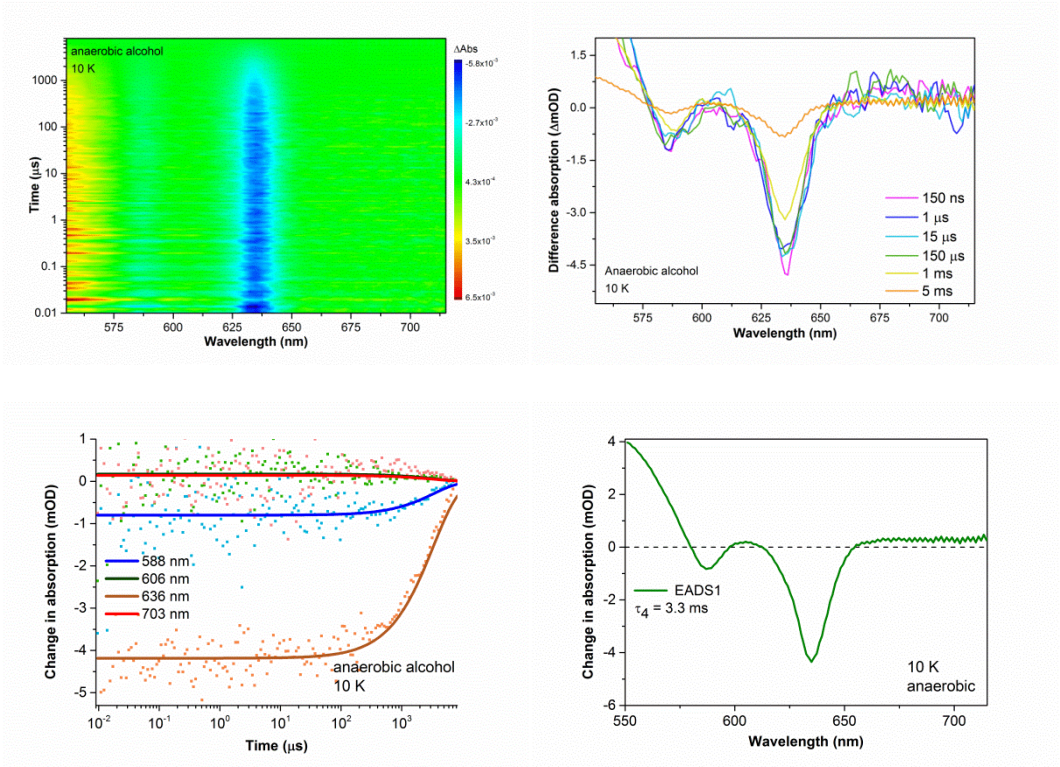

Figure S2.25. Time-resolved visible spectroscopy data for Pchlide in anaerobic alcohol solution at 10 K after photoexcitation at ~450 nm and corresponding fits. Time-resolved difference spectra were recorded between 10 ns and 8.3 ms as described in the experimental section.

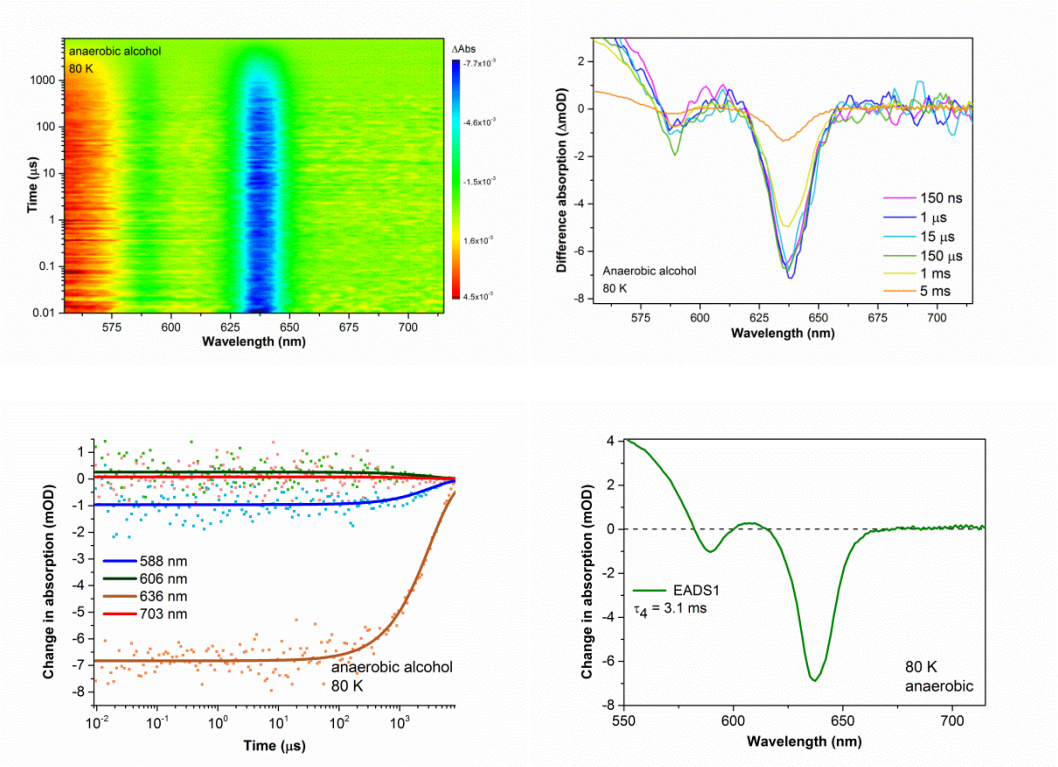

Figure S2.26. Time-resolved visible spectroscopy data for Pchlide in anaerobic alcohol solution at 80 K after photoexcitation at ~450 nm and corresponding fits. Time-resolved difference spectra were recorded between 10 ns and 8.3 ms as described in the experimental section.

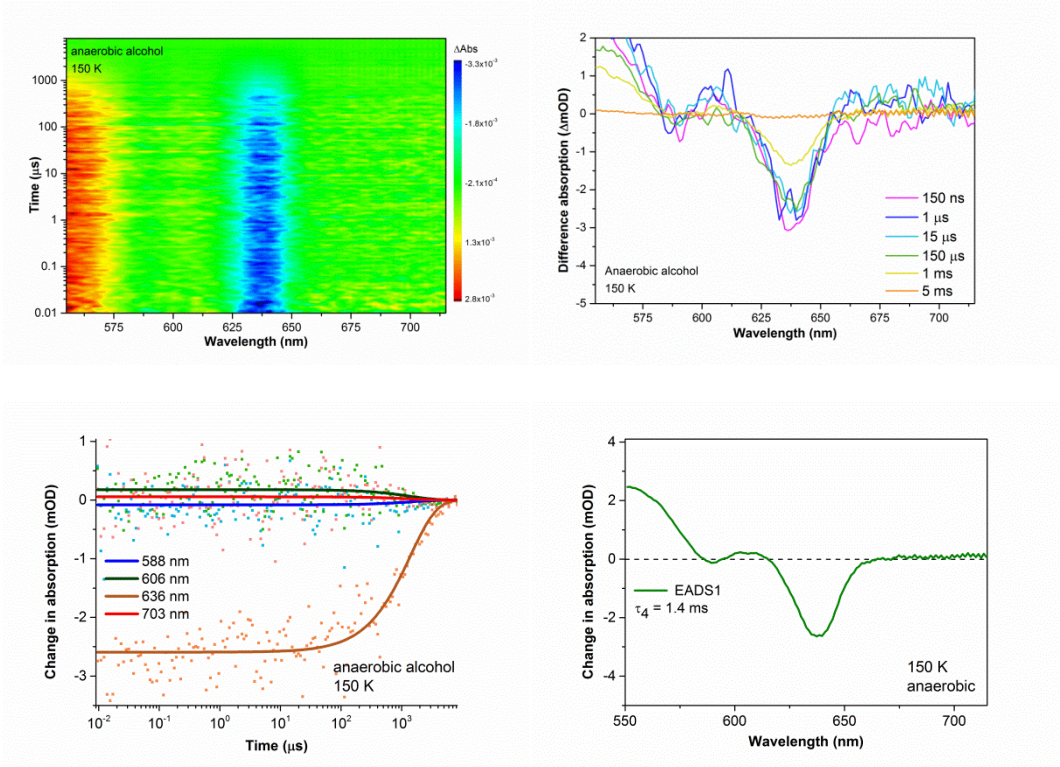

Figure S2.27. Time-resolved visible spectroscopy data for Pchlide in anaerobic alcohol solution at 150 K after photoexcitation at ~450 nm and corresponding fits. Time-resolved difference spectra were recorded between 10 ns and 8.3 ms as described in the experimental section.

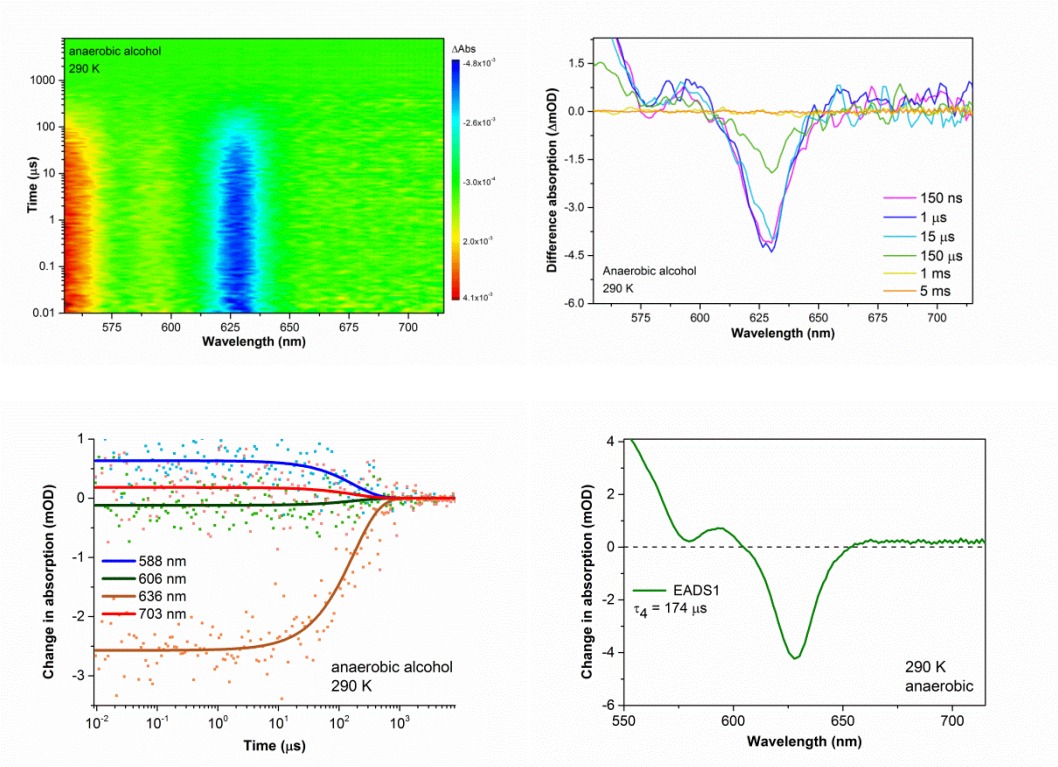

Figure S28. Time-resolved visible spectroscopy data for Pchlide in anaerobic alcohol solution at room temperature after photoexcitation at ~450 nm and corresponding fits. Time-resolved difference spectra were recorded between 10 ns and 8.3 ms as described in the experimental section.

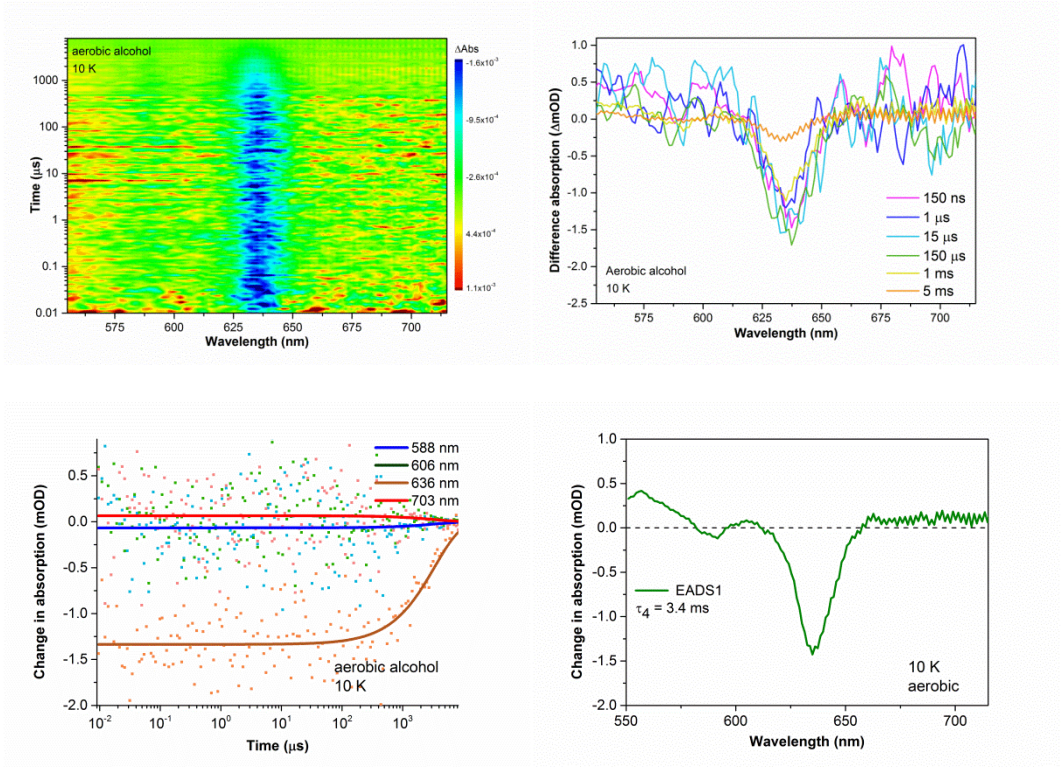

Figure S2.29. Time-resolved visible spectroscopy data for Pchlide in aerobic alcohol solution at 10 K after photoexcitation at ~450 nm and corresponding fits. Time-resolved difference spectra were recorded between 10 ns and 8.3 ms as described in the experimental section.

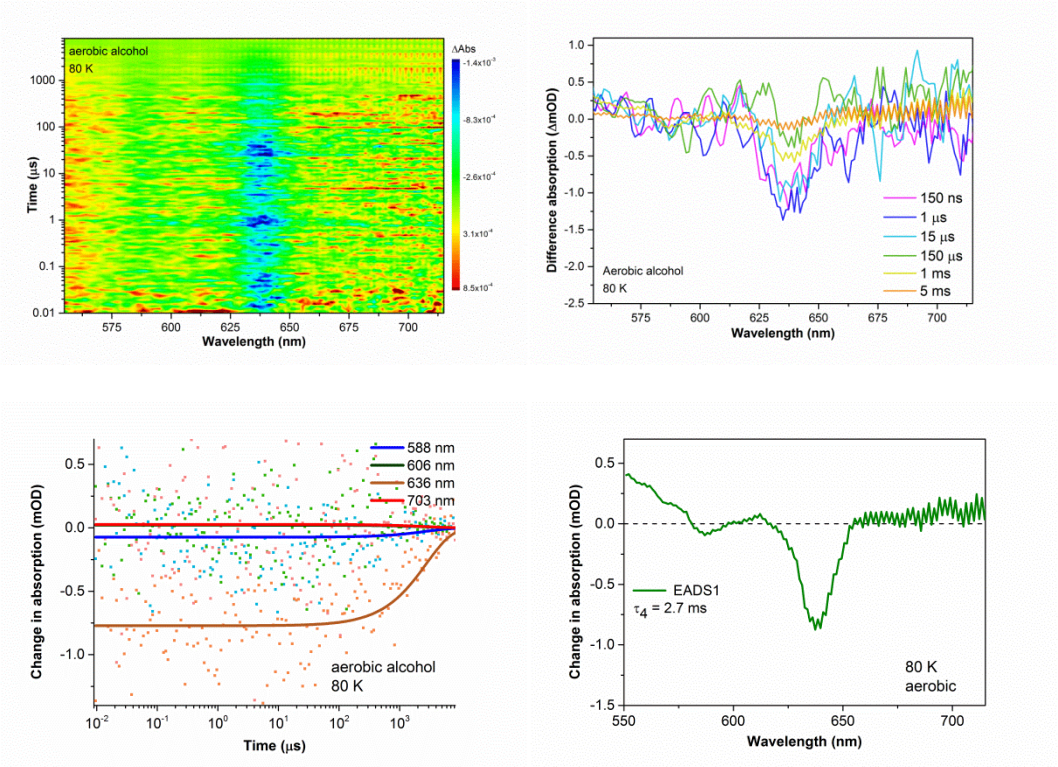

Figure S2.30. Time-resolved visible spectroscopy data for Pchlide in aerobic alcohol solution at 80 K after photoexcitation at ~450 nm and corresponding fits. Time-resolved difference spectra were recorded between 10 ns and 8.3 ms as described in the experimental section.

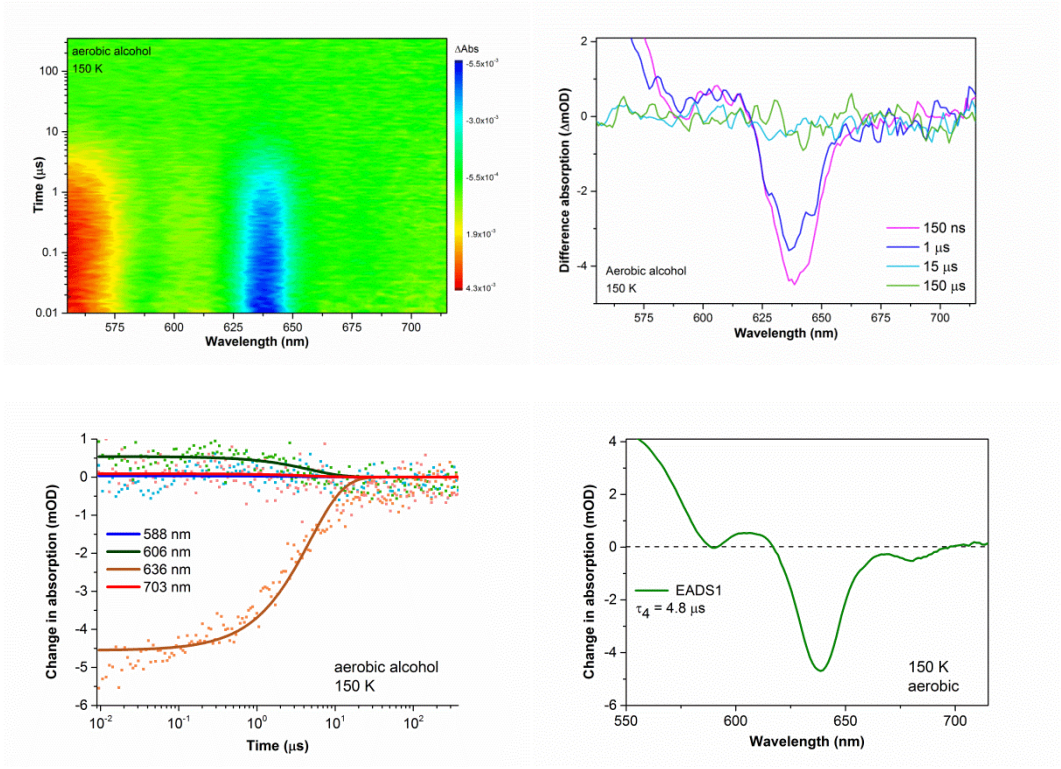

Figure S2.31. Time-resolved visible spectroscopy data for Pchlide in aerobic alcohol solution at 150 K after photoexcitation at ~450 nm and corresponding fits. Time-resolved difference spectra were recorded between 10 ns and 350 μs as described in the experimental section.

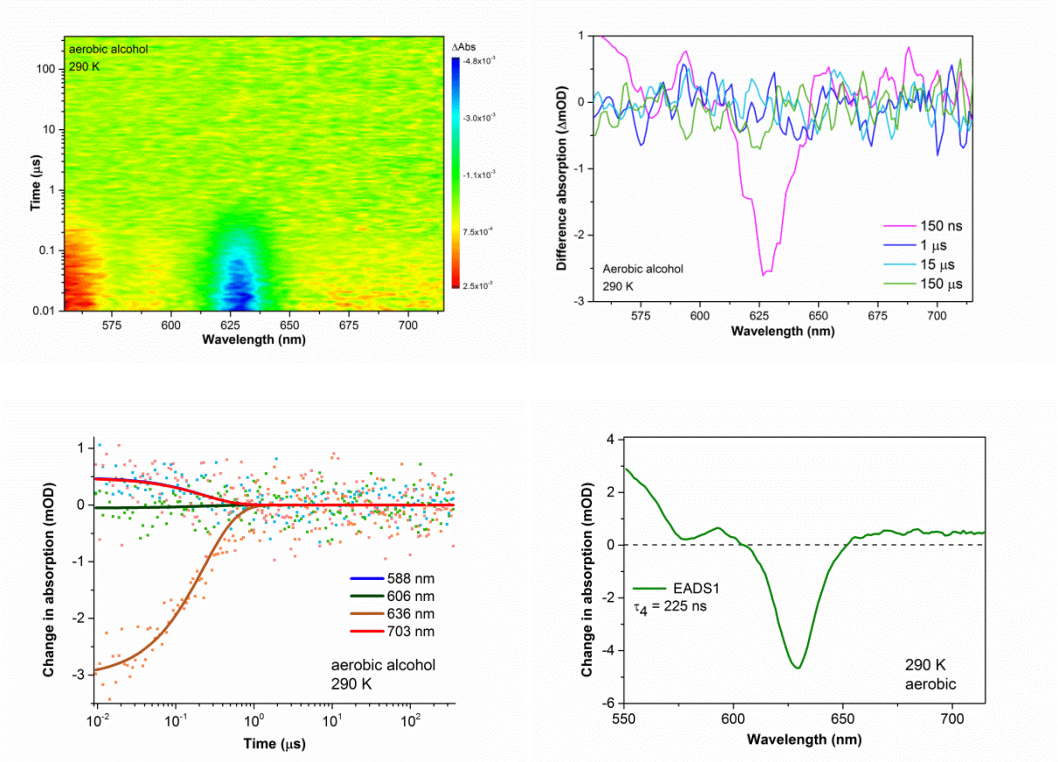

Figure S2.32. Time-resolved visible spectroscopy data for Pchlide in aerobic alcohol solution at room temperature after photoexcitation at ~450 nm and corresponding fits. Time-resolved difference spectra were recorded between 10 ns and 350 μs as described in the experimental section.

Single-wavelength transient absorption

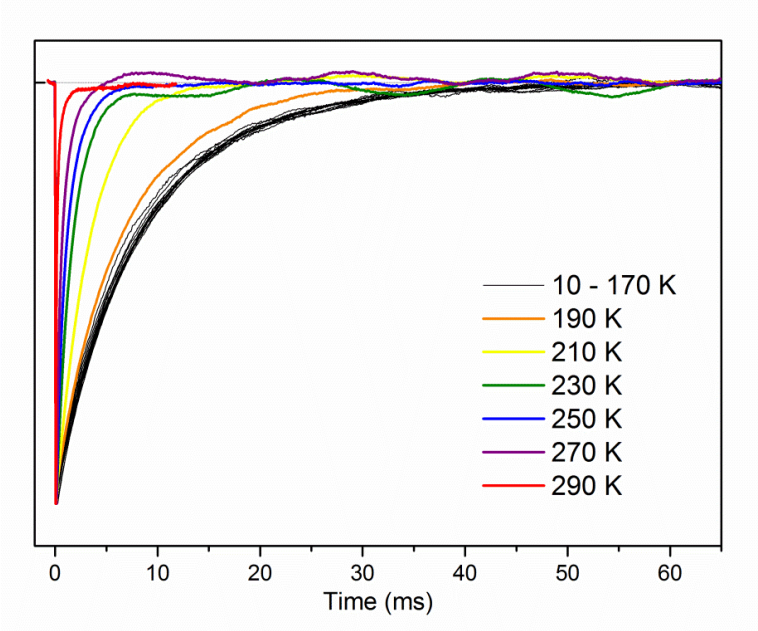

Figure S2.33. Ground state bleach transients measured at 630 nm (which is closely related to the triplet decay) for Pchlide in anaerobic buffer at different temperatures. Samples measured between 10 and 170 K displayed virtually identical decays.

Alcohol solution results

Table S2.1. Lifetimes of the S_1 (τ_1), S_{ICT} (τ_2), solvated S_{ICT} (τ_3) and triplet excited states of Pchlide (τ_4) measured in both aerobic and anaerobic alcohol solution at 10, 80, 150 and 290 K.

	T (K)	τ_1 (ps)	τ_2 (ps)	τ_3 (ns)	τ_4 (μs)
anaerobic	**10**	9 ± 1	175 ± 16	7.8 ± 0.2	3338 ± 62
	80	6.8 ± 0.9	175 ± 16	7.5 ± 0.2	3147 ± 28
	150	4.3 ± 0.1	214 ± 17	6.1 ± 0.1	1392 ± 20
	290	6 ± 1	140 ± 4	4.2 ± 0.1	174 ± 2
aerobic	**10**	6.0 ± 1.4	216 ± 26	8.2 ± 0.3	3382 ± 138
	80	-	-	6.2 ± 0.1	2745 ± 153
	150	4.1 ± 0.5	283 ± 13	6.6 ± 0.8	4.8 ± 0.1
	290	8.6 ± 1.1	214 ± 27	3.3 ± 0.4	0.23 ± 0.01

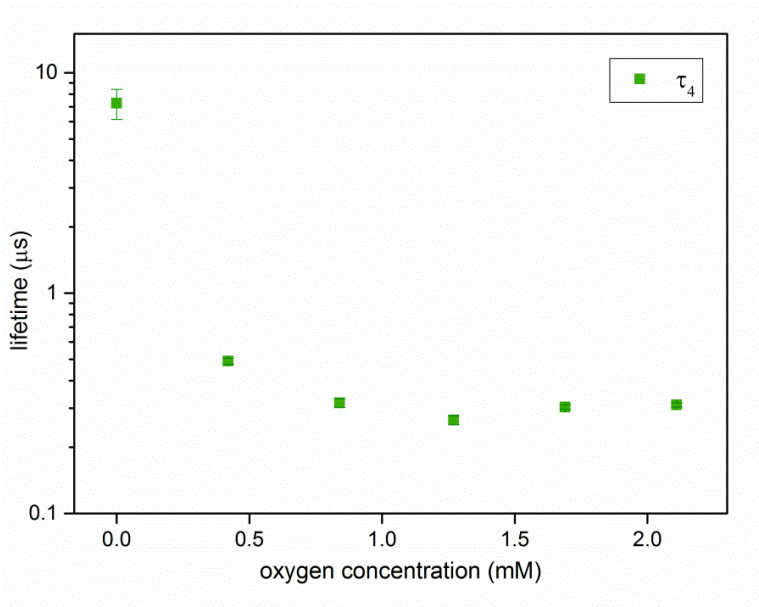

Figure S2.34. Lifetime values (approximately τ_4) obtained from fitting an exponential decay to ground state bleaching (630 nm) flash photolysis time traces. Samples consisted of Pchlide dissolved in mixtures of anaerobic and aerobic alcohol solution at room temperature.

EPR

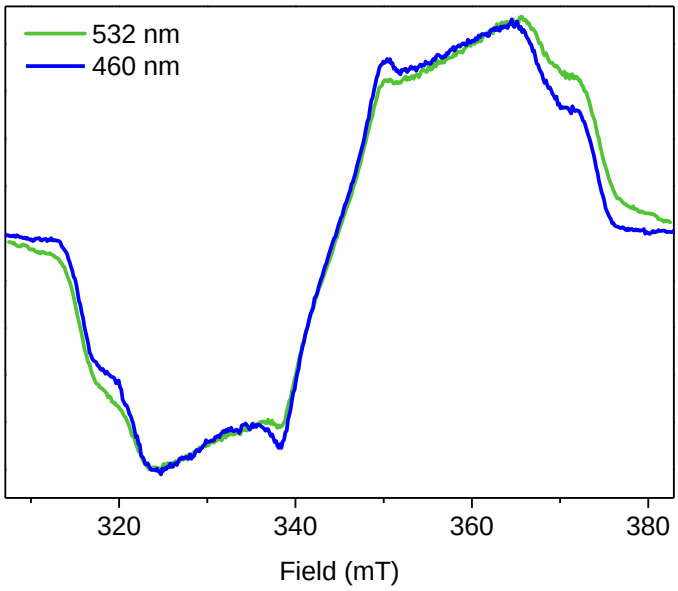

Figure S2.35. Direct-detection field sweep spectra of Pchlide photoexcited using 532 and 460 nm laser pulses reveal the formation of the same triplet state species regardless of the pump wavelength (80 K, Pchlide in degassed methanol solution).

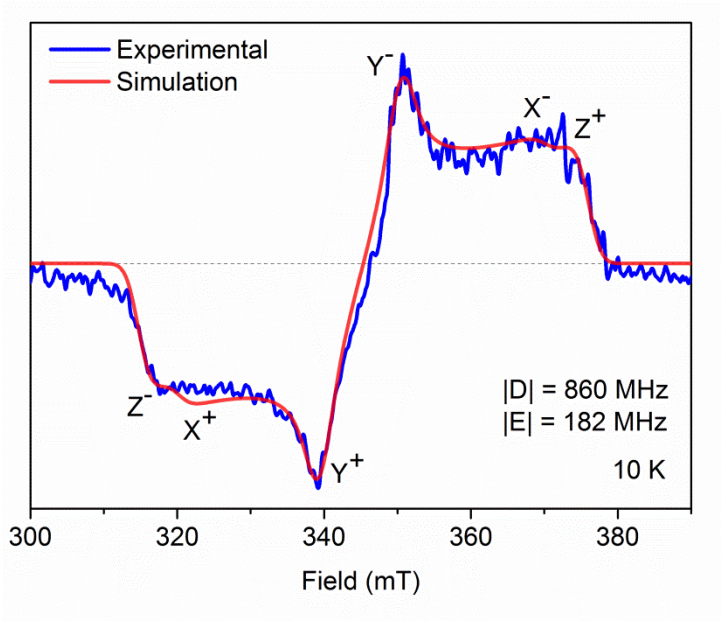

Figure S2.36. Experimental X-band direct detection field sweep spectrum of Pchlide recorded at 10 K in anaerobic aqueous buffer. The spectrum simulation is compared to the experimental one. The triplet sublevels were ordered as |Z| > |X| > |Y| and the six canonical orientations are indicated.

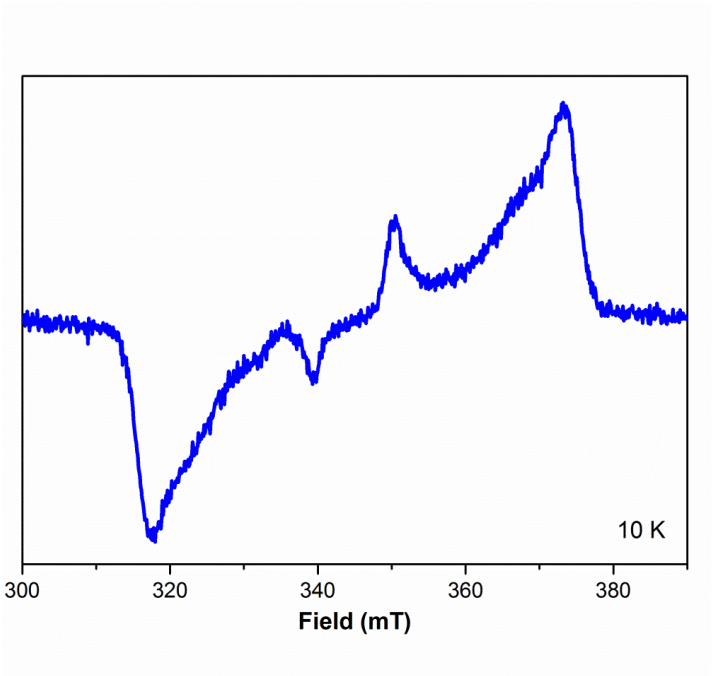

Figure S2.37. Two-pulse ESE field sweep of the Pchlide triplet (anaerobic alcohol solution, 10 K).

3 Excited-state dynamics of POR-bound protochlorophyllide at cryogenic temperatures

Manuscript draft pending submission

Authors: Guillem Brandariz-de-Pedro, Derren J. Heyes, Samantha J. O. Hardman, Michiyo Sakuma, Muralidharan Shanmugam, Stefan Weber, Daniel Nohr, David Collison, Nigel S. Scrutton, Alistair J. Fielding

Contributions: Chapter 3 is a manuscript draft written by GBP with guidance from DJH, SJOH and AJF. Purification of Pchlide was carried out by GBP with help from DJH. Purification of POR was carried out by GBP with help from Sakuma. Sample preparation was carried out by GBP. Ultrafast time-resolved measurements were conducted by SJOH with help from GBP. Laser flash-photolysis measurements were conducted by GBP with help from DJH. Pulse EPR measurements were conducted by GBP. trEPR measurements were carried out by DN with help from GBP. All time-resolved spectroscopy data was analysed by GBP with guidance from DJH and SJOH. All EPR data was analysed by GBP with guidance from AJF.

Excited-state dynamics of POR-bound protochlorophyllide at cryogenic temperatures

Guillem Brandariz-de-Pedro,[†,‡] *Derren J. Heyes,**[,‡] *Samantha J. O. Hardman,*[‡] *Michiyo Sakuma,*[‡] *Muralidharan Shanmugam,*[‡] *Stefan Weber,*[§] *Daniel Nohr,*[§] *David Collison,*[†] *Nigel S. Scrutton,*[‡] *Alistair J. Fielding**[⌉]

[†]School of Chemistry and the Photon Science Institute, University of Manchester, Oxford Road, Manchester M13 9PL, U.K.

[‡]Manchester Institute of Biotechnology, University of Manchester, 131 Princess Street, Manchester M1 7DN, U.K.

[§]Institute of Physical Chemistry, Albert-Ludwigs-Universität Freiburg, 79104 Freiburg, Germany.

[⌉] Liverpool John Moores University, School of Pharmacy and Biomolecular Sciences, Liverpool, L3 3AF.

AUTHOR INFORMATION

Corresponding Author

*E-mail: A.J.Fielding@ljmu.ac.uk

*E-mail: Derren.Heyes@manchester.ac.uk

3.1 ABSTRACT:

The photoreduction of protochlorophyllide, catalysed by protochlorophyllide oxidoreductase (POR), is a crucial step for the biosynthesis of chlorophyll in cyanobacteria, algae and plants. The POR protein has also been argued to play a photoprotective role inside plant cells. The relevance of this reaction lies, in part, to the fact that it is one of the few enzymatic reactions directly initiated by the absorption of light. This makes POR an interesting target of study for future development of light harvesting applications and an excellent candidate for enzymatic catalysis studies, since the reaction can be precisely triggered with a single laser pulse. Much like most enzymatic reactions, very short-lived intermediate species are involved, making the use of ultrafast analytical techniques essential to study such transient species. We have used cryogenic time-resolved absorption measurements to investigate the effects of protein-binding on the formation and decay rates of the Pchlide triplet excited-state. By means of cryo-trapping, we were able to study the excited-state dynamics of the stabilised hydrogen-transfer POR photoreduction intermediate for the first time. The stabilisation of such an intermediate allowed the use of electron paramagnetic resonance (EPR) spectroscopy techniques that operate at longer timescales and can provide novel insights on electron bonding and delocalisation in the intermediate species. We have used time-resolved continuous-wave EPR spectroscopy (trEPR) to provide the first direct characterisation of the excited-state triplet of the hydride-transfer POR reaction intermediate species. By means of three-pulse electron spin echo envelope modulation (3P-ESEEM) measurements, we also carried out a characterisation of the nuclear quadrupole and hyperfine coupling parameters of photoexcited enzyme-bound and free Pchlide.

KEYWORDS electron paramagnetic resonance, protochlorophyllide oxidoreductase, triplet state, photochemistry, time-resolved spectroscopy, excited state

3.2 INTRODUCTION:

The light-driven photoreduction of protochlorophyllide (Pchlide) into chlorophyllide (Chlide), which is catalysed by the enzyme protochlorophyllide oxidoreductase (POR), is an indispensable step for chlorophyll synthesis in photosynthetic organisms (see Figure 3.1).[103,109] Additionally, the POR enzyme has been found to play a photoprotective role in plant cells, reducing the formation of highly reactive radical species generated from photoexcited triplet states in the presence of molecular oxygen.[110,152,153]

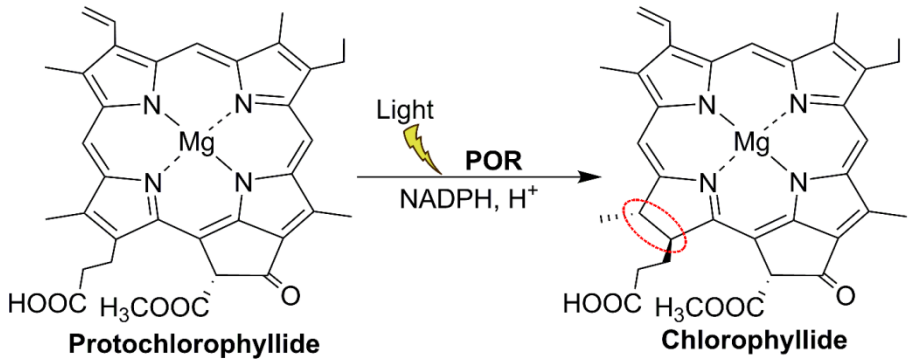

Figure 3.1. Schematic representation of the light-driven reduction of Pchlide.

POR forms a ternary complex with the Pchlide substrate and NADPH cofactor.[154] This complex, which is stable in the dark, reacts upon illumination.[111] The possibility to precisely trigger this reaction with laser pulses makes it an ideal model to study enzymatic catalysis. The photoreduction of Pchlide, which furnishes a *trans* hydrogenation product, has been shown to take place *via* a sequential mechanism in which a hydride from NADPH is transferred to the C17 position of the substrate followed by a thermally activated proton transfer, presumed to be from a Tyr residue in the protein active site, to the C18 position.[110,113,114,116,117,121] These processes have been reported to occur on the µs timescale, which is longer than the formation rate of all the known excited-state species derived from photoexcitation of the substrate, with the slowest-forming species, Pchlide's long-lived triplet state, being formed a few ns after photoexcitation.[22,122,129–134,155] Amongst the species involved in the light-induced dynamics of Pchlide is an intramolecular charge-transfer (ICT) state, which has been subject of many studies and has been previously suggested to favour the hydride

nucleophilic attack from NADPH.[21,122,128,156,157] A recent study on a POR active site mutant has proposed a new sequential reaction mechanism.[110] Despite the extensive research on this reaction, the exact mechanism of photochemistry has not yet been elucidated and the key excited-state species that triggers the reaction chemistry has not been identified. One of the problematic factors in unravelling the reaction mechanism of POR is the transient nature of some of the reaction intermediate species involved, which is prohibitively short for many techniques and limits the study of certain stages of the reaction to the use of ultrafast time-resolved experimental methods. Another limiting factor on the understanding of this biological system lies in the fact that the enzyme crystal structure has not yet been elucidated. This has impeded the characterisation of some basic aspects of the enzymatic process such as determining the geometry of the active site and reaction intermediates, as well as complicating the understanding of which residues are key for the reaction. As a result of this, a range of POR mutants have been studied to assess the role of different active site residues.[110,128] Several studies have used structural homology models based on enzymes from the short-chain dehydrogenase/reductase family, which is related to POR.[158–162] However, none of the enzymes of this family are light-driven and the corresponding homology models do not successfully display a functional active site.[157] A recent publication elaborated a theoretical chemistry protocol to propose a structure of POR that accounts for both its spectral features and enzymatic activity.[163]

In this work we have carried out time-resolved experiments at cryogenic temperatures on a range of POR-bound Pchlide samples, which allowed us to study the effect of POR on the excited state dynamics of the substrate while preventing reaction turnover. Moreover, we have successfully cryo-trapped the hydride-transfer intermediate, which allowed us to study this naturally short-lived species by laser flash photolysis and electron paramagnetic resonance (EPR) spectroscopy. It was also possible to carry out ultrafast absorption measurements that reflect the excited-state dynamics of this intermediate from the photoexcitation of its ground state until complete relaxation, rather than only on the states adopted during normal course of the reaction. EPR is a powerful technique for the study of paramagnetic species that can reveal information about their electron delocalisation, lifetimes and structure. We have successfully used this technique in the past to provide structural information on a light-activated protein and to provide direct evidence of a triplet state in Pchlide excited-state dynamics.[97,155]

In the case of POR, where the lack of a crystal structure has posed great difficulties to the understanding of the enzymatic mechanism, EPR can provide information from a completely new angle through its multiple specialised experimental variants.

3.3 RESULTS AND DISCUSSION:

In order to evaluate the effects of binding to the POR enzyme on the excited-state dynamics of Pchlide we first compared the time-resolved spectroscopic changes of free Pchlide against those of the bound species at cryogenic temperatures in three different samples: an active ternary POR-substrate complex (POR-Pchlide-NADPH), an inactive ternary POR complex (POR-Pchlide-$NADP^+$) and a reaction intermediate obtained by illuminating the active complex at 177 K for 20 minutes with a 450nm LED in order to cryo-trap a state where the hydride has already been transferred from the NADPH to the C17 position of Pchlide. This intermediate, which has been cryo-trapped previously, implies a change to the electronic structure of the substrate due to the addition of two electrons from the added hydride. [114] Time-resolved absorption measurements were carried out after 450 nm laser excitation of the samples. Ultrafast pump-probe spectroscopy and flash-photolysis experimental setups[155] were used to carry out measurements on the ps – 80 μs (Figure 3.2 A1-C1) and 150 μs – 100 ms (Figure 3.2 A2-C2) timescales, respectively.

Time-resolved data of protein samples displayed double peaks in the ground state bleach region (620-650 nm) and peak broadenings due to the presence of residual unbound substrate in the samples (Figure 3.2, S3.3-S3.8). Time-resolved data of the substrate[155] was subtracted from the time-resolved absorption datasets of the protein samples (Figures S3.9-S3.15) to remove the interference of free Pchlide. However, due to differences in the intensity of the excited state absorption features, the subtractions are not perfectly matched over the whole dataset. This makes it a lot more difficult to obtain meaningful information from global analysis of the data, a tool previously used to assign evolution associated difference spectra (EADS) and their lifetimes.[155]

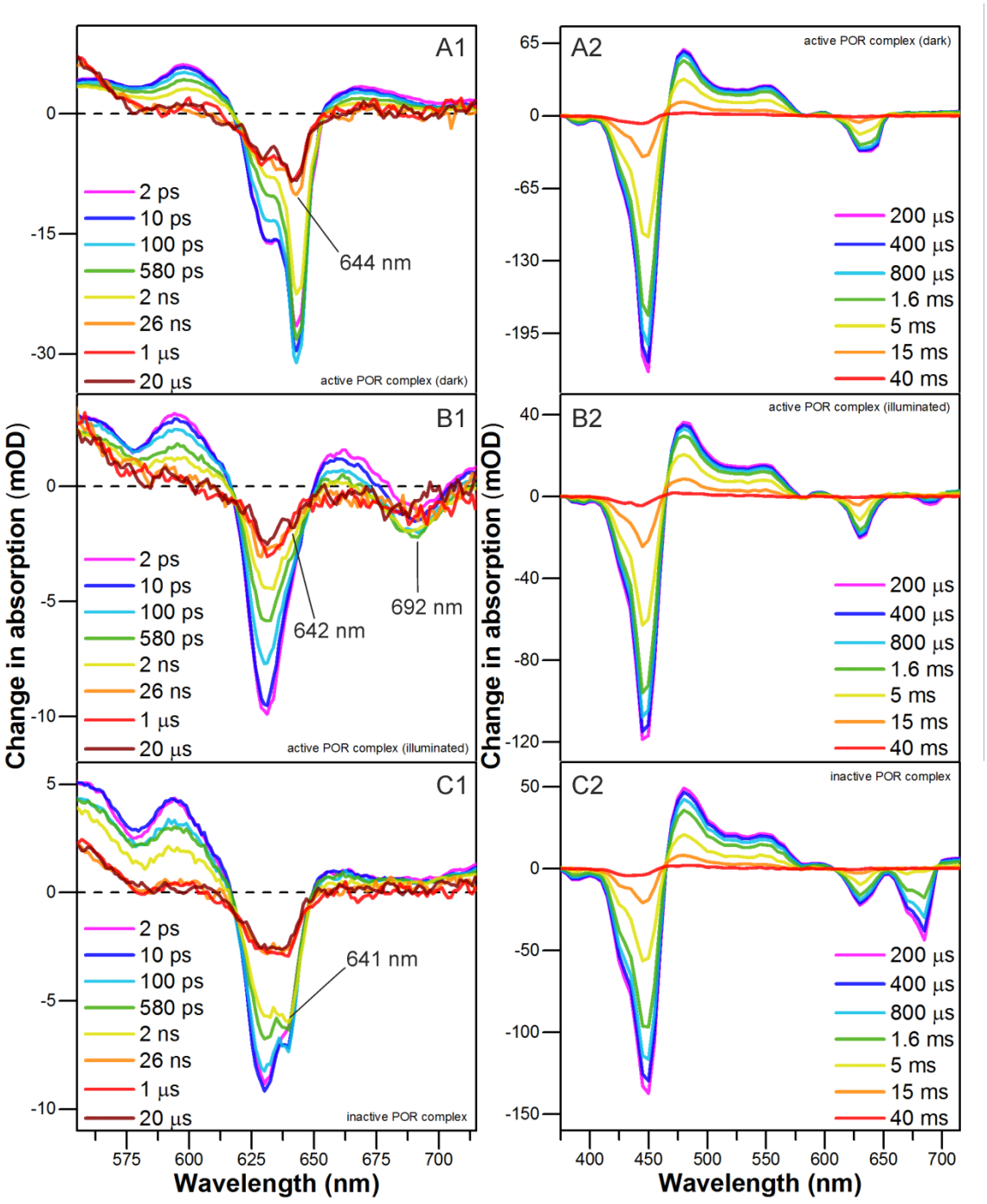

Figure 3.2. Selection of ultrafast (A1-C1) and flash-photolysis (A2-C2) absorption difference spectra of dark active POR complex (A), illuminated active POR complex (B) and inactive POR complex (C) samples.

The main absorptive feature of protein-bound Pchlide samples is red-shifted in comparison to the 631 nm absorption maximum of free Pchlide. The absorption maxima for the active POR complex (dark), active POR complex (after illumination at 177K) and inactive POR complex are 644, ~642 and 641 nm, respectively (Figure 3.2, S3.15). The spectrum of the illuminated active POR complex (Figure S3.15) resembles an

EADS previously observed in ultrafast absorption studies on the POR reaction corresponding to the hydride-transfer intermediate[127], and the spectrum also displays a secondary feature with maximum absorption at 692 nm, coinciding with previous steady state absorption studies.[113]

Due to the difficulty in analysing the data by global analysis the decay rates of the ground-state bleach (GSB) and triplet-state were calculated by fitting the raw (i.e. without the Pchlide only subtraction) transient absorption kinetic traces at 646 nm to a sum of exponentials (Figure 3.3, Table 3.1). This wavelength corresponds to the longer-wavelength isosbestic point of the main ground-state bleach feature of free Pchlide (Figure S3.15), where the signal of the unbound Pchlide is negligible and is likely to have a minimal effect on the POR-bound species spectra. The 692 nm feature of the hydride transfer intermediate was also fitted.

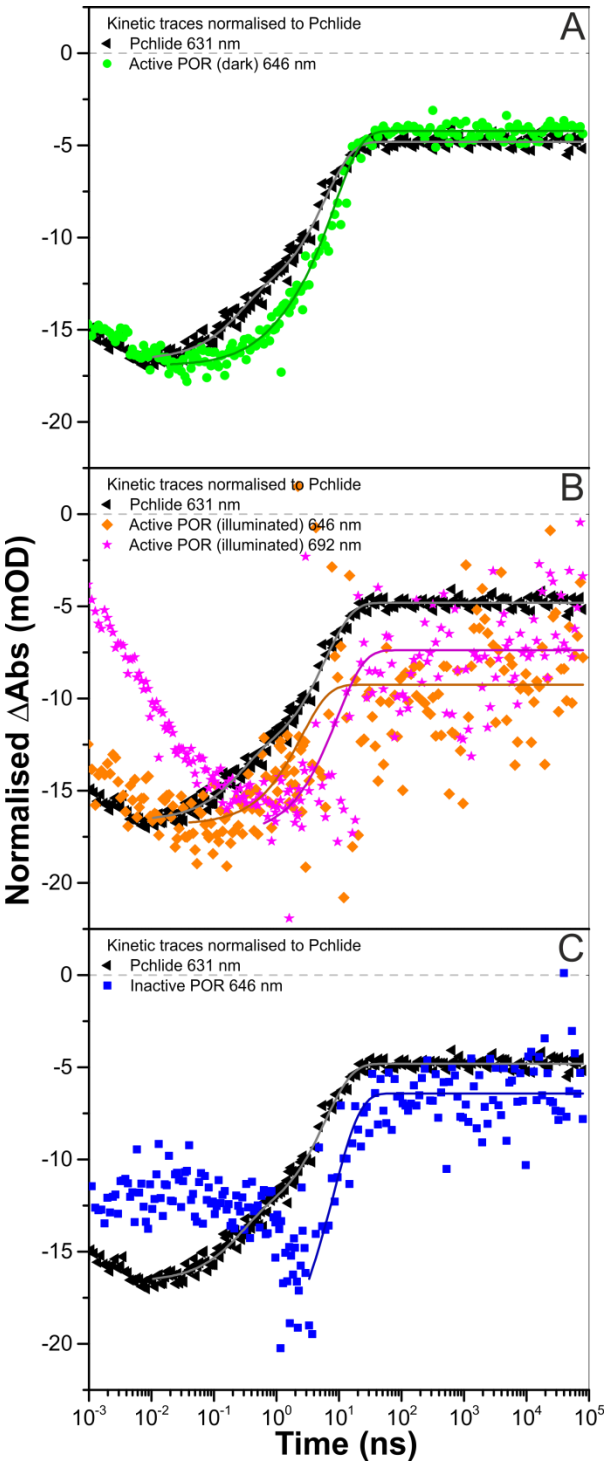

Figure 3.3. Ultrafast time-resolved absorption kinetic traces with corresponding GSB decay fits and free Pchlide reference trace (black triangles). (A) active POR complex (dark), (B) active POR complex (illuminated), (C) inactive POR complex.

The ground state bleach intensity reaches its maximum in just under 10 ps for free Pchlide (Figure 3.3 black trace). For the active POR complex (dark) the maximum intensity of the ground state bleach occurs at ~20 ps (Figure 3.3A green trace). In the case of the illuminated active POR complex, this feature grows in until ~40 ps

(Figure 3.3B orange trace), while the ground state bleach of the 692 nm band only reaches its maximum after ~600 ps (Figure 3.3B pink trace). The maximum intensity of the ground state bleach of the inactive POR complex is observed at ~2 ns (Figure 3.3C blue trace). In this case, part of the signal below 10 ps is most likely due to residual absorption from free Pchlide present in the sample. Early GSB decay lifetimes were obtained from fitting a single exponential decay from the point of maximum intensity of the ground state bleach traces. This decay is due to a combination of ground-state recovery and triplet-state formation. In the case of free Pchlide, the GSB decay of 6 ns exactly matches the triplet formation rate found in our previous work.[155] The early GSB decay was found to take place with lifetimes of 3-9 ns for all of the POR-bound samples (Table 3.1). Triplet decay lifetimes of free Pchlide and active POR were obtained by fitting the kinetic traces of flash photolysis data (time delays >150 μs after excitation) to double exponential decays (Figures S3.16-S3.19). As can be observed in Figure 3.3B-C, the triplet state decay starts to take place at within the ultrafast dataset timescales for inactive POR and illuminated active POR samples. In these cases, the longer components were fit from flash photolysis data (150 μs to 95 ms, Figures S3.17-S3.18) while an estimation of the faster component was calculated by fitting the ultrafast datapoints on the tens of microseconds timescale (Figures S3.20-S3.22). Despite the lower accuracy derived from fitting some of the faster lifetimes close to the dataset limits, all of the POR complex samples displayed significantly shorter triplet lifetimes than free Pchlide (Table 3.1). This finding supports the previously suggested photoprotective role of POR.[110,152,153]

Table 3.1. Lifetimes of monoexponential early GSB decay and double exponential triplet state decay for free and POR-bound Pchlide samples. (*a*: estimation from ultrafast dataset, Figures S3.20-S3.22).

sample	GSB decay (ns)	triplet decay 1 (μs)	triplet decay 2 (μs)
Pchlide	6.0 ± 0.3	1533 ± 280	9614 ± 117
active POR complex (dark)	8.4 ± 0.5	520 ± 167	4243 ± 15
active POR complex (illuminated, 646 nm)	2.5 ± 0.8	34 ± 45[a]	2577 ± 47
active POR complex (illuminated, 692 nm)	9.3 ± 2.5	7.6 ± 4.9[a]	1133 ± 24
inactive POR complex	8.0 ± 1.5	14 ± 23[a]	3007 ± 22

We have also used EPR to evaluate the effect of POR on the geometry of the triplet-state electronic environment. trEPR measurements were carried out at 80 K after 532 nm laser pulse photoexcitation. We measured four samples: Pchlide, active POR complex (dark), inactive POR complex and a hydride-transfer intermediate sample obtained by illuminating an active POR complex at 175 K for 20 minutes with a 450 nm LED inside the EPR cavity before cooling it down to 80 K prior to the measurement. trEPR field-sweep spectra were generated by representing an intensity average of EPR kinetic traces over a range of field positions for each sample (Figure 3.4). The field-sweep spectrum of the active POR complex (dark) was subtracted from that of the illuminated sample to reveal the EPR signature of the hydrogen-transfer reaction intermediate, the unique features of which were overlapping with those of the substrate, presumably due to the active POR complex only partially reacting upon illumination. A set of three illuminated control samples were also prepared and measured by trEPR. Free Pchlide, inactive POR complex and the reaction product, chlorophyllide (Chlide), were illuminated for 20 minutes with a 450 nm LED at 175 K and then measured at 80 K to make sure that the new signal induced by illumination was unique to the active ternary POR complex (Figure S3.23). Experimental zero-field splitting (ZFS) parameters were obtained from simulation of the field-sweep spectra (Figure 3.4).[149]

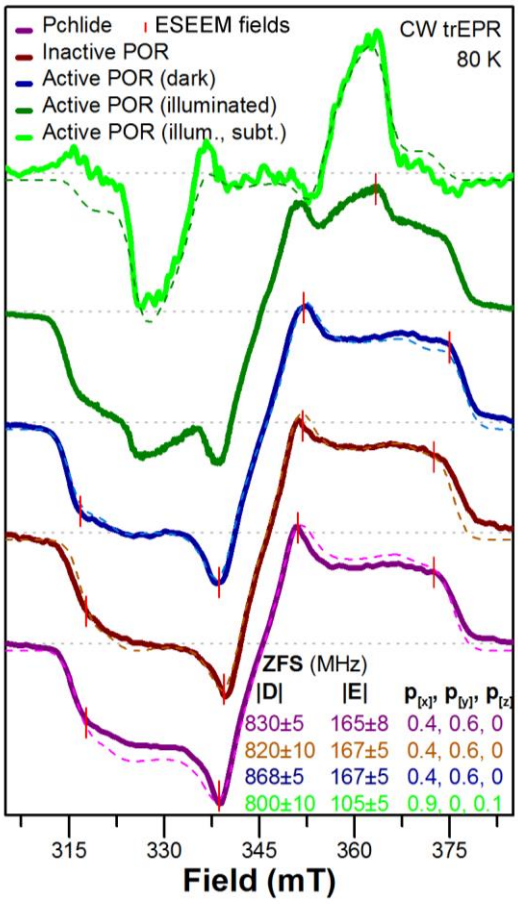

Figure 3.4. Field-sweep trEPR experimental data (solid lines, integration over 100 ns of maximum time-trace signal) including spectral simulations (dashed lines) of free Pchlide (purple), inactive ternary POR complex (brown), active ternary complex (blue), illuminated active ternary complex (dark green) and hydride-transfer intermediate (light green). Zero-field splitting parameters and triplet sublevel populations are given for each compound following the same colour scheme. Field positions selected for ESEEM measurements indicated (red).

The biggest difference between the samples containing intact Pchlide and the hydride transfer intermediate in terms of EPR lineshape is due to a drastic shift of the triplet polarisation pattern. While free Pchlide, inactive ternary POR complex and active ternary POR complex samples exhibit a population of the X and Y sublevels (with a ratio of 4 to 6), the hydride-transfer intermediate exhibits a population of the X and Z sublevels and a different population ratio (9 to 1). It is worth noting that the triplet state of the illuminated sample is not persistent (sample is EPR inactive without laser excitation). This means that a new triplet species is being generated rather than evolving from a polarisation rearrangement of the original substrate triplet. None of the illuminated control samples displayed features resembling those of illuminated active POR (Figure S3.23). The fact that the EPR spectrum of both Pchlide and Chlide display

a very similar lineshape while the illuminated active POR sample is radically different supports the theory that we are looking at the reaction intermediate species. The ternary POR complex samples display very similar ZFS parameters to free Pchlide, suggesting little change of electronic environment. In the case of the active POR complex (dark), the axial component of dipole-dipole interaction, *D*, was found to be larger. This would be consistent with the substrate porphyrin ring adopting a more planar geometry when bound to the POR enzyme as part of the active complex. The cryo-trapped hydride transfer intermediate displays smaller ZFS parameters than the other samples. These results suggest that the substrate adopts a higher symmetry geometry after the nucleophilic hydride addition from NADPH, which is an aspect of the reaction where no consensus has been found yet. This change in geometry could be due to both reaction-induced conformational changes of the active site and a loss of aromaticity of the porphyrin ring induced by the addition of two electrons, aromaticity being one of the factors favouring planarity in cyclic compounds containing delocalised double bonds.[55] Conformational changes have been previously linked to product release steps of the catalytic cycle of POR and were considered to take place in intermediate reaction steps.[21,116,124,132] The ZFS values of free Pchlide differ from those reported in our previous publication by 17-30 MHz.[155] The experimental setup used to acquire the trEPR data of this work consisted of a laboratory-build spectrometer specialising in this kind of measurements while our previous data was acquired in a pulsed-EPR setup converted in order to measure trEPR. The new setup provided us with much higher S/N ratio data and, consequently, a more accurate simulation (Figure S3.24).

EPR also allowed the measurement of the coupling of the triplet state electrons with the porphyrin nitrogen atoms and the evaluation of possible protein-induced changes of the electron delocalisation by means of three-pulse electron spin echo envelope modulation (3P-ESEEM). For pulsed EPR on frozen solution triplet states, a small amount of orientations are excited at a particular field position because of the broadening caused by ZFS, which makes these kind of measurements highly orientation-selective. By measuring at a field position corresponding to one of the turning points of a triplet EPR signature (Figure 3.4, red lines), one can have a close representation of the hyperfine couplings on the direction of the canonical transition associated to that field position. A series of 3P-ESEEM measurements were carried out on the Pchlide, active ternary POR complex (dark), inactive ternary POR complex and the hydride-transfer intermediate

samples from the trEPR measurements. Samples were measured at 10 K with 532 nm laser pulse photoexcitation. The inner- and outermost canonical transitions, Z^-, Y^+, Y^- and Z^+ (~318, ~340, ~352 and ~373 mT), were measured for the Pchlide, active POR (dark) and inactive POR complex samples. In the case of the illuminated active POR samples, one measurement was carried out at the field position corresponding to the X^- orientation (363 mT), which was the most intense, in an attempt to avoid as much intact active POR signal as possible. The microwave pulse sequence can be found in the supporting information. Quadrupole and hyperfine coupling parameters were obtained from simulation of the ESEEM data.[149] The ZFS, quadrupole and hyperfine tensor orientations used for the simulations were calculated with the ORCA quantum Chemistry package (B3LYP, EPR-II basis set).[150,151] A summary of the quadrupole and hyperfine coupling parameters for each sample is presented in Table 3.2. Frequency domain experimental and simulation data are represented in Figure 3.5.

Table 3.2. Quadrupole and hyperfine coupling interaction parameters from 3P-ESEEM spectral simulations.

sample	Q (MHz)	η	A_x (MHz)	A_y (MHz)	A_z (MHz)
Pchlide	0.63 ± 0.04	0.69 ± 0.04	0.6 ± 0.3	0.6 ± 0.4	8 ± 0.4
Inactive POR	0.65 ± 0.04	0.71 ± 0.06	0.6 ± 0.3	-0.5 ± 0.4	6.3 ± 0.5
Active POR (dark)	0.64 ± 0.04	0.7 ± 0.06	0.6 ± 0.3	0.6 ± 0.3	6.3 ± 0.4
Active POR (illum.)	0.65 ± 0.06	0.75 ± 0.12	0.6 ± 0.3	0 ± 0.4	6.3 ± 0.6

Experimental data displayed peaks between 13 and 16 MHz. These matched the calculated proton nuclear frequencies at the different experimental field positions sorted from lower to higher field: ~13.5, ~14.4, ~15.0, 15.4 and ~15.9 MHz. The experimental intensity of the proton signals greatly varied according to the magnetic field. For some of the transitions, especially ~339 mT (Y^+), most of the signal was due to the protons and the S/N ratio of the nitrogen couplings was relatively poor. This can also be observed in the corresponding experimental time traces (Figures S3.25-S3.37). The hyperfine coupling values of Pchlide are relatively close to those found for other porphyrins.[164] However, the Q parameter was found to be much smaller than the one found in other porphyrins and porphine, which generally displayed Q values higher than 2 MHz.[164,165] The simulations for ~318 and ~373 mT field positions displayed the 0.5, ~1.5, 3.1 and ~6.2 MHz features at the right frequency. However, the ~1.5 MHz features appeared at a larger intensity ratio than the one observed in experimental data.

Simulations using two pairs of nitrogens did not offer a substantial improvement of the simulation quality.

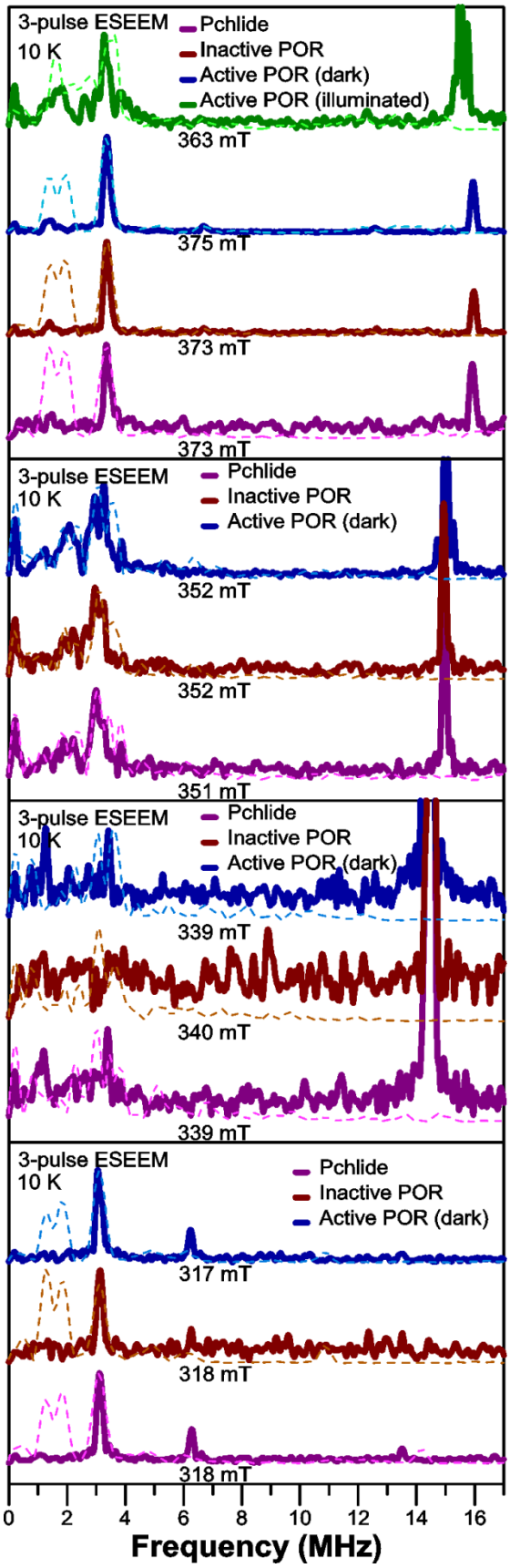

Figure 3.5. 3P-ESEEM frequency-domain experimental data (solid lines) including simulations (dashed lines) of free and POR-bound Pchlide samples. Subplots group data by field position.

This work supports previous findings suggesting a possible photoprotective role of POR by providing a direct comparison between the time-resolved spectral changes of free and POR-bound Pchlide and reveals shorter triplet-state lifetimes for the protein-bound substrate. It also provides the first time-resolved absorption and EPR data on the stable hydride-transfer reaction intermediate in Pchlide photoreduction, revealing significantly distinct properties between the intermediate and both the substrate and product of the reaction. The data in this work allowed fitting of the ns-timescale GSB decay (related to triplet formation) and triplet decay lifetimes of this reaction intermediate. More importantly, our study paves the way for future experiments (at lower Pchlide concentrations to fully remove any unbound substrate) that allow for an accurate global analysis of the data. Identifying the different excited-state species and EADS of this isolated intermediate would allow comparison to the spectral features of the reaction intermediate observed during a complete reaction turnover. This could be crucial to determine the point at which this species is formed and which of the excited states of Pchlide are directly involved in the photoreduction. EPR appears to be a valuable tool for studying this reaction and may provide more information on how POR alters the electron delocalisation of the substrate. Future experiments at lower concentrations with fully bound and fully reacted substrate will help obtain more meaningful EPR data too, especially for pulsed techniques. Currently on-going HYSCORE measurements and simulations could also provide an important improvement on the determination of quadrupole and hyperfine interaction parameters, since this technique has been found to show an advantage over 3P-ESEEM for triplet states in frozen solution samples.[59] Moreover, improved computational results of EPR properties could be achieved by using molecular geometries that take into account binding to the protein in the calculation input.

ASSOCIATED CONTENT

Supporting Information.

The following files are available free of charge. Protein and substrate purification protocol, detailed experimental methods, transient absorption data, EPR data (PDF).

AUTHOR INFORMATION

Notes

The authors declare no competing financial interests.

ACKNOWLEDGMENTS

G.B.-P. acknowledges Early Stage Researcher funding from the European Union's Seventh Framework Programme FP7-PEOPLE-2013-ITN through the 'MAGnetic Innovation in Catalysis' (MAGIC) Initial Training Network (Grant agreement no. 606831). We would like to acknowledge the use of the EPSRC EPR National Service in carrying out this work. NSS is an Engineering and Physical Sciences Research Council (EPSRC) Established Career Fellow (EP/J020192/1). Ultrafast spectroscopy was performed at the Ultrafast Biophysics Facility, Manchester Institute of Biotechnology, as funded by BBSRC Alert14 Award BB/M011658/1.

3.4 SUPPORTING INFORMATION:

Excited-state dynamics of POR-bound protochlorophyllide at cryogenic temperatures

Guillem Brandariz-de-Pedro,[†,‡] Derren J. Heyes,*[,‡] Samantha J. O. Hardman,[‡] Michiyo Sakuma,[‡] Muralidharan Shanmugam,[‡] Stefan Weber,[§] Daniel Nohr,[§] David Collison, [†] Nigel S. Scrutton,[‡] Alistair J. Fielding,*[,⌉]

[†]*School of Chemistry and the Photon Science Institute, University of Manchester, Oxford Road, Manchester M13 9PL, U.K.*

[‡]*Manchester Institute of Biotechnology, University of Manchester, 131 Princess Street, Manchester M1 7DN, U.K.*

[§]*Institute of Physical Chemistry, Albert-Ludwigs-Universität Freiburg, 79104 Freiburg, Germany*

[⌉]*Liverpool John Moores University, School of Pharmacy and Biomolecular Sciences, Liverpool, L3 3AF.*

Corresponding Authors

*E-mail: A.J.Fielding@ljmu.ac.uk

*E-mail: Derren.Heyes@manchester.ac.uk

Contents

3.4.1 Purification of 6xHis-tagged POR from T. elongatus

Expression

BL21 pLysS cells (Agilent) were transformed with the pET9His+POR plasmid.[166] Cell colonies were grown on Luria–Bertani (LB) medium agar plates containing 30 μg/mL kanamycin and 25 μg/mL chloramphenicol and used to grow overnight cultures at 37 °C in flasks containing 100 mL of LB medium and 30 μg/mL kanamycin and 25 μg/mL chloramphenicol. 5 mL of this culture was used to inoculate 2 L flasks containing 500 mL of the same medium and grown at 30 °C for 3 hours. The cells were then grown at 25 °C until an OD_{600} of ~0.6 was reached. Protein expression was induced by adding IPTG (final concentration 0.1 mM). The cells were then incubated overnight at 25 °C and collected by centrifuging the cultures at 6 krpm for 15 minutes. The cell pellets were then stored frozen at -20 °C.

Purification

A cell pellet was resuspended in 150 mL cold Ni-binding buffer (50 mM Tris-HCl pH 7.5, 500 mM NaCl, 5 mM imidazole) containing a tablet of protease inhibitor (Roche Applied Science). 200 μL of DNAse (2500 units/mL) were added to the solution to denature DNA. The cells were disrupted with 20 cycles of sonication (20 second pulse, 1 minute rest) with an ultrasonic homogeniser (Bandelin Sonopuls), centrifuged at 20 krpm for 30 minutes and then the cell debris precipitate was discarded. Protein precipitation was induced by adding 20% NH_4SO_4 to the supernatant solution. The suspension was then centrifuged at 12 krpm for 30 minutes.

Nickel column

The protein pellet was dissolved in ~100 ml of Ni-binding buffer and loaded into a 25 ml nickel-IDA chelating resin (Formedium Ltd) column. The resin and solution were mixed for 30 minutes at 4 °C and left to settle for 5 minutes. After discarding the supernatant, the column was equilibrated with 4 column volumes (cv) of Ni-binding buffer. Subsequently, the column was washed with 6 cv of Ni-wash buffer (50 mM Tris-HCl pH 7.5, 500 mM NaCl, 50 mM imidazole) to remove impurities that, unlike His-tagged POR, do not tightly bind to the chelating resin. Finally, POR was eluted with 6 cv of Ni-elute buffer (50 mM Tris-HCl pH 7.5, 500 mM NaCl, 250 mM imidazole). The elution fraction was precipitated by adding 50% NH_4SO_4 and then centrifuged at 12 krpm for 20 minutes.

Blue sepharose LC

The pellet was resuspended in 100 ml of cold Blue-start buffer (50 mM Tris-HCl pH 7.5, 25 mM NaCl, 1 mM DTT). The solution was then filtered and passed down a 20 ml Blue sepharose column at a 1 ml/min rate. A wash phase consisting of 50 ml Blue-start buffer followed by 50 ml 20% Blue-elute buffer (50 mM Tris-HCl pH 7.5, 2.5 M NaCl, 1 mM DTT) was carried out before elution. The elution cycle consisted of a gradient starting at 20% and going up to 100% Blue-elute buffer over a range of 150 ml. The column was finally washed with 50 ml of 100% Blue-elute buffer. The collected elution fractions containing the most POR were pooled. Precipitation was induced by adding 50% NH_4SO_4 and the suspension was centrifuged at 20 krpm for 30 minutes. After discarding the supernatant, the protein was resuspended in 10 ml activity buffer (50 mM Tris-HCl pH 7.5, 100 mM NaCl, 1 mM DTT), run through a desalting column and concentrated down to ~ 3 ml using 10 kDa MW cutoff Vivaspin concentrators (Sartorius).

Sodium dodecyl sulfate–polyacrylamide gel electrophoresis (SDS-PAGE) was used to evaluate the purity of POR at different stages of the expression and purification. This was carried out using precast gels and a Criterion Gel Imaging System from BioRad.

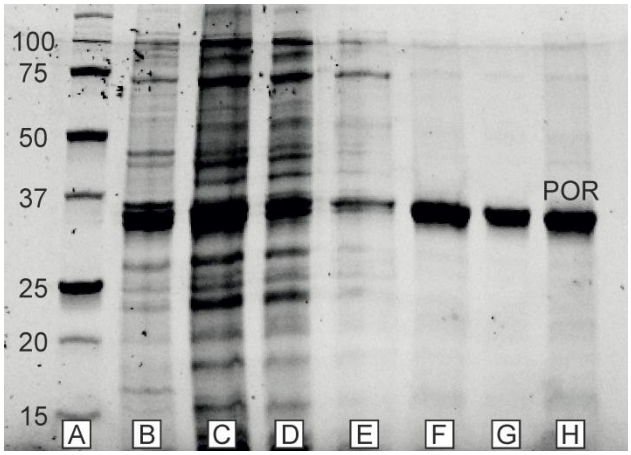

Figure S3.1. SDS-PAGE displaying the protein content at different stages of the purification process. (A) BioRad Precision Plus Protein Standard. (B) Induced cell extract. (C) Disrupted cell extract. (D) Ni column run-through. (E) Ni column wash. (F) Ni column elution. (G) Blue sepharose run-through. (H) Blue sepharose elution.

Concentration determination

The final concentration of POR was determined with a standardised bovine serum albumin (BSA) colorimetric test (BioRad DC Protein Assay). A detergent and a chromophoric reagent were added to solutions containing a range of BSA concentrations, as well as to a range of POR dilutions. The concentration was calculated by measuring the absorbance of the POR dilutions and comparing it to a linear regression of the absorbance of the BSA standard solutions.

3.4.2 Purification of protochlorophillyde

Colonies of *R. capsulatus* ZY5 were grown overnight at 34 °C in three flasks containing 100 mL VN (10 g yeast extract, 1 g K_2HPO_4, 0.5 g $MgSO_4$ per litre and 25 µg/ml rifampycin, pH 7). The culture was then distributed among six flasks containing 1 L VN media. Three polyuretane foam bungs were introduced in each flask for Pchlide to adsorb onto. The culture was grown over 5 days at 34 °C. The foam bungs were then left to dry in a dark, ventilated space at room temperature for a few days. Once dry, the bungs were washed with methanol until most of the green coloration from adsorbed Pchlide had faded. Methanol was then removed from the solution in a rotary evaporator and the pigment precipitate was resuspended in acetone. A small amount of methanol (<2 % total volume) was added to aid resuspension. The acetone suspension was passed

through a pre-equilibrated 50 mL CM Sepharose column (Sigma), which was then washed with acetone (6 cv) until complete removal of carotenoids (orange flow-through). Subsequently, the column was washed with 10 cv of MeOH 1:19 Acetone to remove other subproducts like pheophorbide and phytol. Finally, when the flow-through solution was free of impurities, Pchlide was eluted with MeOH 2:3 Acetone until the flow-through became pale green (20 cv). The Pchlide elution fraction was concentrated down to ~50 ml with a rotary evaporator, then split among black 1.5 ml eppendorfs and left to dry in a dark, ventilated environment at room temperature before being stored at -20 °C.

UV-Vis spectra of the suspension and different fractions were measured at the various stages of the purification process (Cary UV-Vis spectrometer, Agilent Technologies).

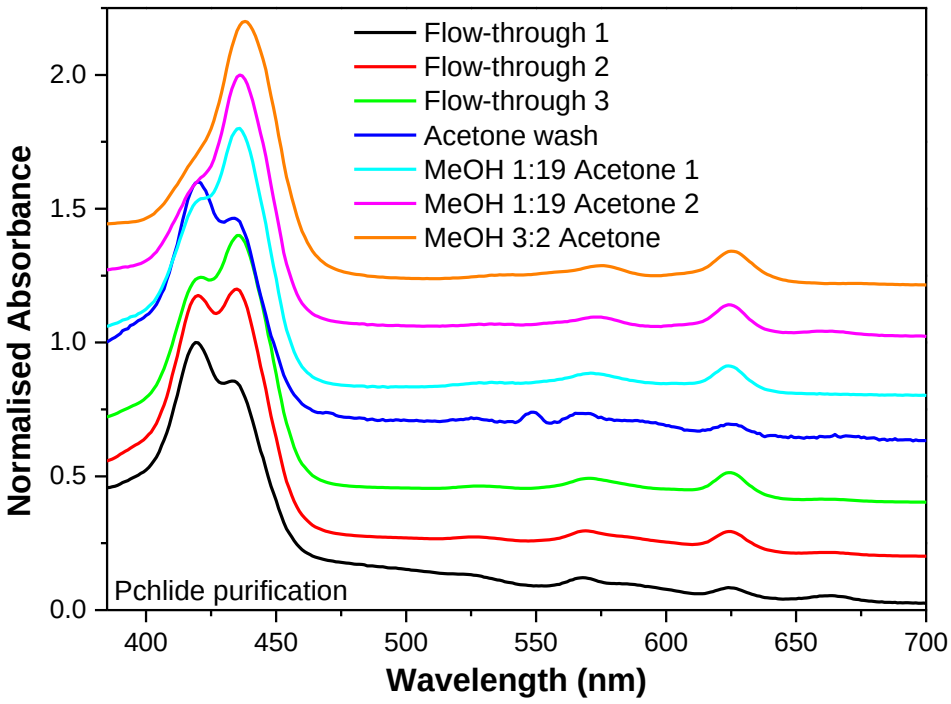

Figure S3.2. UV-Vis spectra of fractions collected throughout the column purification process. Spectra normalised to 1 and offset by 0.2 for clarity.

3.4.3 Ultrafast Pump-Probe Spectroscopy

Excited state dynamics of light-activated reactions on the fs-μs timescale can be followed by means of laser spectroscopy measurements. In a pump-probe setup, a first laser pulse (pump) results in light absorption from the sample, triggering the photolysis events of interest. This is then followed by a second light pulse (probe) that allows for recording absorption at fixed DAF values. It is possible to measure differences in absorption at ultrafast timescales with a time resolution of less than 200 fs. This technique has already been used to study the steps and species involved with photoexcitation of Pchlide on its own and complexed with POR[20–23].

The experimental setup used for ultrafast pump-probe spectroscopy measurements consisted of a cryogen-free cryostat (Oxford Instruments) containing a 2 mm path length sample holder, an OPA generating 450 nm pump pulses, a white light continuum probe and two broadband transient absorption spectrometers as described in a previous publication.[155] All datasets were collected at 10 K on anaerobic samples composed of 50 μM Pchlide, 100 μM POR, NADP cofactor, 40 v% glycerol, 20 m/v% sucrose, 50 mM Tris-HCl, pH 7.5, 1 v% Genapol. Active POR contained 1 mM NADPH and was prepared and kept in the dark. Inactive POR contained 5 mM $NADP^+$. The cryotrapped hydride-transfer reaction intermediate sample was prepared by illuminating an active POR sample with ~900 mW 455 nm radiation generated by a Thorlabs M455L3 LED for 20 minutes at 177 K before being cooled down to 10 K. The datasets from the two spectrometers were merged for each sample as described previously, forming final datasets with a 1 ps to 80 μs time range.[127]

3.4.4 Flash Photolysis

Slower time-resolved measurements were carried out using the laser flash photolysis technique. This method involves illuminating the sample with a high-power flash or laser pulse in order to generate transient concentrations of intermediates that are high enough to be measured. In this kind of measurements, the concentration of reactants, intermediates or products can be followed as a function of delay after flash (DAF). This type of kinetic measurements is appropriate for measuring on μs-s timescales and is an invaluable tool to study photochemical processes.[1]

Sample cuvettes (1 cm path length) were contained in a liquid nitrogen cryostat (Opstistat DN, Oxford Instruments). The rest of the setup consisted of an OPO (pumped by a Nd:YAG laser) achieving 450 nm 15 mJ pulses and a spectrometer measuring single-wavelength absorption transients (750 to 375 nm, 150 μs to 95 ms) as described in a previous publication.[155] The datasets were composed by averaging four sets of measurements at 80K on anareobic samples composed of 20 μM Pchlide, 120 μM POR, NADP cofactor, 40 v% glycerol, 20 m/v% sucrose, 50 mM Tris-HCl, pH 7.5, 1 v% Genapol. Active POR contained 1 mM NADPH and was prepared and kept in the dark. Inactive POR contained 5 mM $NADP^+$. The cryotrapped hydride-transfer reaction intermediate sample was prepared by illuminating an active POR sample with ~900 mW 455 nm radiation generated by a Thorlabs M455L3 LED for 20 minutes at 177 K before being cooled down to 80 K.

3.4.5 Time-resolved absorption spectroscopy data analysis

In order to characterise the spectral properties of each of the POR-bound species, free Pchlide data under the same conditions (from previous work[155]) were subtracted from each dataset. In the case of ultrafast pump-probe spectroscopy measurements, the original datasets were subtracted separately and then merged. The resulting Pchlide-subtracted datasets displayed a good visual representation of the excited-state dynamics of the different POR-bound species and were used to assess the most relevant time-traces to study for each sample. Pchlide-subtracted time-resolved spectra were also averaged over the 30 ns – 1 μs time frame, in which the triplet state is the only appreciable species in order to compare the main features of the triplet species from the various samples (Figure S3.15).The time-traces selected for kinetic analysis of the raw data correspond to the isosbestic point of Pchlide (646 nm) for the primary spectral features in all POR samples and an isolated secondary feature in the hydride-transfer intermediate sample (692 nm) in order to minimise the effect of residual free Pchlide on the fitting of excited-state dynamics. In the case of raw flash photolysis data, time-traces corresponding to the isosbestic wavelength of the main features of POR-bound species were plotted in order to observe the kinetics of free Pchlide present in the protein samples. According to this, the 625 nm traces were chosen for all samples. Moreover, in the case of active POR (dark) the 630 nm trace was also plotted, as the isosbestic point

of bound Pchlide in this sample falls between these two wavelengths. For each sample, the selected traces were plotted alongside the 645 nm traces, which correspond to the isosbestic point of free Pchlide, thus displaying the kinetics of the POR-bound species at hand. Figures S3.16-S3.18 display the triplet decay of the Pchlide present in each sample alongside its POR-bound counterpart.

3.4.6 Time-resolved CW EPR

An OPO system (BBO VIS/IR, Opta) pumped by a Nd:YAG laser (GCR 190-10, Spectra Physics) and tuned to deliver 532 nm pulses (6 ns, ~2.3 mJ, 10 Hz) was used to generate the photoexcited triplet states of free and POR-bound Pchlide samples. X-band trEPR measurements were performed on a laboratory-built spectrometer based on a Bruker ESP380E with a Bruker microwave bridge (ER 046 MRT, Bruker) and equipped with a laboratory-built nitrogen gas-flow cryostat at a temperature of 80 K. The measurements were performed using a critically coupled dielectric resonator (ER 4118X-MD5, Bruker) and a Teledyne LeCroy 9354A transient recorder. Laser-induced baseline distortions were corrected by subtracting a signal measured at an off-resonant field position. Samples consisted of anaerobic solutions of Pchlide and POR contained in 3 mm inner diameter quartz tubes (250 µM Pchlide, 900 µM POR, NADP cofactor, 40 v% glycerol, 20 m/v% sucrose, 50 mM Tris-HCl, pH 7.5, 1 v% Genapol). Active POR contained 2.5 mM NADPH and was prepared and kept in the dark. Inactive POR contained 12.5 mM $NADP^+$. The cryotrapped hydride-transfer reaction intermediate sample was prepared by illuminating an active POR sample with ~900 mW 455 nm radiation generated by a Thorlabs M455L3 LED for 20 minutes at 175 K before being cooled down to 80 K. All samples were stored in liquid nitrogen for subsequent pulsed EPR measurements. Simulations of the trEPR triplet spectra were performed using the Easyspin software extension for Matlab.[149]

3.4.7 Three-pulse ESEEM

A Nd:YAG laser (Minilite, Continuum) frequency doubled to deliver 532 nm (~5 ns, ~6 mJ, 10 Hz) was used to generate the photoexcited triplet species of free and POR-bound Pchlide samples. X-band three-pulse ESEEM measurements were performed on

an X-band Bruker Elexsys E580 spectrometer equipped with a cryogen-free cryostat (ER 4118HV-CF58 FlexLine Cryogen-Free, Bruker) and a Bruker MD5 resonator. The stimulated-echo envelope was obtained using the pulse sequence $\pi/2 \rightarrow \tau \rightarrow \pi/2 \rightarrow T \rightarrow \pi/2 \rightarrow \tau \rightarrow$echo with mw pulses of lengths $t_{\pi/2}$ = 16 ns and t_{π} = 32 ns. The initial T length was of 64 ns and was incremented by 8 ns per point (1024 points total). A standard 4 step cycle was used to suppress artifacts and eliminate unwanted echoes. Three different τ values (100, 160 and 200 ns) were used to minimise the effect of signal supression. Measurements were carried out at field positions corresponding to the outer- and innermost emission and absorption transitions (Z^-, Y^+, Y^- and Z^+ transitions) of each sample (same samples from trEPR measurements). For the illuminated active POR sample, the field position corresponding to the maximum absorption feature was chosen. The recorded time-domain ESEEM signals were processed with a home-written Matlab script consisting of a polynomial baseline correction, Hamming window data apodisation, zero-filling and Fourier transform. The hyperfine tensor and nuclear quadrupole parameters were obtained from simulating the baseline-corrected time-domain traces and final frequency domain data using the pepper function within the Easyspin software extension for Matlab.[149] The g and ZFS tensors were kept fixed to the values from previous trEPR simulations, whereas ZFS, hyperfine and nuclear quadrupole tensor orientations were set to the values obtained from a DFT calculation using the B3LYP hybrid functional and the EPR-II basis set (6-31G(d) basis set for Mg) in ORCA, as previously described by Sinnecker.[150,151,167] The orientation of the hyperfine, quadrupole and g tensors respect to the ZFS tensor were defined by the following sets of Euler angles (ZYZ rotation): hyperfine α = 31.4°, β = -2.3°, γ = -104.7°, quadrupole α = -2.3°, β = -88.2°,γ = -72.5°, g α = -12.6°, β = -92.6°, γ =101.9°. The hyperfine and quadrupole orientations corresponding to the three remaining ^{14}N nuclei are related by symmetry.

3.4.8 Supporting data

Raw time-resolved absorption spectroscopy data

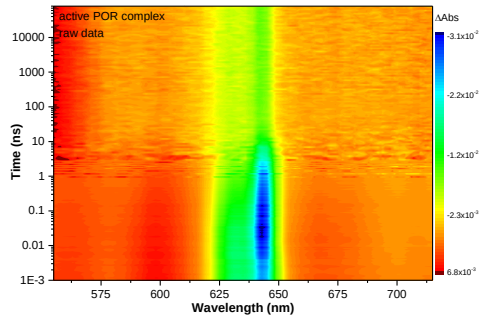

Figure S3.3. Time-resolved visible spectroscopy data for the active POR complex in anaerobic buffer at 10 K after photoexcitation at ~450 nm. Time-resolved difference spectra were recorded between 1 ps and 80 μs.

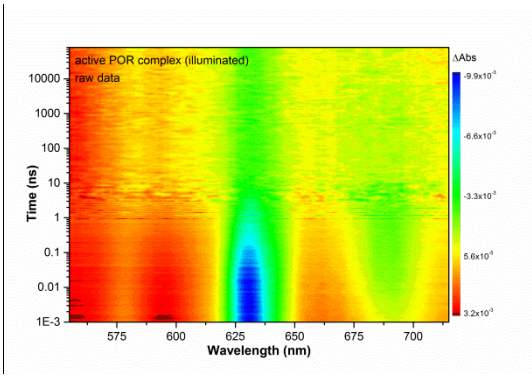

Figure S3.4. Time-resolved visible spectroscopy data for illuminated active POR complex in anaerobic buffer at 10 K after photoexcitation at ~450 nm. Time-resolved difference spectra were recorded between 1 ps and 80 μs.

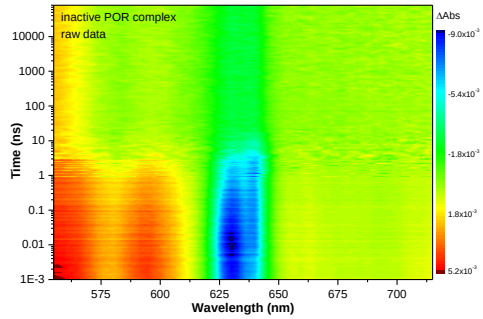

Figure S3.5. Time-resolved visible spectroscopy data for inactive POR complex in anaerobic buffer at 10 K after photoexcitation at ~450 nm. Time-resolved difference spectra were recorded between 1 ps and 80 μs.

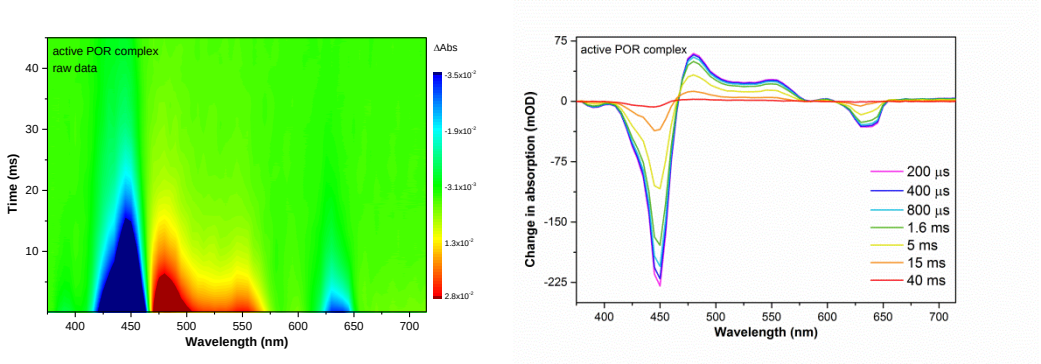

Figure S3.6. Time-resolved visible spectroscopy data and selected spectra for the active POR complex in anaerobic buffer at 80 K after photoexcitation at 450 nm. Kinetic transients were recorded at single-wavelengths between 375 and 750 nm over 85ms.

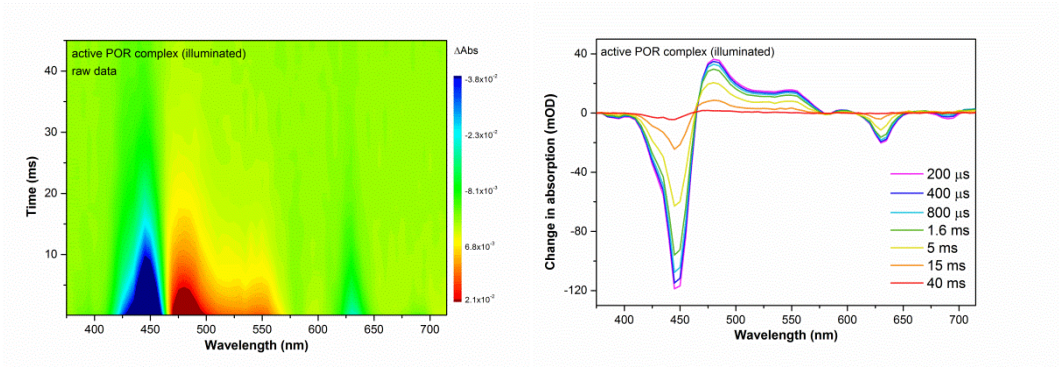

Figure S3.7. Time-resolved visible spectroscopy data and selected spectra for illuminated active POR complex in anaerobic buffer at 80 K after photoexcitation at 450 nm. Kinetic transients were recorded at single-wavelengths between 375 and 750 nm over 85ms.

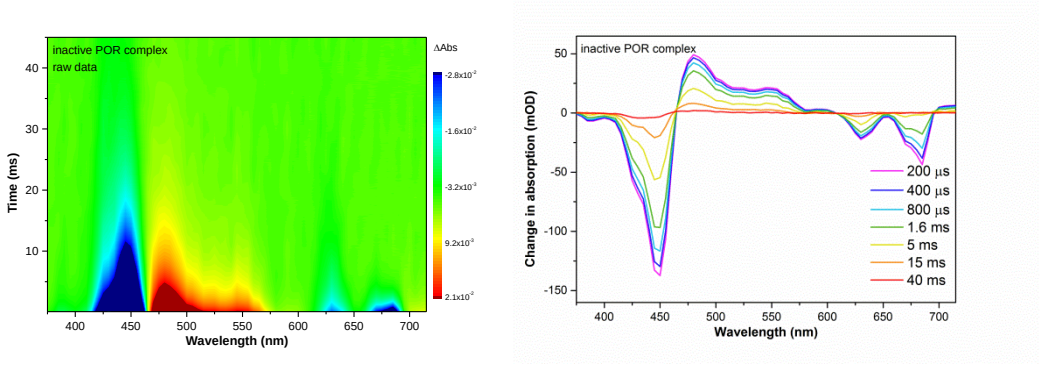

Figure S3.8. Time-resolved visible spectroscopy data and selected spectra for inactive POR complex in anaerobic buffer at 80 K after photoexcitation at 450 nm. Kinetic transients were recorded at single-wavelengths between 375 and 750 nm over 85ms.

Pchlide-subtracted ultrafast absorption spectroscopy datasets

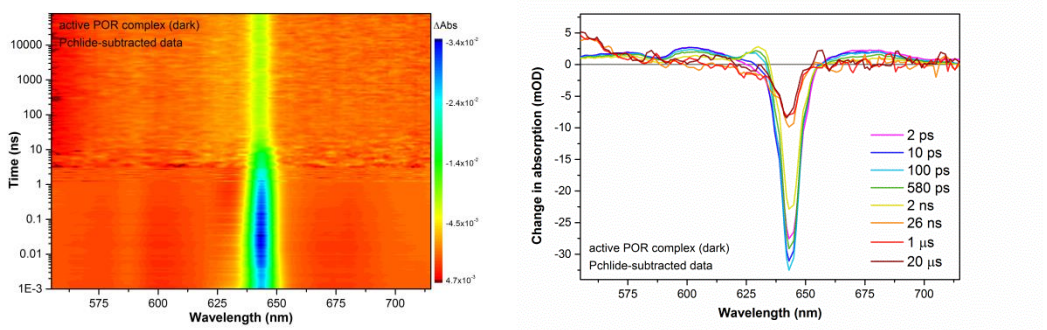

Figure S3.9. Time-resolved visible spectroscopy data and selected spectra for the active POR complex after subtracting the time-resolved spectral changes of free Pchlide as described in the experimental section.

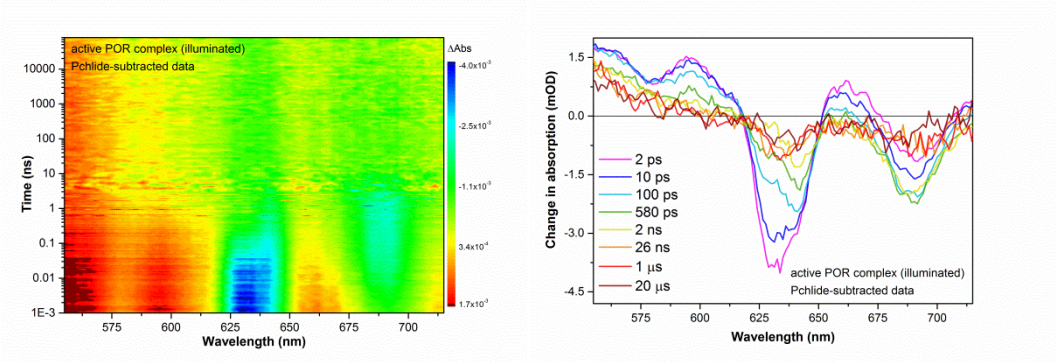

Figure S3.10. Time-resolved visible spectroscopy data and selected spectra for illuminated active POR complex after subtracting the time-resolved spectral changes of free Pchlide as described in the experimental section.

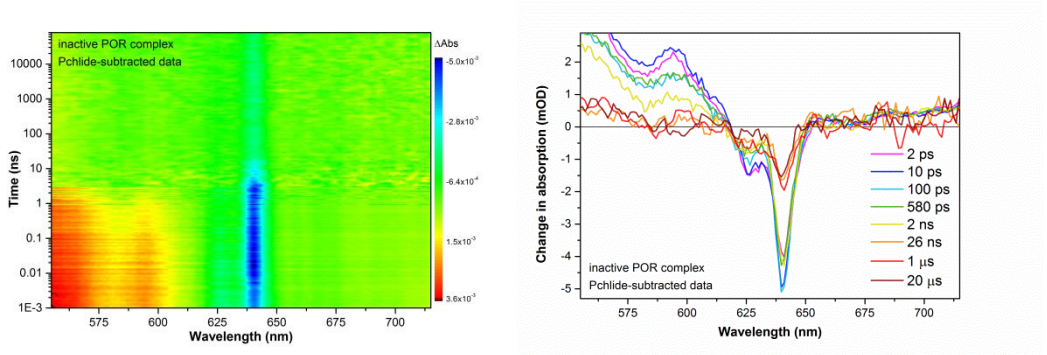

Figure S3.11. Time-resolved visible spectroscopy data and selected spectra for inactive POR complex after subtracting the time-resolved spectral changes of free Pchlide as described in the experimental section.

Pchlide-subtracted flash-photolysis spectroscopy datasets

Note: The subtracted ms-timescale Pchlide dataset had been recorded up to 675 nm. Wavelengths above that have been left blank in this section to maintain the aspect ratio of raw data plots and make direct visual comparison more straightforward.

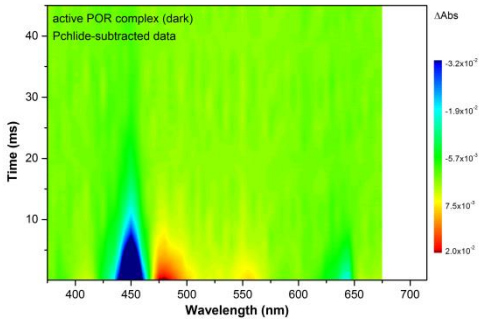

Figure S3.12. Time-resolved flash-photolysis data for the active POR complex after subtracting the time-resolved spectral changes of free Pchlide as described in the experimental section.

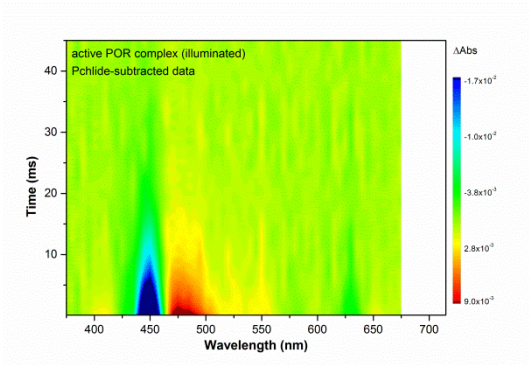

Figure S3.13. Time-resolved flash-photolysis data for illuminated active POR complex after subtracting the time-resolved spectral changes of free Pchlide as described in the experimental section.

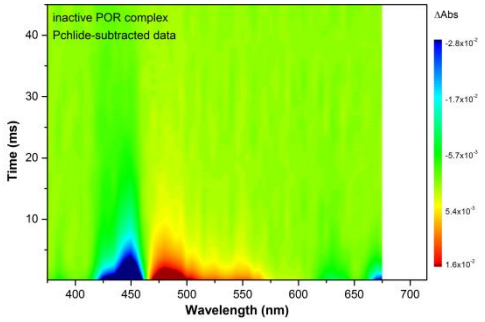

Figure S3.14. Time-resolved flash-photolysis data for inactive POR complex after subtracting the time-resolved spectral changes of free Pchlide as described in the experimental section.

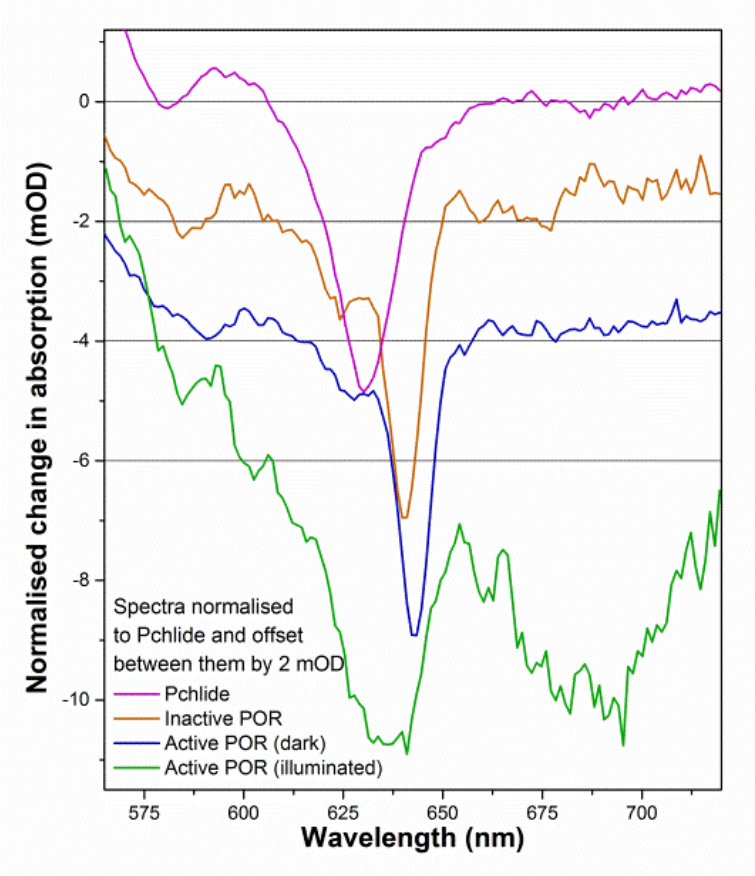

Figure S3.15. Comparison of normalised triplet spectra (averaged 30 ns-1 µs) from free Pchlide and Pchlide-subtracted POR-complex samples. Spectra were normalised using the major ground state bleach feature to that of unbound Pchlide. Spectra are vertically offset by 2 mOD.

Single-wavelength transient absorption

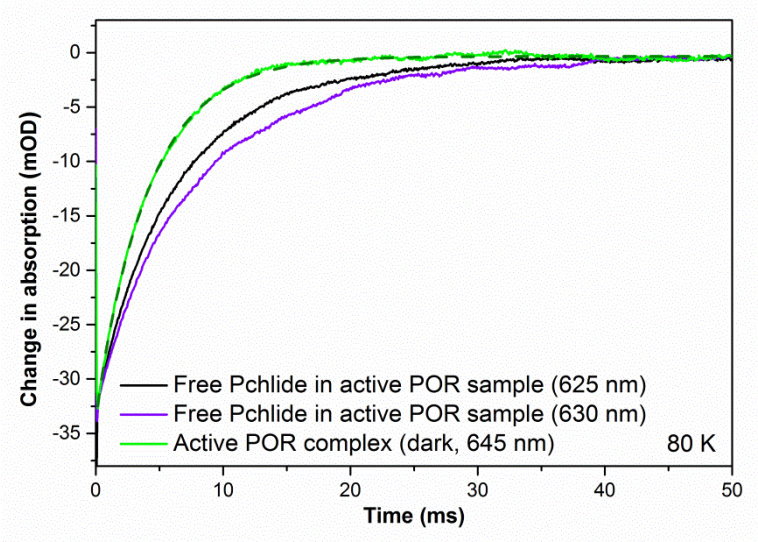

Figure S3.16. Ground state bleach transients measured at 625/630 nm and 645 nm (which correspond to the triplet decay of free- and bound-Pchlide respectively) for the active POR complex (dark). The trace corresponding to POR-bound Pchlide displayed a faster decay.

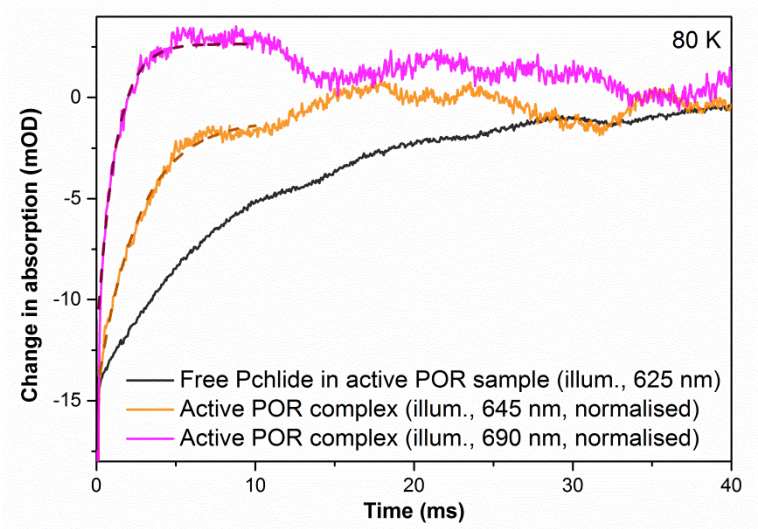

Figure S3.17. Ground state bleach transients measured at 625 (which corresponds to the triplet decay of free Pchlide), 645 and 690 nm (which correspond to the triplet decay of the hydrogen transfer intermediate) for illuminated active POR complex. The traces corresponding to the POR-bound reaction intermediate displayed faster decays.

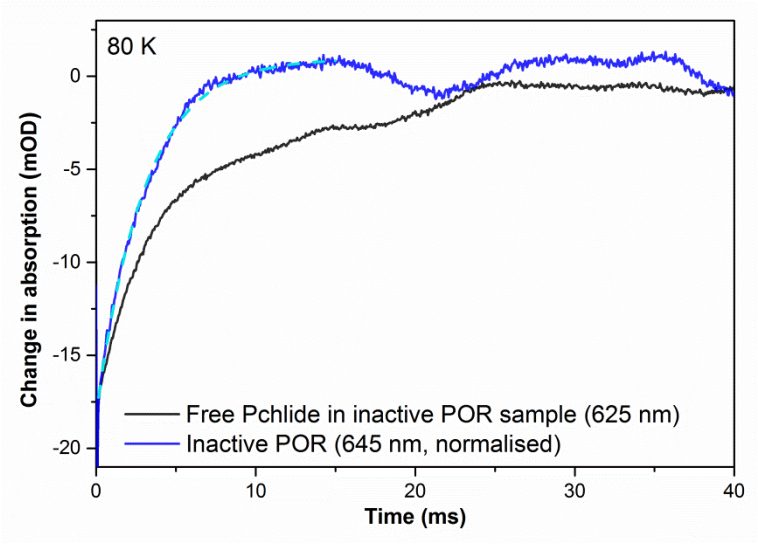

Figure S3.18. Ground state bleach transients measured at 625 nm and 645 nm (which correspond to the triplet decay of free- and bound-Pchlide respectively) for inactive POR complex. The trace corresponding to POR-bound Pchlide displayed a faster decay.

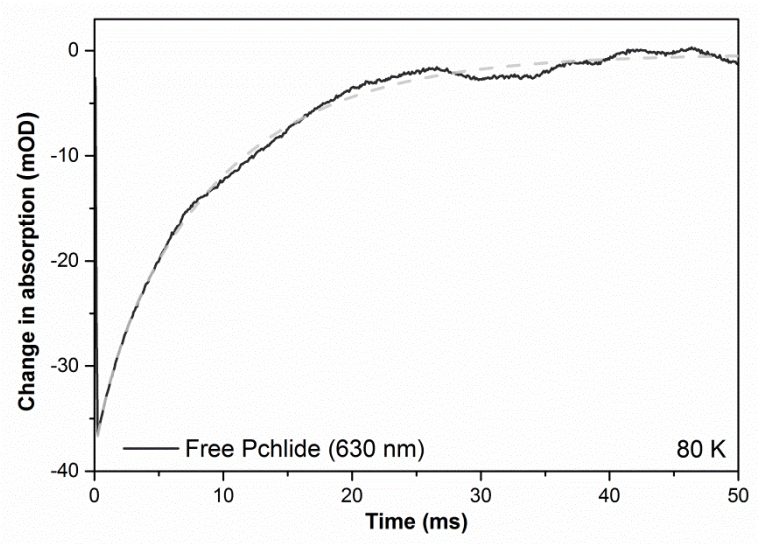

Figure S3.19. Ground state bleach kinetic trace of a free Pchlide sample.[155]

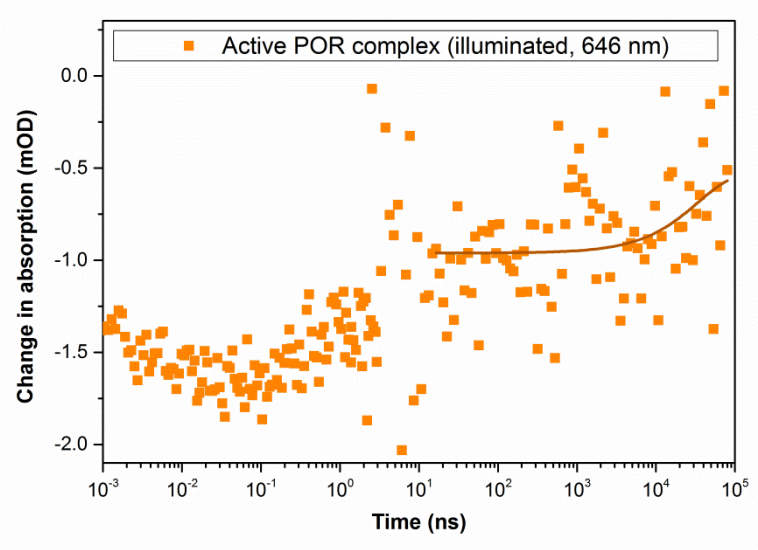

Figure S3.20. Ultrafast time-resolved absorption kinetic trace of the active POR complex (646 nm) with corresponding triplet-state decay estimation fit.

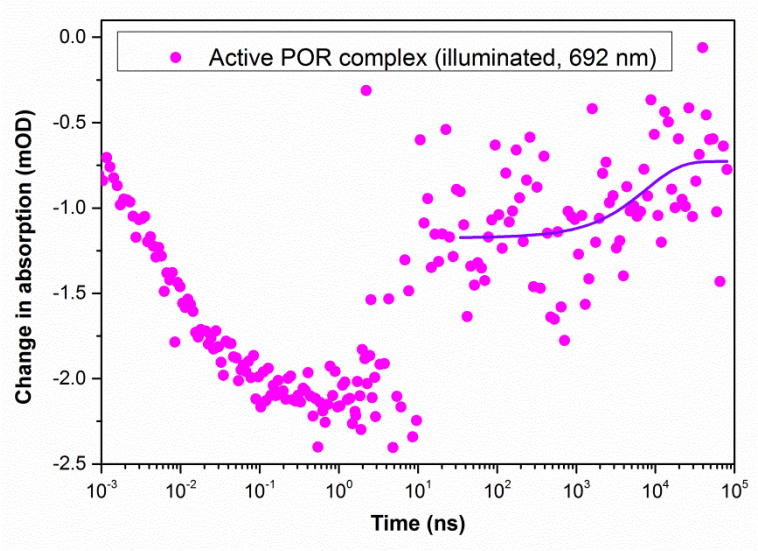

Figure S3.21. Ultrafast time-resolved absorption kinetic trace of the active POR complex (692 nm) with corresponding triplet-state decay estimation fit.

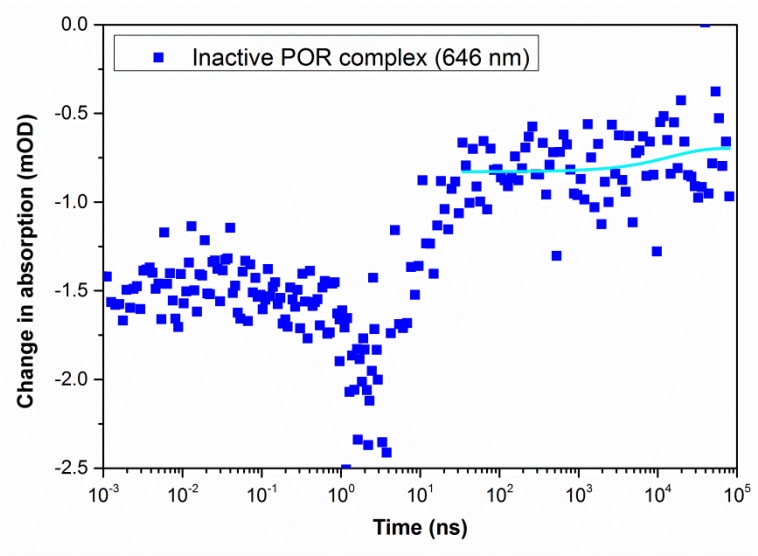

Figure S3.22. Ultrafast time-resolved absorption kinetic trace of the inactive POR complex (646 nm) with corresponding triplet-state decay estimation fit.

EPR

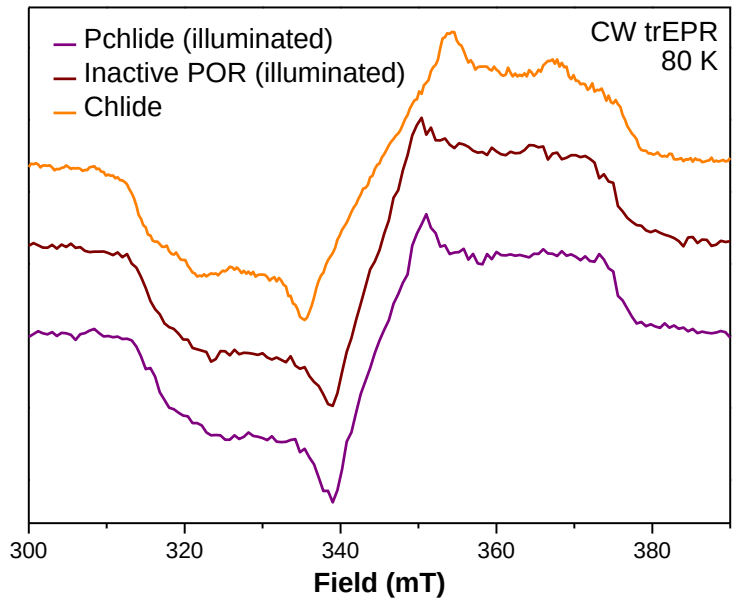

Figure S3.23. Field-sweep trEPR experimental data (integration over 100 ns of maximum time-trace signal) of illuminated free Pchlide, illuminated inactive POR and illuminated Chlide samples. None of these reference samples display the features observed in the illuminated active POR sample.

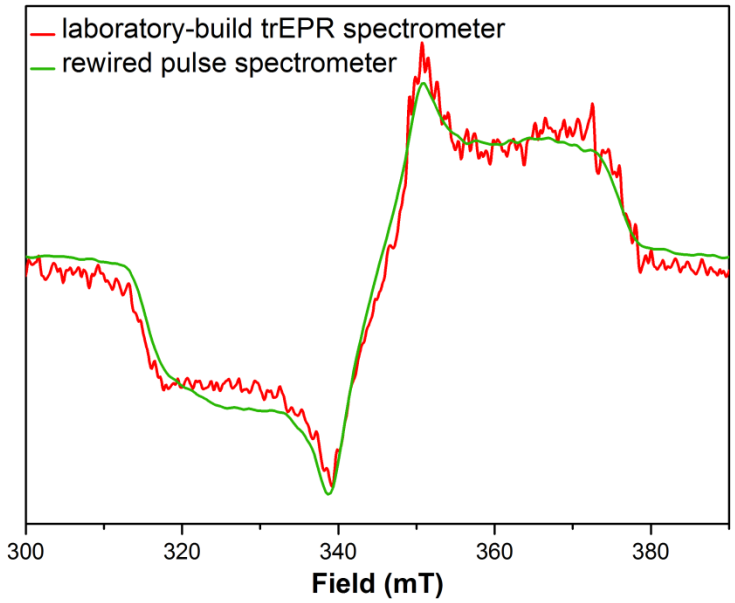

Figure S3.24. Field-sweep trEPR spectrum of Pchlide in anaerobic aqueous buffer recorded on the experimental setup used in the present work (green, 80 K) overlaid with the spectrum recorded in our previous trEPR setup (red, 10 K).

ESEEM data

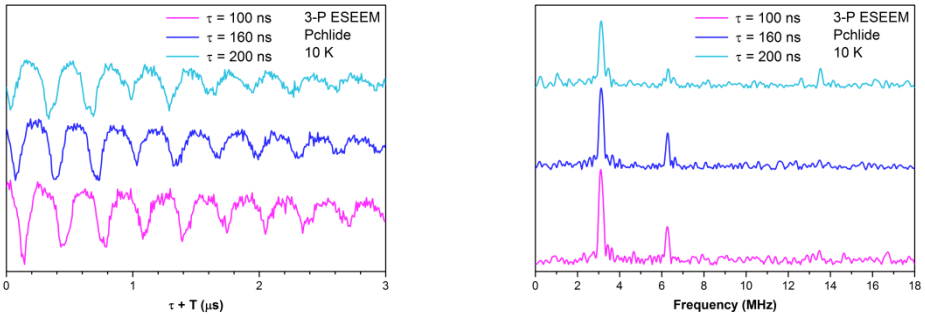

Figure S3.25. Three-pulse ESEEM experimental time traces and FT spectra of Pchlide measured at 318 mT using 100 ns (pink), 160 ns (dark blue) and 200 ns (cyan) τ pulses.

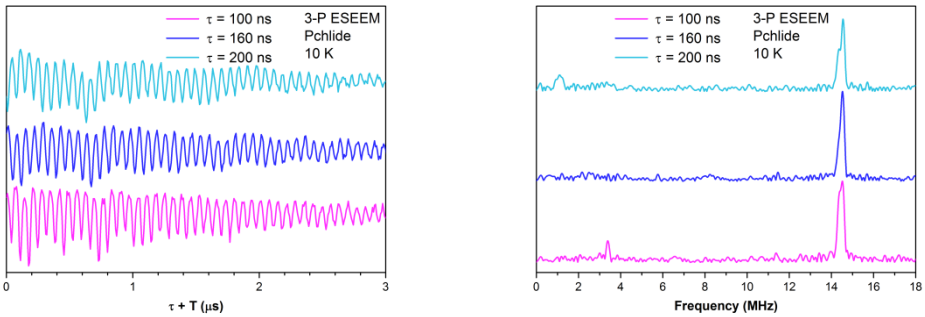

Figure S3.26. Three-pulse ESEEM experimental time traces and FT spectra of Pchlide measured at 339 mT using 100 ns (pink), 160 ns (dark blue) and 200 ns (cyan) τ pulses.

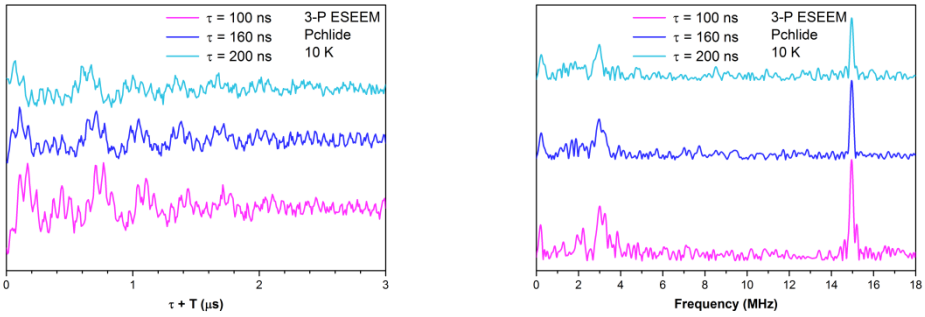

Figure S3.27. Three-pulse ESEEM experimental time traces and FT spectra of Pchlide measured at 351 mT using 100 ns (pink), 160 ns (dark blue) and 200 ns (cyan) τ pulses.

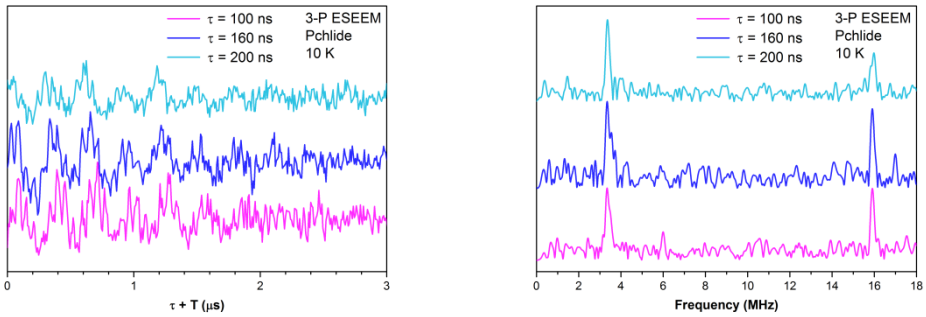

Figure S3.28. Three-pulse ESEEM experimental time traces and FT spectra of Pchlide measured at 373 mT using 100 ns (pink), 160 ns (dark blue) and 200 ns (cyan) τ pulses.

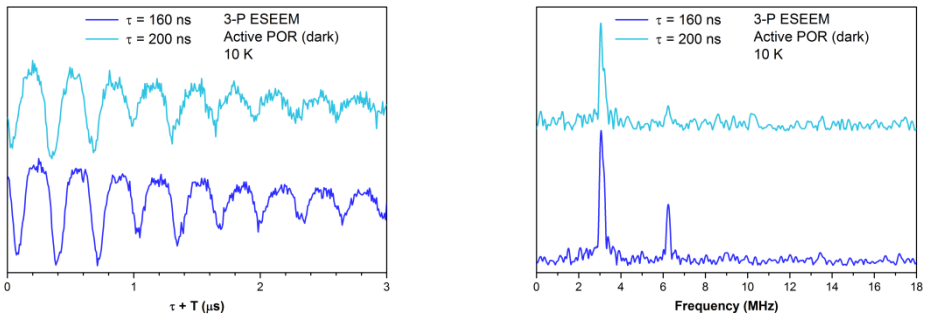

Figure S3.29. Three-pulse ESEEM experimental time traces and FT spectra of active POR complex (dark) measured at 317 mT using 160 ns (dark blue) and 200 ns (cyan) τ pulses.

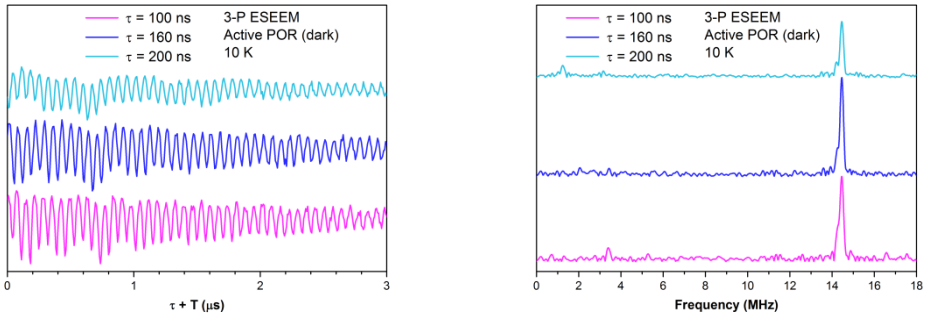

Figure S3.30. Three-pulse ESEEM experimental time traces and FT spectra of active POR complex (dark) measured at 338.5 mT using 100 ns (pink), 160 ns (dark blue) and 200 ns (cyan) τ pulses.

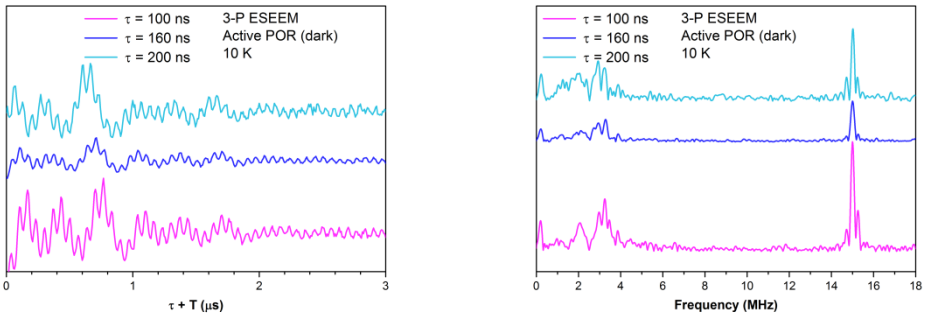

Figure S3.31. Three-pulse ESEEM experimental time traces and FT spectra of active POR complex (dark) measured at 352 mT using 100 ns (pink), 160 ns (dark blue) and 200 ns (cyan) τ pulses.

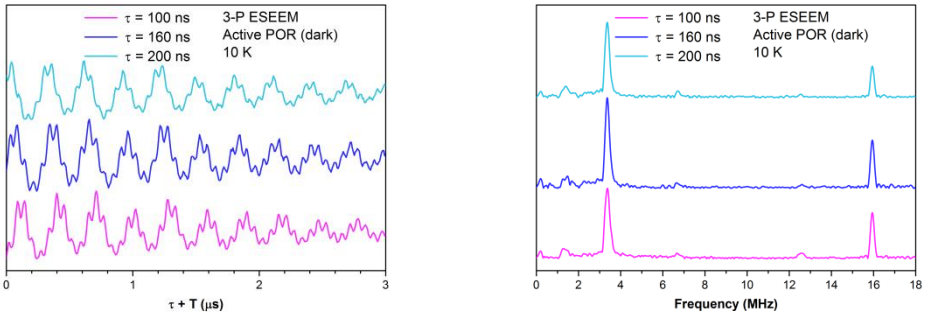

Figure S3.32. Three-pulse ESEEM experimental time traces and FT spectra of active POR complex (dark) measured at 375 mT using 100 ns (pink), 160 ns (dark blue) and 200 ns (cyan) τ pulses.

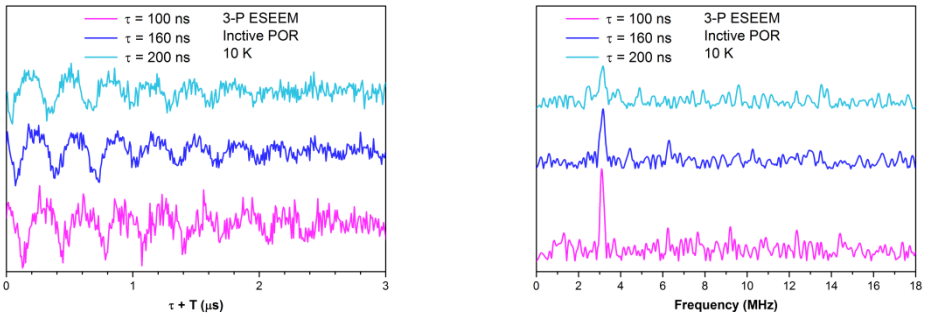

Figure S3.33. Three-pulse ESEEM experimental time traces and FT spectra of inactive POR complex measured at 318 mT using 100 ns (pink), 160 ns (dark blue) and 200 ns (cyan) τ pulses.

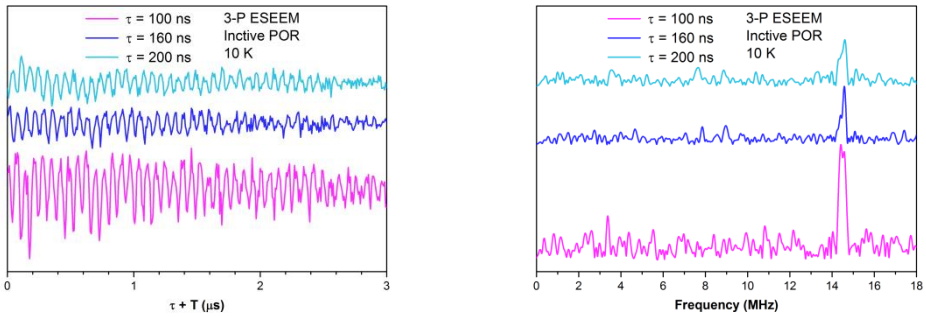

Figure S3.34. Three-pulse ESEEM experimental time traces and FT spectra of inactive POR complex measured at 339.5 mT using 100 ns (pink), 160 ns (dark blue) and 200 ns (cyan) τ pulses.

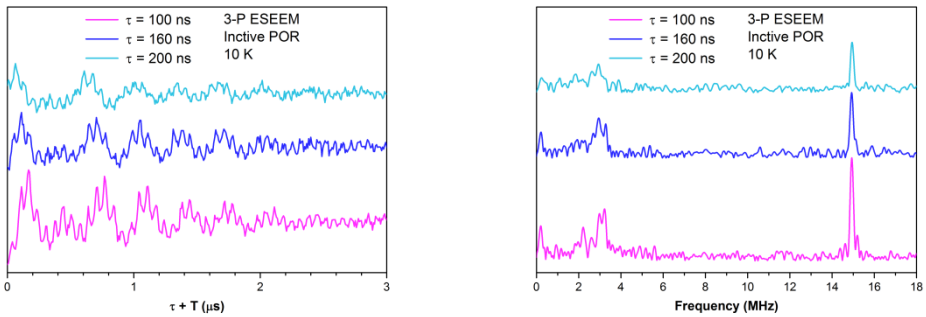

Figure S3.35. Three-pulse ESEEM experimental time traces and FT spectra of inactive POR complex measured at 351.5 mT using 100 ns (pink), 160 ns (dark blue) and 200 ns (cyan) τ pulses.

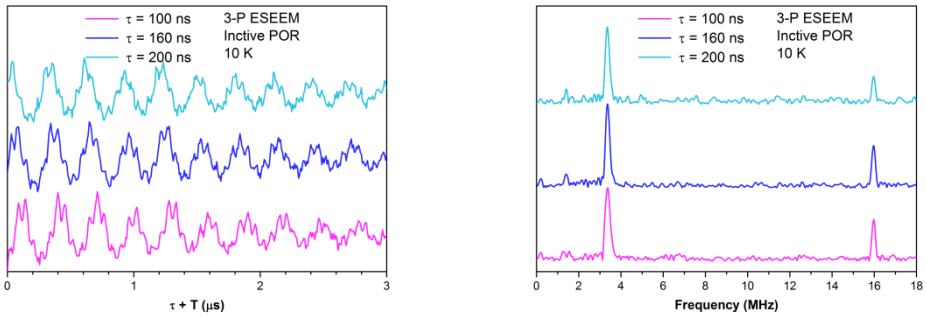

Figure S3.36. Three-pulse ESEEM experimental time traces and FT spectra of inactive POR complex measured at 373 mT using 100 ns (pink), 160 ns (dark blue) and 200 ns (cyan) τ pulses.

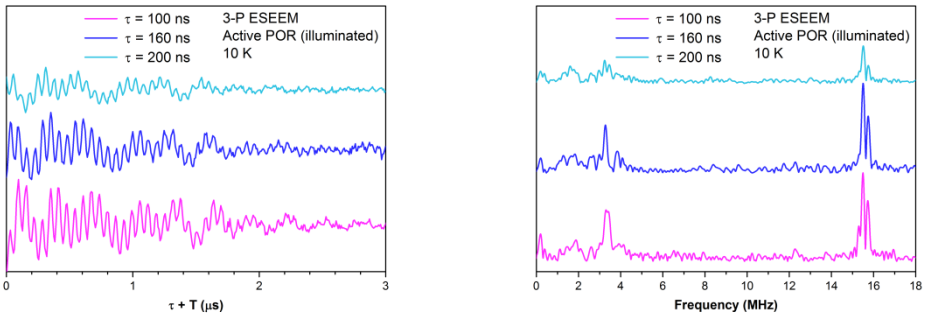

Figure S3.37. Three-pulse ESEEM experimental time traces and FT spectra of active POR complex (illuminated) measured at 363 mT using 100 ns (pink), 160 ns (dark blue) and 200 ns (cyan) τ pulses.

4 Excited-state studies on the triplet state of protochlorophyllide analogues at cryogenic temperatures

Manuscript draft pending submission

Authors: Guillem Brandariz-de-Pedro, Derren J. Heyes, Samantha J. O. Hardman, Nicholas F. Chilton, Stefan Weber, Daniel Nohr, David Collison, Nigel S. Scrutton, Alistair J. Fielding

Contributions: Chapter 4 is a manuscript draft written by GBP with guidance from DJH, SJOH and AJF. Final CASSCF calculations are pending to be added to the main text. Sample preparation was carried out by GBP. Laser flash-photolysis measurements were conducted by GBP. trEPR measurements were conducted by DN with help from GBP. DFT calculations were carried out by GBP. CASSCF calculations on compound A were conducted by NFC. CASSCF calculations on compounds B-H are being conducted by GBP. All time-resolved spectroscopy data was analysed by GBP with guidance from DJH and SJOH. All EPR data was analysed by GBP with guidance from AJF.

Excited-state studies on the triplet state of protochlorophyllide analogues at cryogenic temperatures

Guillem Brandariz-de-Pedro,[†,¶,‡] *Derren J. Heyes,**[,‡] *Samantha J. O. Hardman,*[‡] *Nicholas F. Chilton,*[†] *Stefan Weber,*[§] *Daniel Nohr,*[§] *David Collison,*[†] *Nigel S. Scrutton,*[‡] *Alistair J. Fielding**[⌉]

[†]School of Chemistry, University of Manchester, Oxford Road, Manchester M13 9PL, U.K.

[¶]The Photon Science Institute, University of Manchester, Oxford Road, Manchester M13 9PL, U.K.

[‡]Manchester Institute of Biotechnology, University of Manchester, 131 Princess Street, Manchester M1 7DN, U.K.

[§]Institute of Physical Chemistry, Albert-Ludwigs-Universität Freiburg, 79104 Freiburg, Germany

[⌉] Liverpool John Moores University, School of Pharmacy and Biomolecular Sciences, Liverpool, L3 3AF.

Corresponding Authors

*E-mail: A.J.Fielding@ljmu.ac.uk

*E-mail: Derren.Heyes@manchester.ac.uk

4.1 ABSTRACT:

The protochlorophyllide (Pchlide) pigment is the substrate of the enzyme protochlorophyllide oxidoreductase (POR), which catalyses a reaction with a major role in both plant development and the biosynthesis of chlorophyll. The enzymatic reduction of Pchlide by POR is a light-driven process that is highly dependent on the complex excited-state properties of the substrate. The fact that the crystal structure of POR is to date unavailable has posed difficulties in terms of fully understanding the ternary structure and reaction mechanism of the enzyme. The study of substrate analogues has brought insight about the regions of Pchlide that are crucial for the reaction and their role in photochemistry, providing more detailed understanding of this biological system. In this work we have expanded on our previous room temperature sub-μs time-resolved studies by carrying out experiments at cryogenic temperatures. We have measured the decay kinetics of the excited-state triplet species for a range of Pchlide analogues in aqueous buffer and compared them to our previous results. Working at cryogenic temperatures has allowed the characterisation of the paramagnetic triplet state of Pchlide analogues by means of electron paramagnetic resonance (EPR) spectroscopy. We have also tested the accuracy of density functional theory methods in predicting trends in experimental EPR data for this family of compounds. The ability to compare the electronic properties of substrate analogues to their excited-state kinetic properties has allowed us to better understand the factors behind their suitability as a substrate and support our previous findings.

KEYWORDS electron paramagnetic resonance, protochlorophyllide, analogues, triplet state, photochemistry, time-resolved spectroscopy, excited state

4.2 INTRODUCTION:

Protochlorophyllide (Pchlide) is a precursor of chlorophyll with an important role in plant development. Pchlide forms a ternary complex with the enzyme protochlorophyllide oxidoreductase (POR) and the NADPH cofactor, which accumulates in etioplasts of dark-grown plants in the form of organised networks called prolamellar bodies. Absorption of light by the POR complex in seedlings leads to the dismantlement of these structures and the transformation of etioplasts into chloroplasts, releasing chlorophyll and triggering transformations in plant growth.[108,168] Pchlide is the chromophore responsible for harnessing light to drive the POR reaction. In this reaction, POR catalyses the photoreduction of the C17-C18 double bond in the *D*-ring of Pchlide (Figure 4.1), which produces chlorophyllide (Chlide). The reaction involves a hydride transfer from the NADPH cofactor to the C17 position of Pchlide, followed by a proton transfer from an active site residue to the C18 position.[104,108,109]

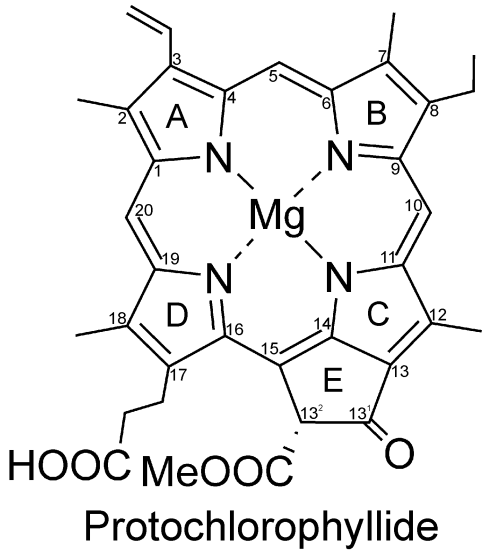

Figure 4.1. Schematic representation of the protochlorophyllide pigment displaying the main ring and Carbon atom labels.

The current lack of a POR crystal structure has implied an added difficulty to achieving a full understanding of the ternary structure of POR and the protein-substrate interactions occurring in the POR active site. Protein homology studies based on the short-chain dehydrogenase family of enzymes have provided important advances in obtaining a ternary structure model of POR. However, they have not been able to provide a model that also accounts for the active site reactivity.[157] A recent study presented a computational model based on homology modelling and simulations of

spectral features to gain insight into the enzymatic processes of POR.[163] Another approach to deciphering the photochemistry is to better understand which parts of the substrate are crucial for catalysis. Studies of POR reactivity using substrate analogues have provided important insights about which regions of the molecule are important for enzyme activity.[169,170] It was revealed that substitution of the Mg atom by a Zn atom maintained enzymatic activity. However, removal of the metal atom or replacement by either Co, Cu or Ni led to substrate inactivity.[169] Modifications to the acid chain at the C17 of the substrate were found to render the substrate unsuitable for POR catalysis and it has subsequently been suggested that the structural properties of this substituent play a role in active-site binding.[121,169] The *D*- and *E*-rings of Pchlide have been found to play a crucial role in its reactivity and any modifications to their structure resulted in loss of activity. However, POR is more tolerant to modifications on the *B* ring, such as substituting the C8 ethyl group by a vinyl group, which does not affect substrate activity.[170,171] The carbonyl group at the $C13^1$ position of the substrate has been suggested to play a key role in the formation of an internal charge-transfer (ICT) state that is believed to induce a high polarisation of the double bond that facilitates the nucleophilic hydride addition.[22,127,130,133,172] In addition to activity assays, time-resolved spectroscopy studies on Pchlide analogues are necessary in order to understand the precise role and effect of individual substituent groups on the overall reactivity and excited-state properties of the substrate. A previous study on the excited-state dynamics of Pchlide analogues over the ps to µs timescale revealed that analogues with changes on the C17 carboxylic acid group or an opening of the *E*-ring displayed similar excited-state dynamics to Pchlide. These involved a sequential decay from an excited singlet state into an ICT singlet state on the order of a few ps leading to a solvation of the ICT state with lifetimes of tens of picoseconds. This was followed by an intersystem crossing from the solvated ICT singlet state into a long-lived triplet state with a lifetime of a few ns and, finally, a decay of the triplet state back to the ground state with a lifetime of ~250 ns.[137] Removal of the metal atom, substitution of Mg by Zn and substitution of the $C13^1$ carbonyl group by a hydroxyl altered the excited-state dynamics and revealed a sequential decay involving only three species. This was interpreted as a change in formation and solvation of the ICT state for these analogues, suggesting that the central Mg atom and $C13^1$ carbonyl are important for charge separation within the substrate and strengthening its interaction with solvent molecules.[137] Analogues containing modifications to the $C13^1$ carbonyl also displayed

the biggest changes in static absorption spectra, featuring broader and less intense absorption bands on the red region of the visible spectrum, stripping away the characteristic green colour of Pchlide and chlorophylls from said analogues.[137]

4.3 RESULTS AND DISCUSSION:

We studied a series of Pchlide analogues with structural modifications to the metal atom and rings *D* and *E*, which have previously been found to be crucial for POR activity.[121,137,169,170] The compounds of interest differ from Pchlide (compound **A**) in the following (Figure 4.2): chlorophyllide (compound **B**), the reaction product of POR, contains a reduced C17 double bond, protopheophorbide (compound **C**) has had the metal atom removed, Zn protopheophorbide (compound **D**) has had the Mg atom replaced by Zn, 13,15-dimethyl ester protochlorophyllide (compound **E**) contains a double ester resulting in the opening of ring E, C17-methyl ester protochlorophyllide (compound **F**) contains a methyl propionate ester on the C17 position instead of an acid group, 13-OH-Pchlide (compound **G**) contains a hydroxyl group instead of a carbonyl on the $C13^1$ position, chlorophyll c (compound **H**) has an acrylic acid rather than a propionic acid substituent at the C17 position. UV-Vis absorption spectra of the studied compounds can be found in Figure S4.1. This study is a follow up to our previous work on Pchlide analogues at room temperature, which revealed that the $C13^1$ position is crucial for the formation of the excited-state ICT species.[137]

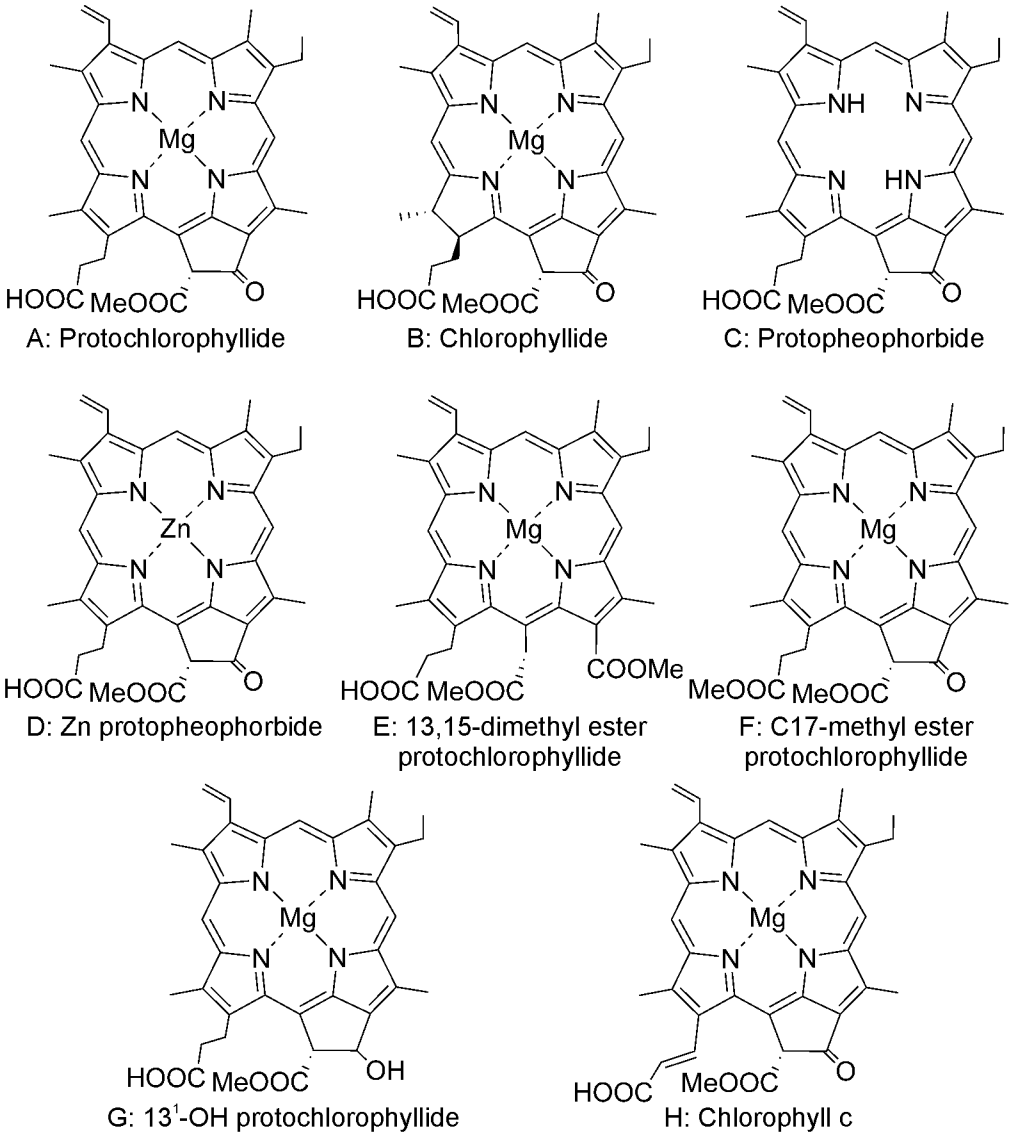

Figure 4.2. Schematic representation of the Pchlide analogues studied in this work.

Ultrafast time resolved visible and IR spectroscopy studies on Pchlide analogues in methanol have provided crucial information on the role of various structural characteristics of Pchlide during its early excited-state dynamics.[137] Different studies also found that solvent polarity has a great effect on the excited-state dynamics of Pchlide and that, while early steps leading to triplet formation remain similar, triplet decay kinetics display more pronounced changes.[130,132,134,155] In order to investigate the differences in triplet-state decay kinetics between Pchlide analogues in aqueous solution we carried out laser flash photolysis measurements at cryogenic temperatures on compounds **C**-**H**. Time-resolved datasets were recorded on a ms timescale after laser excitation of the samples at 430 nm (Figure 4.3, S4.2-S4.7). The ground state bleach features (~550-650 nm) of Pchlide analogues in aqueous buffer appeared to be red-

shifted in comparison to the triplet state spectral features of those analogues previously studied in methanol solution (compounds **C**-**G**, Figure 4.3).[137]

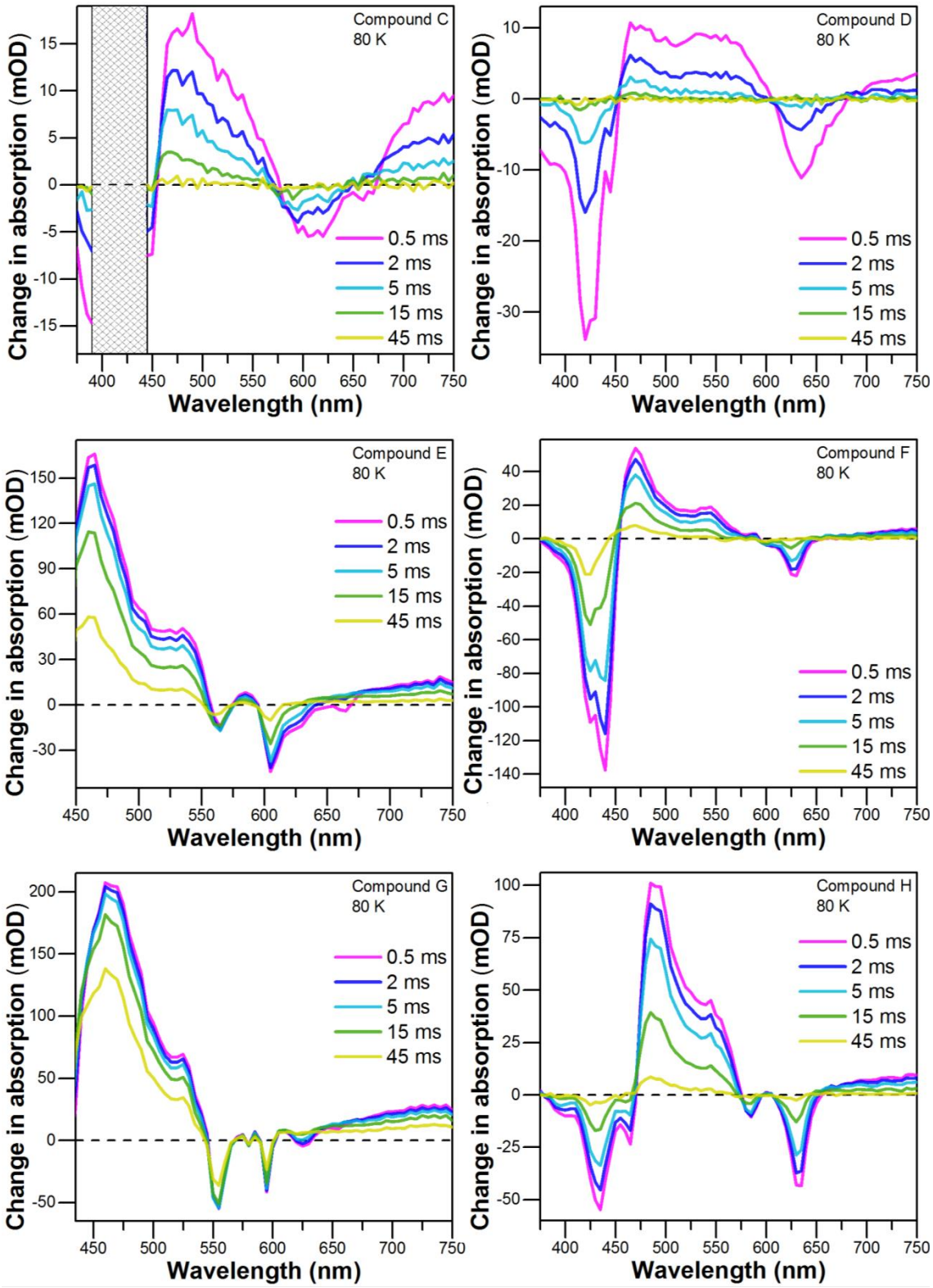

Figure 4.3. Selected time-resolved spectra at 0.5, 2, 5, 15 and 45 ms delay times after 430 nm laser flash for compounds C-H at 80K in anaerobic aqueous buffer.

The time-resolved spectral changes of the datasets were fit to a two-component exponential sequential model by means of global analysis.[148] The resulting lifetimes and calculated evolution associated difference spectra (EADS) can be found in Table 4.1 and Figures S4.2-S4.7, respectively. In accordance to our previous study, compounds **C**-**H** displayed lifetimes much longer than those found for Pchlide analogues in methanol at room temperature.[137,155] The EADS corresponding to the slower component from global analysis of compounds **C**-**F** and compound **H** displayed blue-shifted, less intense spectral features than the faster component EADS (Figures S4.2-S4.7). For compound **G**, similarly to previous results on compound **A**,[155] the blue shift is not so apparent.

Table 4.1. Biexponential triplet decay lifetimes of Pchlide analogues from global analysis[148] of flash photolysis data. (*a*: data from previous publication).[155]

	τ_1 (ms)	τ_2 (ms)
A	7.5 ± 0.1[a]	22.3 ± 0.1[a]
B	-	-
C	2.26 ± 0.01	14.4 ± 0.1
D	1.73 ± 0.01	12.1 ± 0.1
E	14.3 ± 0.1	48.2 ± 0.1
F	9.7 ± 0.1	47.3 ± 0.1
G	23.6 ± 70.1	94.5 ± 0.1
H	7.4 ± 0.1	22.4 ± 0.1

Compound **H**, with 7.5 and ~22 ms components, displayed identical triplet lifetimes to Pchlide at 80 K.[155] Compounds containing changes in the carboxylic acid group or an opening of ring E (compounds **E** and **F**) displayed lifetimes twice as long as Pchlide. Studies in methanol had displayed identical excited state dynamics and very similar triplet decay lifetimes between these compounds and Pchlide.[137] Compounds where the metal atom had been removed (compound **C**) or substituted by Zn (compound **D**) displayed triplet decay lifetimes about half as long as those of Pchlide. These results also contrast with previous findings in methanol where, although changes in the metal atom reflected altered sub-nanosecond excited-state dynamics, the triplet state appeared to decay at a similar rate (compound **D**) or slower (compound **C**) than that displayed by Pchlide.[137] The only compound without a C13 carbonyl group (compound **G**) displayed much longer (~4x) triplet decay lifetimes than Pchlide. The substitution of the carbonyl group by a hydroxyl had the biggest impact in excited-state properties, which

is in accordance with previous work, where this analogue was also found to have the longest triplet lifetime and altered sub-nanosecond excited state dynamics.[137]

In order to evaluate the effect of structural changes on the EPR signature of the excited-state triplet of Pchlide we carried out time-resolved continuous wave EPR (trEPR) measurements on compounds **B**-**H**. trEPR time traces were recorded at 80 K after photoexcitation with 532 nm laser pulses over a range of magnetic field positions. Field-sweep spectra were obtained from integration of the trEPR time traces and simulated in order to obtain experimental zero-field splitting (ZFS) parameters of each compound (Figure 4.4, Table 4.2).[149] The *D* and *E* parameters represent the axial and transversal components of ZFS, respectively. These are directly related to the symmetry level of the spatial distribution of the electrons responsible for the studied paramagnetic species. A larger *D* value is associated to a compression along the z axis of the molecule (more planar) while larger *E* values are associated to differences in electron distribution along the molecule x and y axes (more rhombic).[41] We have previously used EPR to reveal possible changes in the geometry of a POR reaction intermediate.[173]

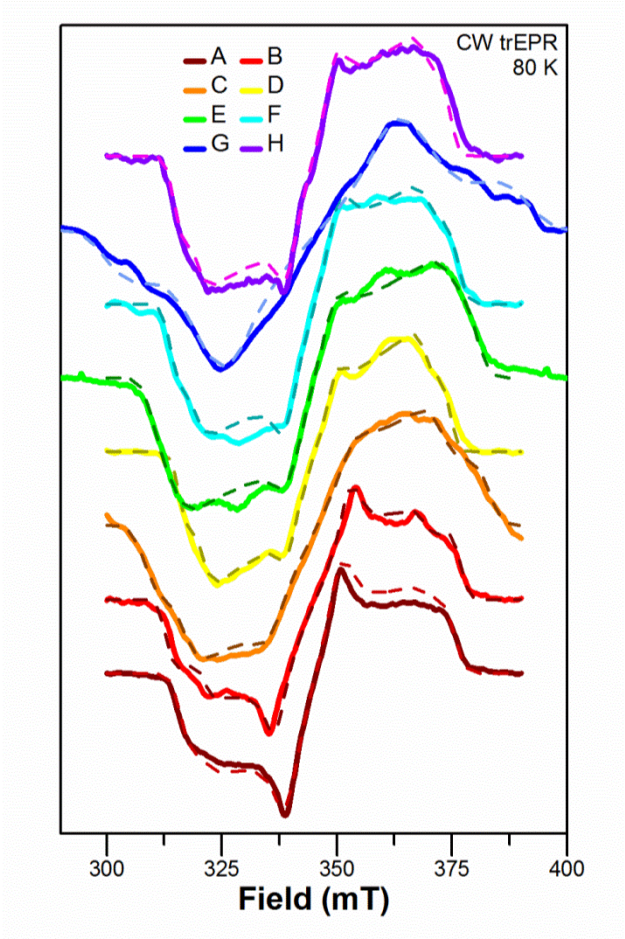

Figure 4.4. Field-sweep trEPR experimental data (solid lines, integration over 100 ns of maximum time-trace signal) including spectral simulations (dashed lines) of compounds A (burgundy), B (red), C (orange), D (yellow), E (green), F (light blue), G (dark blue) and H (violet).

Density functional theory (DFT) calculations were carried out to predict ZFS parameters for compounds **B-H** (Table 4.2).[150,151] Although this method had been found to be inaccurate for ZFS calculations on systems displaying high electron delocalisation, it could correctly predict trends when used to compare porphyrin analogues.[164,174]

Table 4.2. ZFS parameters of Pchlide analogues from simulation of experimental data and DFT calculations. (*a*: data from unpublished work,[173] *b*: data from previous publication.)[155]

compound	$p_{[x]}$, $p_{[y]}$, $p_{[z]}$	$\|D\|$ exp. (MHz)	$\|E\|$ exp. (MHz)	$\|D\|$ DFT (MHz)	$\|E\|$ DFT (MHz)
A	0.4, 0.6, 0	830 ± 5[a]	165 ± 8[a]	648[b]	166[b]
B	0.4, 0.6, 0	897 ± 20	147 ± 8	579	159
C	0.5, 0.5, 0	1040 ± 20	175 ± 20	592	170
D	0.5, 0.5, 0	824 ± 9	174 ± 5	655	164
E	0.5, 0.5, 0	980 ± 15	230 ± 9	651	181
F	0.5, 0.5, 0	870 ± 10	180 ± 7	641	167
G	0.6, 0.4, 0	1280 ± 12	90 ± 10	721 ± 2	166 ± 1
H	0.5, 0.5, 0	840 ± 20	180 ± 5	643	169

The EPR spectra of compounds **A**-**H** display a similar lineshape due to, in part, the triplet-state nature of the studied species and their similar triplet sublevel populations revealed by the simulations. Compounds **A**-**H** exhibit a population of X and Y triplet sublevels with a ratio close to 1:1. Changes in the sublevel populations generally imply drastic changes in EPR lineshape, as observed in our previous work.[173] Removal of the metal atom of Pchlide (compound **C**), opening of the ring E (compound **E**) and substitution of the C13 carbonyl group by a hydroxyl (compound **G**) had the biggest effect on the triplet EPR signature, which was greatly broadened due to an increase of the axial ZFS parameter from $|D|$ = 830 MHz to ~1000 MHz for compounds **C** and **E** and up to 1280 MHz for compound **G**. The analogue with a C13 hydroxyl group (compound **G**) also displayed a change in the sign of the *E* parameter, implying a bigger change on the distribution of the unpaired electrons within the molecule plane. The fact that compound **G** is a mixture of two $C13^1$-OH isomers might be a reason contributing to the apparently greater linewidth in this spectrum with generally broad features. Compounds **B**, **D**, **F** and **H** displayed very similar ZFS parameters to Pchlide, indicating a smaller impact of substitution of the metal centre by a Zn atom and modifications on the C17 double bond and acid group to the electronic properties of the triplet state of Pchlide. DFT calculations correctly predicted an increase of the axial ZFS parameter for compound **G** although, unlike in previous studies involving porphyrins, they did not predict a change in sign of the transversal parameter.[164] DFT calculations also correctly predicted the axial parameter being similar between compounds **A**, **D**, **F** and **H**. The calculations underestimated the relative value of the axial ZFS parameter of compounds **B**, **C** and **E** in comparison to **A**.

Carrying out experiments at cryogenic temperatures has allowed the use of EPR on several Pchlide analogues for the first time and has expanded on previous room temperature time-resolved spectroscopy findings. This work provided a characterisation of the triplet-state kinetics of Pchlide analogues in aqueous solution. A combination of time-resolved absorption and EPR measurements revealed that removal of the metal centre, opening of the porphyrin E ring and substitution of the C13 carbonyl by a hydroxyl had the biggest impact on both the electronic and kinetic properties of Pchlide. Substitution of the metal centre by a Zn atom affected the kinetics of triplet decay but preserved the electronic properties, which is in accordance with this compound conserving its reactivity.[169,170] The fact that changes to the C17 propionic acid group displayed very little variation in the measured electronic properties of the analogue triplet states reinforces the theory that the reason behind compounds **F** and **H** being unsuitable POR substrates is an impairment in active site.[175] Currently on-going complete active space self-consistent field (CASSCF) calculations on Pchlide analogues could provide better predictions of electronic properties of this family of compounds than DFT. While DFT is able to provide accurate predictions of ZFS for radicals, CASSCF has been shown to better predict properties in highly delocalised systems due to its multiconfigurational nature that can account for dynamic correlation in near-degenerate states, such as those found in porphyrins.[150,174] At the same time, as this method is highly resource-demanding with larger molecules, basis sets and active spaces it has limited the amount of use it has seen in the past. CASSCF calculations of the electron localisation in the porphyrin system for the ground state singlet, lowest-energy excited-state singlet and lowest-energy excited-state triplet could help us better understand the differences in electronic properties caused by changes in Pchlide functional groups, as well as providing more information on which excited-state species is directly involved in triggering the reaction chemistry.

ASSOCIATED CONTENT

Supporting Information

The following files are available free of charge. Detailed experimental methods, steady-state UV-Vis data, raw transient absorption data, EPR data (PDF).

AUTHOR INFORMATION

Notes

The authors declare no competing financial interests.

ACKNOWLEDGMENTS

G.B.-P. acknowledges Early Stage Researcher funding from the European Union's Seventh Framework Programme FP7-PEOPLE-2013-ITN through the 'MAGnetic Innovation in Catalysis' (MAGIC) Initial Training Network (Grant agreement no. 606831). We would like to acknowledge the use of the EPSRC EPR National Service in carrying out this work. NSS is an Engineering and Physical Sciences Research Council (EPSRC) Established Career Fellow (EP/J020192/1).

4.4 SUPPORTING INFORMATION:

Excited-state studies on the triplet state of protochlorophyllide analogues at cryogenic temperatures

Guillem Brandariz-de-Pedro,[†,ℸ,‡] Nicholas F. Chilton,[†] Derren J. Heyes,*[,‡] Samantha J. O. Hardman,[‡] Stefan Weber,[§] Daniel Nohr,[§] David Collison, Nigel S. Scrutton,[‡] Alistair J. Fielding,*[, ⅂]

[†]*School of Chemistry, University of Manchester, Oxford Road, Manchester M13 9PL, U.K.*

[ℸ]*The Photon Science Institute, University of Manchester, Oxford Road, Manchester M13 9PL, U.K.*

[‡]*Manchester Institute of Biotechnology, University of Manchester, 131 Princess Street, Manchester M1 7DN, U.K.*

[§]*Institute of Physical Chemistry, Albert-Ludwigs-Universität Freiburg, 79104 Freiburg, Germany*

[⅂]*Liverpool John Moores University, School of Pharmacy and Biomolecular Sciences, Liverpool, L3 3AF.*

Corresponding Authors

*E-mail: A.J.Fielding@ljmu.ac.uk

*E-mail: Derren.Heyes@manchester.ac.uk

Contents

4.4.1 Synthesis of protochlorophyllide analogues

The compounds studied in this work were prepared according to literature methods[137] and already available within the Scrutton research group. UV-Vis steady-absorption spectra of the compounds were measured on a Cary 50 spectrophotometer (Agilent Technologies).

4.4.2 Flash Photolysis

Sample cuvettes (1 cm path length) were contained in a liquid nitrogen cryostat (Opstistat DN, Oxford Instruments). An OPO (pumped by a Nd:YAG laser) achieving 430 nm 15 mJ pulses and a spectrometer were used to photoexcite and measure single-wavelength absorption transients (750 to 375 nm, 500 μs to 95 ms) as described in a previous publication.[155] The datasets were generated by averaging four sets of measurements at 80K on anareobic samples, which consisted of compounds **C-H** diluted to a concentration where the absorbance at 430 nm was equal to that of 20 μM Pchlide in 40 v% glycerol, 20 m/v% sucrose, 50 mM Tris-HCl, pH 7.5, 1 v% Genapol.

Time-resolved absorption data was globally analysed in order to translate the time-dependent spectral changes to a series of lifetimes and evolution associated difference spectra by using a sequential biexponential decay model as previously optimised for Pchlide flash photolysis data.[148,155] Some of the measured kinetic traces around the Soret band were left out of the global analysis of the data due to the transient recorder failing to register their intensity.

4.4.3 Time-resolved CW EPR

Time-resolved continuous-wave EPR (trEPR) datasets were measured after laser excitation at 532 nm using the experimental setup described in our previous work.[173] Samples consisted of anaerobic solutions of compounds **B**-**H** diluted to a concentration where the absorbance at 532 nm was equal to that of 250 µM Pchlide and were contained in 3 mm inner diameter quartz tubes. (40 v% glycerol, 20 m/v% sucrose, 50 mM Tris-HCl, pH 7.5, 1 v% Genapol). Simulations of the trEPR triplet spectra were performed using the Easyspin software extension for Matlab.[149]

4.4.4 Density functional theory calculations

Density functional theory (DFT) calculations of the ZFS parameters of Pchlide analogues triplet state were performed using the ORCA software package with a B3LYP hybrid functional and the EPR-II basis set as previously described by Sinnecker.[150,151]

4.4.5 Supporting Data

UV-Vis spectra of Pchlide analogues

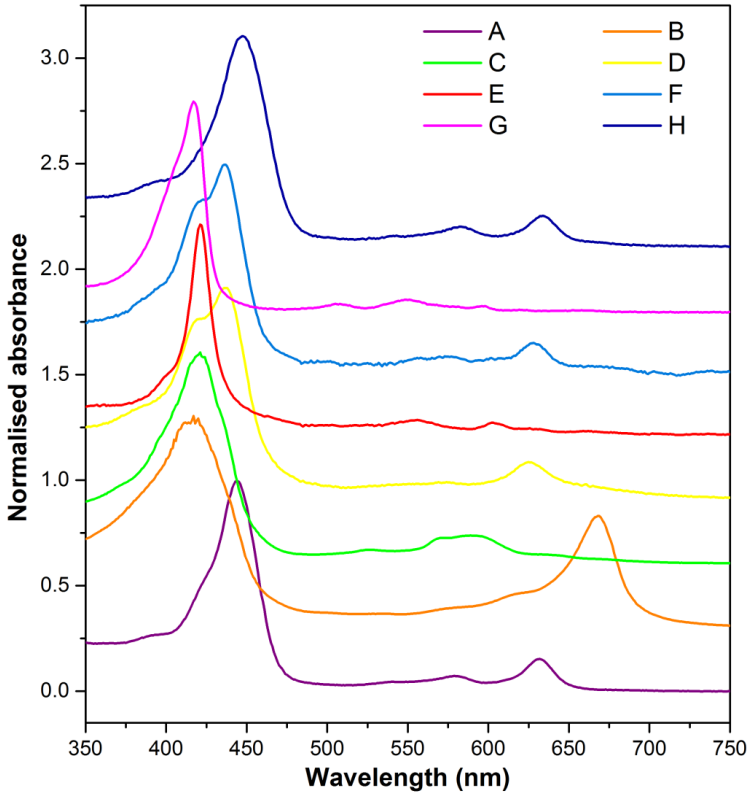

Figure S4.1. Steady-state UV-Vis absorption spectra of Pchlide analogues at room temperature. The spectra are offset from each other for clarification.

Raw time-resolved absorption spectroscopy data and triplet decay fits

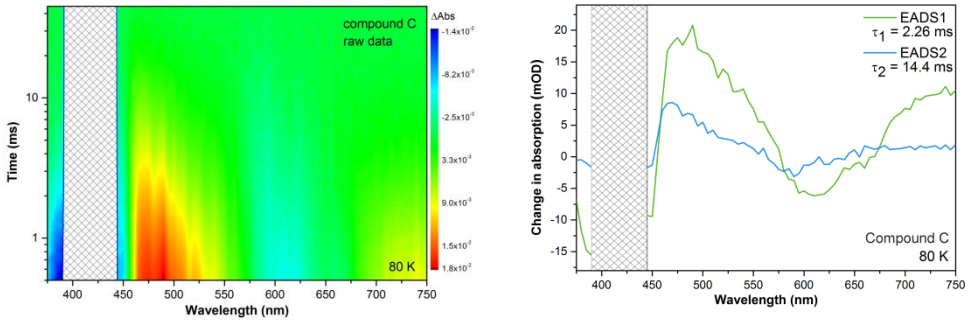

Figure S4.2. Time-resolved visible spectroscopy data and evolution associated difference spectra (EADS) for protopheophorbide (compound **C**) in anaerobic buffer at 10 K after photoexcitation at ~430 nm. Time-resolved difference spectra were recorded between 0.5 and 45 ms. The EADS were obtained from fitting the time-resolved absorption data to a sequential double exponential model.

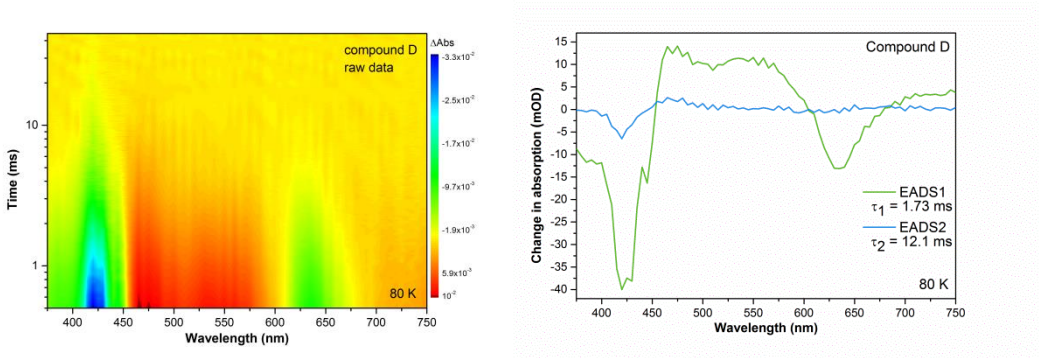

Figure S4.3. Time-resolved visible spectroscopy data and evolution associated difference spectra (EADS) for Zn protopheophorbide (compound **D**) in anaerobic buffer at 10 K after photoexcitation at ~430 nm. Time-resolved difference spectra were recorded between 0.5 and 45 ms. The EADS were obtained from fitting the time-resolved absorption data to a sequential double exponential model.

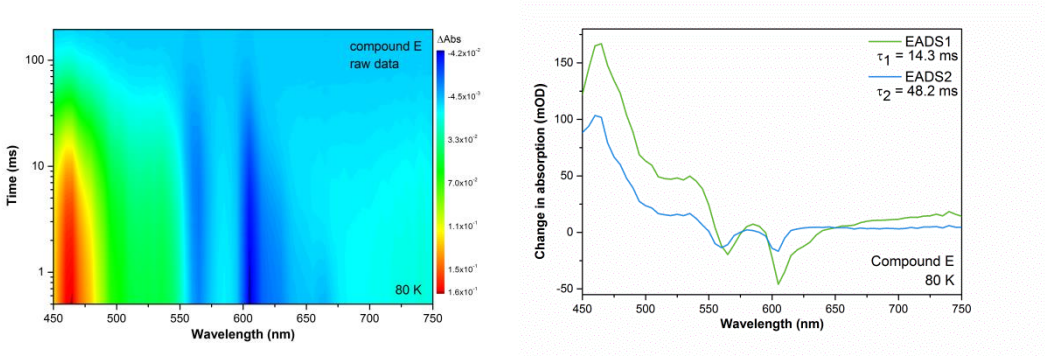

Figure S4.4. Time-resolved visible spectroscopy data and evolution associated difference spectra (EADS) for 13,15-dimethyl ester protochlorophyllide (compound **E**) in anaerobic buffer at 10 K after photoexcitation at ~430 nm. Time-resolved difference spectra were recorded between 0.5 and 195 ms. The EADS were obtained from fitting the time-resolved absorption data to a sequential double exponential model.

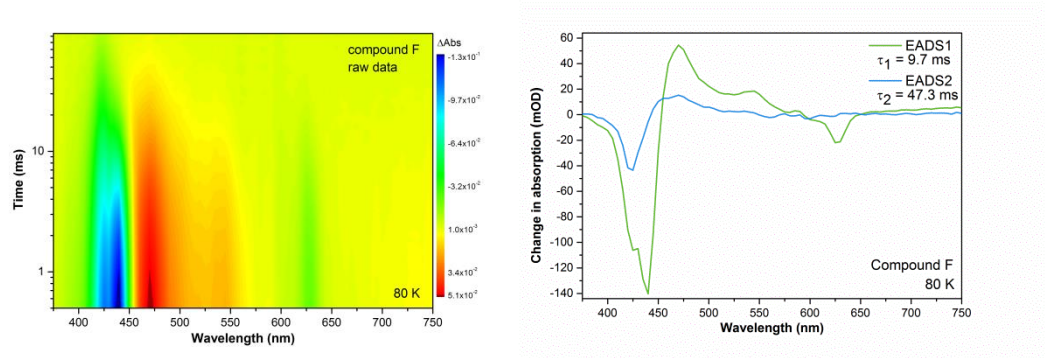

Figure S4.5. Time-resolved visible spectroscopy data and evolution associated difference spectra (EADS) for C17-methyl ester protochlorophyllide (compound **F**) in anaerobic buffer at 10 K after photoexcitation at ~430 nm. Time-resolved difference spectra were recorded between 0.5 and 95 ms. The EADS were obtained from fitting the time-resolved absorption data to a sequential double exponential model.

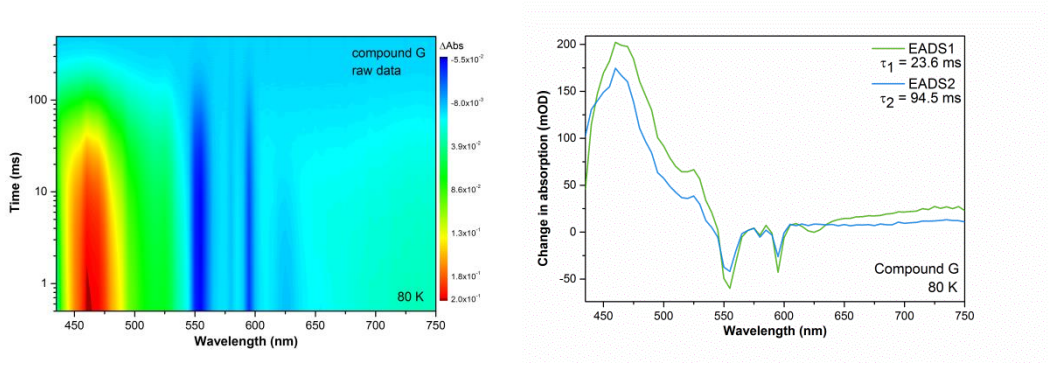

Figure S4.6. Time-resolved visible spectroscopy data and evolution associated difference spectra (EADS) for 13^1-OH-Pchlide (compound **G**) in anaerobic buffer at 10 K after photoexcitation at ~430 nm. Time-resolved difference spectra were recorded between 0.5 and 495 ms. The EADS were obtained from fitting the time-resolved absorption data to a sequential double exponential model.

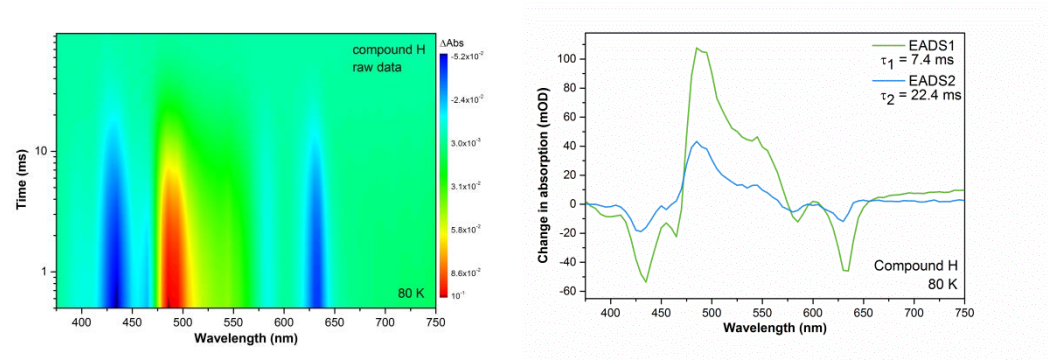

Figure S4.7. Time-resolved visible spectroscopy data and evolution associated difference spectra (EADS) for chlorophyll c (compound **H**) in anaerobic buffer at 10 K after photoexcitation at ~430 nm. Time-resolved difference spectra were recorded between 0.5 and 95 ms. The EADS were obtained from fitting the time-resolved absorption data to a sequential double exponential model.

5 Conclusions

Experiments at cryogenic temperatures on protochlorophyllide oxidoreductase have opened up a new range of possibilities to study this light-driven biological system.

A combination of time-resolved absorption and EPR studies on the Pchlide substrate allowed us to confirm the triplet nature of the long-lived species formed during the excited-state relaxation process and characterise its EPR signature. This triplet state was found to form on the nanoseconds timescale and displayed lifetimes of tens of milliseconds at cryogenic temperatures.

The work conducted during this thesis revealed that the triplet state of Pchlide interacts with oxygen in solution and that binding to the POR enzyme reduces the lifetime of this triplet. These are relevant findings to support a photoprotective role of POR in plants, where it would reduce the amount of highly reactive and potentially hazardous oxygen species inside of plant cells.

Working at cryogenic temperatures also allowed us to generate and stabilise the highly transient hydride-transfer reaction intermediate of POR, where a hydrogen from the NADPH cofactor has been transferred to the C17 position of Pchlide. It was possible to detect a change towards higher symmetry geometry setting of the hydride-transfer intermediate in comparison to both the substrate and product of the reaction by means of trEPR. This information is highly relevant given the scarcity of structural information on the reaction intermediate and the POR active site due to the lack of a crystal structure of the protein in the literature.

Cryo-trapping allowed investigations of this intermediate species, until now mostly unexplored, and paved the way for future studies that could provide further insight on the nature of this species, the intricacies surrounding its formation, its geometry and the reaction mechanism of POR. Elucidation of the transient spectral components of the hydride-transfer intermediate could reveal the exact excited-state species responsible for the enzyme reaction chemistry.

3P-ESEEM measurements provided an insight into the electronic coupling in the triplet state of free Pchlide and protein-bound Pchlide. Pulsed EPR techniques offer a much wider selection of tools to investigate paramagnetic species and the interaction of

electrons with neighbouring atoms that could be used to decipher how POR tunes the electronic environment of the substrate in order to trigger the reaction chemistry.

The study of Pchlide analogue compounds allowed expanding the knowledge of the substrate functional groups relevant for the photochemistry and reactivity of Pchlide. Investigation of electronic properties of Pchlide analogues with a combination of time-resolved absorption and EPR spectroscopy provided results supporting the idea that the C17 propionic acid chain is important for active site binding. It was shown that removal or substitution of the metal centre, as well as modification of the C13 carbonyl group of Pchlide had the biggest overall impact on the excited-state properties of the substrate. Further experimental and computational work on protochlorophyllide analogues, based on the measurements presented here, could provide relevant information to determine the nature of the reactive state and reveal further implications of structural modifications on the substrate.

6 References

1. Wayne CE. Photochemistry. Oxford: Oxford University Press; 1996.

2. Turro NJ, Ramamurthy V, Scaiano JC. Modern Molecular Photochemistry of Organic Molecules. 2010 hardc. Sausalito, California: University Science Books; 2010.

3. Wardle B. Principles and applications of photochemistry. Hoboken, N.J: Wiley; 2008.

4. Klessinger M, Michl J. Excited States and Photochemistry of Organic Molecules. 1st ed. Weinheim: Wiley-VCH; 1995.

5. Lakowicz JR. Principles of Fluorescence Spectroscopy. 3rd ed. Boston, MA: Springer US; 2006.

6. Turro NJ. Modern molecular photochemistry. Mill Valley, Calif.: University Science Books; 1991.

7. Barltrop JA, Coyle JD. Excited States in Organic Chemistry. London: John Wiley & Sons Ltd; 1975.

8. Braslavsky SE. Glossary of terms used in Photochemistry. Pure Appl Chem 2007;79(3):293–465.

9. Liu R. "You're repulsive!"--Teaching VSEPR in a not-so-elegant way. J Chem Educ 2005;82(4):558–60.

10. Shenkuan N. The physical basis of Hund's rule - orbital contraction effects. J Chem Educ 1992;69(10):800–3.

11. Rioux F. Hund's Multiplicity Rule Revisited. J Chem Educ 2007;84(2):358–60.

12. Yoon S, Kukura P, Stuart CM, Mathies RA. Direct observation of the ultrafast intersystem crossing in tris(2,2′-bipyridine)ruthenium(II) using femtosecond stimulated Raman spectroscopy. Mol Phys 2006;104(8):1275–82.

13. Lytle FE, Hercules DM. Luminescence of tris(2,2'-bipyridine)ruthenium(II) dichloride. J Am Chem Soc 1969;91(2):253–7.

14. Crosby GA, Demas JN. Quantum efficiencies on transition metal complexes. II. Charge-transfer luminescence. J Am Chem Soc 1971;93(12):2841–7.

15. Porter G. Flash photolysis and spectroscopy. A new method for the study of free radical reactions. Proc R Soc A 1950;200(1061):284–300.

16. Bailey DN, Hercules DM. Topics in chemical instrumentation XX. flash photolysis - A technique for studying fast reactions. J Chem Educ 1965;42(2):A83–94.

17. Kühn O, Lochbrunner S. Ultrafast Spectroscopy. In: Encyclopedia of applied physics. New York, NY: VCH Publishers; 2009. page 629.

18. Lytle FE, Parrish RM, Barnes WT. An Introduction to Time-Resolved Pump/Probe Spectroscopy. Appl Spectrosc 1985;39(3):444–51.

19. Laptenok SP, Borst JW, Mullen KM, van Stokkum IHM, Visser AJWG, van Amerongen H. Global analysis of Förster resonance energy transfer in live cells measured by fluorescence lifetime imaging microscopy exploiting the rise time of acceptor fluorescence. Phys. Chem. Chem. Phys.2010;12(27):7593–602.

20. Hanf R, Fey S, Dietzek B, Schmitt M, Reinbothe C, Reinbothe S, et al. Protein-induced excited-state dynamics of protochlorophyllide. J Phys Chem A 2011;115:7873–81.

21. Heyes DJ, Hardman SJO, Mansell D, Gardiner JM, Scrutton NS. Mechanistic reappraisal of early stage photochemistry in the light-driven enzyme protochlorophyllide oxidoreductase. PLoS One 2012;7(9):e45642.

22. Dietzek B, Tschierlei S, Hermann G, Yartsev A, Pascher T, Sundström V, et al. Protochlorophyllide a: A Comprehensive Photophysical Picture. Chemphyschem 2009;10(1):144–50.

23. Sytina O a, Heyes DJ, Hunter CN, Alexandre MT, van Stokkum IHM, van Grondelle R, et al. Conformational changes in an ultrafast light-driven enzyme determine catalytic activity. Nature 2008;456(7224):1001–4.

24. Vij DR. Handbook of Applied Solid State Spectroscopy. Boston, MA: Springer US; 2006.

25. Eaton GR. Foundations of modern EPR . Singapore ; World Scientific; 1998.

26. Weil JA, Bolton JR. Electron paramagnetic resonance : elementary theory and practical applications. 2nd ed. Hoboken, N.J: Wiley-Interscience; 2007.

27. Schweiger A, Jeschke G. Principles of pulse electron paramagnetic resonance. Oxford: Oxford University Press; 2001.

28. Drescher M, Jeschke G. EPR Spectroscopy Applications in Chemistry and Biology. Berlin, Heidelberg: Springer Berlin Heidelberg; 2012.

29. Forbes MDE. Symposium-in-Print Time-Resolved (CW) Electron Paramagnetic Resonance Spectroscopy: An Overview of the Technique and Its Use in Organic Photochemistry. 1997;65(1):73–81.

30. Pickett HM. General rotational relaxation matrix: Linewidths for oxygen, their interrelation and relation to theory. J Chem Phys 1975;63(5):2153–61.

31. Hicks RG, editor. Stable radicals : fundamentals and applied aspects of odd-electron compounds. Oxford: Wiley-Blackwell; 2010.

32. Spaeth JM, Tkach I, Greulich-Weber S, Overhof H. High-field optically detected EPR and ENDOR of semiconductor defects using W-band microwave Fabry-Pérot resonators. Magn Reson Chem 2005;43(S1):S153–65.

33. Lee CE, Oh DK, Jin J-I, Nam B-K. EPR study of the PPV conducting polymers. Synth Met 1995;69(1):425–6.

34. Eaton GR. Quantitative EPR. New York: Springer; 2010.

35. Abragam A, Bleaney B. Electron paramagnetic resonance of transition ions. Oxford: Clarendon Press; 1970.

36. Möbius K, Savitsky A, Schnegg A, Plato M, Fuchs M. High-field EPR spectroscopy applied to biological systems: characterization of molecular switches for electron and ion transfer. Phys Chem Chem Phys 2005;7(1):19–42.

37. Janzen EG. Spin Trapping. Acc Chem Res 1971;4(1):31–40.

38. Abragam A, Pryce MHL. Theory of the Nuclear Hyperfine Structure of Paramagnetic Resonance Spectra in Crystals. Proc R Soc London Ser A, Math Phys Sci 1951;205(1080):135–53.

39. BioSpin B. Multi-frequency EPR [Internet]. [cited 2019 Mar 12];Available from: https://www.bruker.com/products/mr/epr/multifrequency-epr/multi-frequency-epr.html

40. Raymond Hagen W. Biomolecular EPR Spectroscopy. Boca Raton: CRC Press; 2008.

41. Waals JH. EPR of photo-excited triplet states: A personal account. Appl. Magn. Reson.2001;20(4):545–61.

42. Kottis P, Lefebvre R. Calculation of the Electron Spin Resonance Line Shape of Randomly Oriented Molecules in a Triplet State. I. The Δ m =2 Transition with a Constant Linewidth. J Chem Phys 1963;39(2):393–403.

43. Wasserman E, Snyder LC, Yager WA. ESR of the Triplet States of Randomly Oriented Molecules. J Chem Phys 1964;41(6):1763–72.

44. Stevenson RC. Triplet state EPR spectra. J Magn Reson 1984;57:24–42.

45. Eaton SS, More KM, Sawant BM, Eaton GR. Use of the EPR Half-Field Transition To Determine the Interspin Distance and the Orientation of the Interspin Vector in Systems with Two Unpaired Electrons. J Am Chem Soc 1983;105(22):6560–7.

46. Levanon H, Norris JR. The Photoexcited Triplet State and Photosynthesis. Chem Rev 1978;78(3):185–98.

47. Atherton NM. Principles of electron spin resonance. Chichester: Ellis Horwood; 1993.

48. El-Sayed MA. Multiple resonance techniques in the study of the magnetic, radiative and non-radiative properties of the triplet state. Pure Appl Chem 1970;24(3):475–94.

49. Bersohn M, Baird JC. An introduction to electron paramagnetic resonance. New York: Benjamin; 1966.

50. Hanna MW. Quantum mechanics in chemistry. 3rd ed. Menlo Park, Calif.: Benjamin/Cummings; 1981.

51. Lin TS. Electron spin echo spectroscopy of organic triplets. Chem Rev 1984;84(1):1–15.

52. Angiolillo PJ, Lin VS-Y, Vanderkooi JM, Therien MJ. EPR Spectroscopy and Photophysics of the Lowest Photoactivated Triplet State of a Series of Highly Conjugated (Porphinato)Zn Arrays. J Am Chem Soc 1995;117(50):12514–27.

53. Ringe D, Petsko GA. How Enzymes Work. Science 2008;320(5882):1428–9.

54. Lund A, Shiotani M, Shimada S. Principles and Applications of ESR Spectroscopy. Dordrecht : Springer Netherlands; 2011.

55. Minkin VI. Glossary of terms used in theoretical organic chemistry. Pure Appl Chem 1999;71(10):1919–81.

56. Taguchi AT, O'Malley PJ, Wraight CA, Dikanov SA, O'Malley PJ, Wraight CA, et al. Nuclear Hyperfine and Quadrupole Tensor Characterization of the Nitrogen Hydrogen Bond Donors to the Semiquinone of the QB Site in Bacterial Reaction Centers: A Combined X- and S-Band 14,15N ESEEM and DFT Study. J Phys Chem B 2014;118(6):1501–9.

57. James TL. Nuclear magnetic resonance in biochemistry : principles and applications. London: Academic Press; 1975.

58. Deligiannakis Y, Louloudi M, Hadjiliadis N. Electron spin echo envelope modulation (ESEEM) spectroscopy as a tool to investigate the coordination environment of metal centers. Coord Chem Rev 2000;204(1):1–112.

59. Tait C, Neuhaus P, Anderson H, Timmel C, Carbonera D, Valentin M. HYSCORE on Photoexcited Triplet States. Appl Magn Reson 2015;46(4):389–409.

60. Kaminker I, Han S. Amplification of Dynamic Nuclear Polarization at 200 GHz by Arbitrary Pulse Shaping of the Electron Spin Saturation Profile. J Phys Chem Lett 2018;9(11):3110.

61. Tait CE, Stoll S. ENDOR with band-selective shaped inversion pulses. J Magn Reson 2017;277:36–44.

62. Spindler PE, Zhang Y, Endeward B, Gershernzon N, Skinner TE, Glaser SJ, et al. Shaped optimal control pulses for increased excitation bandwidth in EPR. J Magn Reson 2012;218:49–58.

63. Pribitzer S, Segawa TF, Doll A, Jeschke G. Transverse interference peaks in chirp FT-EPR correlated three-pulse ESEEM spectra. J Magn Reson 2016;272:37–45.

64. Harm H, Rupert CS. Analysis of photoernzymatic repair of UV lesions in DNA by single light flashes. XI. Light-induced activation of the yeast photoreactivating enzyme. Mutat Res Mol Mech Mutagen 1976;34(1):75–92.

65. Harm W. Analysis of photoenzymatic repair of UV lesions in DNA by single light flashes XII. Evidence for enhanced photolysis of enzyme—substrate complexes by a 2-photon reaction. Mutat Res Mol Mech Mutagen 1979;60(2):121–33.

66. Hug DH, O'Donnell PS, Hunter JK. Light Activation of Enzymes. Photochem Photobiol 1980;32(6):841–8.

67. Menon BRKK, Waltho JP, Scrutton NS, Heyes DJ. Cryogenic and laser photoexcitation studies identify multiple roles for active site residues in the light-driven enzyme protochlorophyllide oxidoreductase. J Biol Chem 2009;284(27):18160–6.

68. Aubert C, Vos MH, Mathis P, Eker APM, Brettel K. Intraprotein radical transfer during photoactivation of DNA photolyase. Nature 2000;405(6786):586.

69. Johannissen LO, Hay S, Scrutton NS, Sutcliffe MJ. Proton tunneling in aromatic amine dehydrogenase is driven by a short-range sub-picosecond promoting vibration: Consistency of simulation and theory with experiment. J Phys Chem B 2007;111(10):2631–8.

70. Alhambra C, Corchado JC, Sánchez ML, Gao J, Truhlar DG. Quantum dynamics of hydride transfer in enzyme catalysis. J Am Chem Soc 2000;122(34):8197–203.

71. Scrutton NS, Louise Groot M, Heyes DJ, Groot ML, Heyes DJ. Excited state dynamics and catalytic mechanism of the light-driven enzyme protochlorophyllide oxidoreductase. Phys Chem Chem Phys 2012;14(25):8818–24.

72. The International Organization for Standardization. ISO 21348 Definitions of Solar Irradiance Spectral Categories [Internet]. 2007;Available from: http://www.spacewx.com/pdf/SET_21348_2004.pdf

73. Brash DE. UV mutagenic photoproducts in Escherichia coli and human cells: a molecular genetics perspective on human skin cancer. Photochem Photobiol 2008;48(1):59–66.

74. Alberts B, Johnson A, Lewis J, Morgan D, Raff M, Roberts K, et al. Molecular biology of the cell. 6th ed. New York, NY: Garland Science, Taylor and Francis Group; 2015.

75. Friedberg EC. DNA damage and repair. Nature 2003;421(January):436–40.

76. Cory S, Adams JM. The Bcl2 family: regulators of the cellular life-or-death switch. Nat Rev Cancer 2002;2:647–56.

77. Essen L-O. Photolyases and cryptochromes: common mechanisms of DNA repair and light-driven signaling. Curr Opin Struct Biol 2006;16(1):51–9.

78. Yasuhira S, Yasui A. Visible light-inducible photolyase gene from the goldfish Carassius auratus. J Biol Chem 1992;267:25644–7.

79. Yasui A, Eker AP, Yasuhira S, Yajima H, Kobayashi T, Takao M, et al. A new class of DNA photolyases present in various organisms including aplacental mammals. EMBO J 1994;13(24):6143.

80. Sancar A. Structure and function of DNA photolyase. Biochem 1994;33(1):2–9.

81. Kato T, Todo T, Ayaki H, Ishizaki K, Morita T, Mitra S, et al. Cloning of a marsupial DNA photolyase gene and the lack of related nucleotide sequences in placental mammals. Nucleic Acids Res 1994;22(20):4119.

82. Mees A, Klar T, Gnau P, Hennecke U, Eker APM, Carell T, et al. Crystal structure of a photolyase bound to a CPD-like DNA lesion after in situ repair. Science 2004;306:1789–93.

83. Müller M, Carell T. Structural biology of DNA photolyases and cryptochromes. Curr Opin Struct Biol 2009;19(3):277–85.

84. Yasui A, Laskowski W. Determination of the number of photoreactivating enzyme molecules per haploid Saccharomyces cells. Int J Radiat Biol Relat Stud Phys Chem Med 1975;28:511–8.

85. Henry AA, Jimenez R, Hanway D, Romesberg FE. Preliminary characterization of light harvesting in E. coli DNA photolyase. Chembiochem 2004;5:1088–94.

86. Voet D. Biochemistry. 4th ed. Hoboken, N.J.: Wiley; 2011.

87. Förster T. Transfer Mechanisms of Electronic Excitation Energy. Radiat Res Suppl 1960;2:326–39.

88. Gindt YM, Schelvis JPM, Thoren KL, Huang TH. Substrate binding modulates the reduction potential of DNA photolyase. J Am Chem Soc 2005;127:10472–3.

89. Langenbacher T, Zhao X, Bieser G, Heelis PF, Sancar A, Michel-Beyerle ME. Substrate and temperature dependence of DNA photolyase repair activity examined with ultrafast spectroscopy. J Am Chem Soc 1997;119:10532–6.

90. Kim S, Sancar A. Evidence from photoinduced EPR for a radical intermediate during photolysis of cyclobutane thymine dimer by DNA photolyase. J Am Chem Soc 1992;(9):4442–3.

91. IV AM, Stanley RRJ, MacFarlane IV AW. Cis-Syn thymidine dimer repair by DNA photolyase in real time. Biochemistry 2003;42:8558–68.

92. Weber S. Light-driven enzymatic catalysis of DNA repair: a review of recent biophysical studies on photolyase. Biochim Biophys Acta 2005;1707(1):1–23.

93. Park HW, Kim ST, Sancar A, Deisenhofer J. Crystal structure of DNA photolyase from Escherichia coli. Science 1995;268:1866–72.

94. Brettel K, Byrdin M. Reaction mechanisms of DNA photolyase. Curr Opin Struct Biol 2010;20(6):693–701.

95. Sorigué D, Légeret B, Cuiné S, Blangy S, Moulin S, Billon E, et al. An algal photoenzyme converts fatty acids to hydrocarbons. Science 2017;357(6354):903–7.

96. Scrutton NS. Enzymes make light work of hydrocarbon production. Science 2017;357(6354):872–3.

97. Weber S, Richter G, Schleicher E, Bacher A, Möbius K, Kay CW. Substrate binding to DNA photolyase studied by electron paramagnetic resonance spectroscopy. Biophys J 2001;81:1195–204.

98. Kay CW, Feicht R, Schulz K, Sadewater P, Sancar A, Bacher A, et al. EPR, ENDOR, and TRIPLE resonance spectroscopy on the neutral flavin radical in Escherichia coli DNA photolyase. Biochemistry1999;38(51):16740–8.

99. Sanders D, Wiest O. A model for the enzyme-substrate complex of DNA photolyase and photodamaged DNA. J Am Chem Soc 1999;121(22):5127–34.

100. Hahn J, Michel-Beyerle ME, Rosch N. Binding of pyrimidine model dimers to the photolyase enzyme: A molecular dynamics study. J Phys Chem B 1999;103(11):2001–7.

101. Antony J, Medvedev DM, Stuchebrukhov AA. Theoretical study of electron transfer between the photolyase catalytic cofactor FADH(-) and DNA thymine dimer. J Am Chem Soc 2000;122(6):1057–65.

102. Rüdiger W. Chlorophyll metabolism: From outer space down to the molecular level. Phytochemistry 1997;46(7):1151–67.

103. Beale SI. Enzymes of chlorophyll biosynthesis. Photosynth Res 1999;60:43–73.

104. Lebedev N, Timko MP. Protochlorophyllide photoreduction. Photosynth Res 1998;58(1):5–23.

105. Reinbothe C, El Bakkouri M, Buhr F, Muraki N, Nomata J, Kurisu G, et al. Chlorophyll biosynthesis: spotlight on protochlorophyllide reduction. Trends Plant Sci 2010;15(11):614–24.

106. Armstrong CA, Runge S, Frick C, Sperling U, Apel K. ldentification of NADPH : Protochlorophyllide Oxidoreductases A and B : A Branched Pathway for Light- Dependent Chlorophyll Biosynthesis in Arabidopsis thaliana. Plant Physiol 1995;(108):1505–17.

107. Muraki N, Nomata J, Ebata K, Mizoguchi T, Shiba T, Tamiaki H, et al. X-ray crystal structure of the light-independent protochlorophyllide reductase. Nature 2010;465:110–4.

108. Masuda T, Takamiya K. Novel Insights into the Enzymology, Regulation and Physiological Functions of Light-dependent Protochlorophyllide Oxidoreductase in Angiosperms. Photosynth Res 2004;81(1):1–29.

109. Heyes DJ, Hunter CN. Making light work of enzyme catalysis: protochlorophyllide oxidoreductase. Trends Biochem Sci 2005;30(11):642–9.

110. Archipowa N, Kutta RJ, Heyes DJ, Scrutton NS. Stepwise Hydride Transfer in a Biological System: Insights into the Reaction Mechanism of the Light-Dependent Protochlorophyllide Oxidoreductase. Angew Chemie Int Ed 2018;2682–6.

111. Griffiths BWT. Reconstitution of Chlorophyilide Formation by Isolated Etioplast Membranes EnLcmpex. Biochem J 1978;174:681–92.

112. Heyes D, Menon B, Sakuma M, Scrutton N. Conformational Events during Ternary Enzyme-Substrate Complex Formation Are Rate Limiting in the Catalytic Cycle of the Light-Driven Enzyme Protochlorophyllide. Biochemistry 2008;47:10991–8.

113. Heyes DJ, Ruban A V, Wilks HM, Hunter CN. Enzymology below 200 K: the kinetics and thermodynamics of the photochemistry catalyzed by protochlorophyllide oxidoreductase. Proc Natl Acad Sci U S A 2002;99:11145–50.

114. Heyes DJ, Heathcote P, Rigby SEJ, Palacios M a, van Grondelle R, Hunter CN. The first catalytic step of the light-driven enzyme protochlorophyllide oxidoreductase proceeds via a charge transfer complex. J Biol Chem 2006;281(37):26847–53.

115. Heyes DJ, Hunter CN, van Stokkum IHM, van Grondelle R, Groot ML. Ultrafast enzymatic reaction dynamics in protochlorophyllide oxidoreductase. Nat Struct Biol 2003;10(6):491–2.

116. Heyes DJ, Hunter CN. Identification and characterization of the product release steps within the catalytic cycle of protochlorophyllide oxidoreductase. Biochemistry 2004;43:8265–71.

117. Heyes DJ, Ruban A V, Hunter CN. Protochlorophyllide oxidoreductase: dark reactions of a light-driven enzyme. Biochemistry 2003;42(2):523.

118. Heyes DJ, Scrutton NS. Conformational changes in the catalytic cycle of protochlorophyllide oxidoreductase: what lessons can be learnt from dihydrofolate reductase? Biochem Soc Trans 2009;37:354–7.

119. Begley TP, Young H. Protochlorophyllide reductase. 1. Determination of the regiochemistry and the stereochemistry of the reduction of protochlorophyllide to chlorophyllide. J Am Chem Soc 1989;111(8):3095–6.

120. Vimlesh Valera, Margaret Fung, Andreas N. Wessler WRR. Synthesis of 4R- and 4S-tritium labeled NADPH for the determination of the coenzyme stereospecificity of NADPH: Protochlorophyllide oxidoreductase. Biochem Biophys Res Commun 1987;148(1):515–20.

121. Wilks HM, Timko MP. A light-dependent complementation system for analysis of NADPH:protochlorophyllide oxidoreductase: Identification and mutagenesis of two conserved residues that are essential for enzyme activity. Proc Natl Acad Sci USA 1995;92(3):724–8.

122. Heyes DJ, Sakuma M, de Visser SP, Scrutton NS. Nuclear quantum tunneling in the light-activated enzyme protochlorophyllide oxidoreductase. J Biol Chem 2009;284(6):3762–7.

123. Menon BRKK, Davison PA, Hunter CN, Scrutton NS, Heyes DJ. Mutagenesis alters the catalytic mechanism of the light-driven enzyme protochlorophyllide oxidoreductase. J Biol Chem 2010;285(3):2113.

124. Heyes DJ Scrutton NS SM, Heyes DJ, Sakuma M, Scrutton NS. Laser excitation studies of the product release steps in the catalytic cycle of the light-driven enzyme protochlorophyllide oxidoreductase (POR). 2007;282(44):32015–20.

125. Sytina O a, Alexandre MT, Heyes DJ, Hunter CN, Robert B, van Grondelle R, et al. Enzyme activation and catalysis: characterisation of the vibrational modes of substrate and product in protochlorophyllide oxidoreductase. Phys Chem Chem Phys 2011;13(6):2307–13.

126. Schmitt M, Dietzek B, Hermann G, Popp J. Femtosecond time-resolved spectroscopy on biological photoreceptor chromophores. Laser Photonics Rev 2007;1(1):57–78.

127. Heyes DJ, Hardman SJO, Hedison TM, Hoeven R, Greetham GM, Towrie M, et al. Excited-State Charge Separation in the Photochemical Mechanism of the Light-Driven Enzyme Protochlorophyllide Oxidoreductase **. Angew Chemie - Int Ed 2015;54(5):1512–5.

128. Menon BRK, Hardman SJOO, Scrutton NS, Heyes DJ. Multiple active site residues are important for photochemical efficiency in the light-activated enzyme protochlorophyllide oxidoreductase (POR). J Photochem Photobiol B Biol 2016;161:236–43.

129. Colindres-Rojas M, Wolf MMN, Gross R, Seidel S, Dietzek B, Schmitt M, et al. Excited-state dynamics of protochlorophyllide revealed by subpicosecond infrared spectroscopy. Biophys J 2011;100(1):260–7.

130. Dietzek B, Maksimenka R, Siebert T, Birckner E, Kiefer W, Popp J, et al. Excited-state processes in protochlorophyllide a – a femtosecond time-resolved absorption study. Chem Phys Lett 2004;397(1–3):110–5.

131. Dietzek B, Kiefer W, Yartsev A, Sundström V, Schellenberg P, Grigaravicius P, et al. The excited-state chemistry of protochlorophyllide a: A time-resolved fluorescence study. ChemPhysChem 2006;7(8):1727–33.

132. Sytina OA, van Stokkum IHM, Heyes DJ, Hunter CN, van Grondelle R, Groot ML. Protochlorophyllide excited-state dynamics in organic solvents studied by time-resolved visible and mid-infrared spectroscopy. J Phys Chem B 2010;114(C):4335–44.

133. Dietzek B, Tschierlei S, Hanf R, Seidel S, Yartsev A, Schmitt M, et al. Dynamics of charge separation in the excited-state chemistry of protochlorophyllide. Chem Phys Lett 2010;492(1–3):157–63.

134. Dietzek B, Kiefer W, Hermann G, Popp J, Schmitt M. Solvent effects on the excited-state processes of protochlorophyllide: a femtosecond time-resolved absorption study. J Phys Chem B 2006;110(9):4399–406.

135. Rodriguez J, Kirmaier C, Holten D. Optical properties of metalloporphyrin excited states. J Am Chem Soc 1989;111(17):6500–6.

136. Zhao G-J, Han K-L. Site-specific solvation of the photoexcited protochlorophyllide a in methanol: formation of the hydrogen-bonded intermediate state induced by hydrogen-bond strengthening. Biophys J 2008;94(1):38–46.

137. Heyes DJ, Hardman SJO, Mansell D, Ní Cheallaigh A, Gardiner JM, Johannissen LO, et al. Excited-State Properties of Protochlorophyllide Analogues and Implications for Light-Driven Synthesis of Chlorophyll. J Phys Chem B 2017;121(6):1312–20.

138. Hanf R, Tschierlei S, Dietzek B, Seidel S, Hermann G, Schmitt M, et al. Probing the structure and Franck-Condon region of protochlorophyllide a through analysis of the Raman and resonance Raman spectra. J Raman Spectrosc 2010;41:414–23.

139. Patterson LK, Porter G, Topp MR. Oxygen quenching of singlet and triplet states. Chem Phys Lett 1970;7(6):612–4.

140. Gijzeman OLJ, Kaufman F, Porter G. Oxygen quenching of aromatic triplet states in solution. Part 1. J Chem Soc Faraday Trans 2 Mol Chem Phys 1973;69(0):708–20.

141. Lebedev NN, Krasnovsky AA, Litvin FF. Phosphorescence of protochlorophyll(ide) and chlorophyll(ide) in etiolated and greening bean leaves - Assignment of spectral bands. Photosynth Res 1991;30(1):7–14.

142. Hutchison CA, Mangum BW. Paramagnetic Resonance Absorption in Naphthalene in Its Phosphorescent State. J Chem Phys 1958;29(1):952–3.

143. Yager WA, Wasserman E, Cramer RMR. ESR Observation of Δm=1 Transitions of Triplet States in Glasses. J Chem Phys 1962;37(1):1148–9.

144. Thurnauer MC, Norris JR. The ordering of the zero field triplet spin sublevels in the chlorophylls. A magnetophotoselection study. Chem Phys Lett 1977;47(1):100–5.

145. Cohen AJ, Mori-Sánchez P, Yang W. Challenges for Density Functional Theory. Chem Rev 2012;112(1):289–320.

146. Schmidt J, Antheunis DA, van der Waals JH. The dynamics of populating and depopulating the phosphorescent triplet state as studied by microwave induced delayed phosphorescence. Mol Phys 1971;22(1):1–17.

147. Di Valentin M, Ceola S, Agostini G, Giacometti GM, Angerhofer A, Crescenzi O, et al. Pulse ENDOR and density functional theory on the peridinin triplet state involved in the photo-protective mechanism in the peridinin-chlorophyll a-protein from Amphidinium carterae. Biochim Biophys Acta - Bioenerg 2008;1777(3):295–307.

148. Snellenburg JJ, Laptenok SP, Seger R, Mullen KM, van Stokkum IHM. Glotaran : A Java -Based Graphical User Interface for the R Package TIMP. J Stat Softw 2012;49(3):1–22.

149. Stoll S, Schweiger A. EasySpin, a comprehensive software package for spectral simulation and analysis in EPR. J Magn Reson 2006;178(1):42–55.

150. Sinnecker S, Neese F. Spin-spin contributions to the zero-field splitting tensor in organic triplets, carbenes and biradicals - A density functional and Ab initio study. J Phys Chem A 2006;110(44):12267–75.

151. Neese F. The ORCA program system. Wiley Interdiscip Rev Comput Mol Sci 2012;2(1):73–8.

152. Sperling U, Cleve B, Frick G, Apel K, Armstrong GA. Overexpression of light-dependent PORA or PORB in plants depleted of endogenous POR by far-red light enhances seedling survival in white light and protects against photooxidative damage. Plant J 1997;12(3):649–58.

153. Buhr F, El Bakkouri M, Valdez O, Pollmann S, Lebedev N, Reinbothe S, et al. Photoprotective role of NADPH:protochlorophyllide oxidoreductase A. Proc Natl Acad Sci U S A 2008;105(34):12629–34.

154. Virgin HI, Kahn A, Wettstein D. The physiology of chlorophyll formation in relation to structural changes in chloroplasts. Photochem Photobiol 1963;2(2):83–91.

155. Brandariz-de-Pedro G, Heyes DJ, Hardman SJO, Shanmugam M, Jones AR, Weber S, et al. Direct Evidence of an Excited-State Triplet Species upon Photoactivation of the Chlorophyll Precursor Protochlorophyllide. J Phys Chem Lett 2017;8(6):1219–23.

156. Heyes DJ, Sakuma M, Scrutton NS. Solvent-Slaved protein motions accompany proton but not hydride tunneling in light-activated protochlorophyllide oxidoreductase. Angew Chem Int Ed Engl 2009;48(21):3850–3.

157. Townley HE, Sessions RB, Clarke AR, Dafforn TR, Trevor Griffiths W, Griffiths WT, et al. Protochlorophyllide oxidoreductase: A homology model examined by site-directed mutagenesis. Proteins 2001;44(3):329–35.

158. Filling C, Berndt KD, Benach J, Knapp S, Prozorovski T, Nordling E, et al. Critical residues for structure and catalysis in short-chain dehydrogenases/reductases. J Biol Chem 2002;277(28):25677.

159. Kallberg Y, Persson B. Prediction of coenzyme specificity in dehydrogenases-reductases. A hidden Markov model-based method and its application on complete genomes. FEBS J 2006;273(6):1177–84.

160. Kavanagh KL, Jörnvall H, Persson B, Oppermann U. Medium- and short-chain dehydrogenase/reductase gene and protein families. Cell Mol Life Sci 2008;65(24):3895–906.

161. Gabruk M, Mysliwa-Kurdziel B. Light-Dependent Protochlorophyllide Oxidoreductase: Phylogeny, Regulation, and Catalytic Properties. Biochemistry 2015;54(34):5255.

162. Dahlin C, Aronsson H, Wilks HM, Lebedev N, Sundqvist C, Timko MP. The role of protein surface charge in catalytic activity and chloroplast membrane association of the pea NADPH: Protochlorophyllide oxidoreductase (POR) as revealed by alanine scanning mutagenesis. Plant Mol Biol 1999;39(2):309–23.

163. Gholami S, Nenov A, Rivalta I, Bocola M, Bordbar AK, Schwaneberg U, et al. Theoretical Model of the Protochlorophyllide Oxidoreductase from a Hierarchy of Protocols. J Phys Chem B 2018;122(31):7668.

164. Tait CE, Neuhaus P, Anderson HL, Timmel CR. Triplet state delocalization in a conjugated porphyrin dimer probed by transient EPR techniques. J Am Chem Soc 2015;150427063742002.

165. Singel DJ, van Der Poel WAJA, Schmidt J, van Der Waals JH, de Beer R. Complete determination of 1 4 N hyperfine and quadrupole interactions in the metastable triplet state of free-base porphin via electron spin echo envelope modulation. J Chem Phys 1984;81(12):5453–61.

166. Heyes DJ, Martin GEM, Reid RJ, Hunter CN, Wilks HM. NADPH:protochlorophyllide oxidoreductase from Synechocystis: overexpression, purification and preliminary characterisation. FEBS Lett 2000;483(1):47–51.

167. Francl MM, Pietro WJ, Hehre WJ, Binkley JS, Gordon MS, Defrees DJ, et al. Self-consistent molecular orbital methods. XXIII. A polarization-type basis set for second-row elements. J Chem Phys 1982;77(7):3654–65.

168. Franck F, Sperling U, Frick G, Pochert B. Regulation of etioplast pigment-protein complexes, inner membrane architecture, and protochlorophyllide a chemical heterogeneity by light-dependent NADPH: Protochlorophyllide oxidoreductases A and B. Plant Physiol 2000;124(4):1678–96.

169. Griffiths WT. Substrate-specificity studies on protochlorophyllide reductase in barley (Hordeum vulgare) etioplast membranes. Biochem J 1980;186(1):267.

170. Klement H, Helfrich M, Oster U, Schoch S, Ru W, Rüdiger W. Pigment-free NADPH:protochlorophyllide oxidoreductase from Avena sativa L. Purification and substrate specificity. Eur J Biochem 1999;265(3):862–74.

171. Rüdiger W, Böhm S, Helfrich M, Schulz S, Schoch S. Enzymes of the last steps of chlorophyll biosynthesis: modification of the substrate structure helps to understand the topology of the active centers. Biochemistry 2005;44(32):10864.

172. Raskin V, Schwartz A. The charge-transfer complex between protochlorophyllide and NADPH: an intermediate in protochlorophyllide photoreduction. Photosynth Res 2002;74(2):181–6.

173. Brandariz-de-Pedro G, Heyes DJ, Hardman SJO, Sakuma M, Shanmugam M, Weber S, et al. Unpublished work.

174. Loboda O, Minaev B, Vahtras O, Schimmelpfennig B, Ågren H, Ruud K, et al. Ab initio calculations of zero-field splitting parameters in linear polyacenes. Chem Phys 2003;286(1):127–37.

175. Derren Heyes personal communication.